

Receiver Autonomous Integrity Monitoring Schemes for Global Navigation Satellite Systems

Author:

Jiang, Yiping

Publication Date:

2014

DOI:

<https://doi.org/10.26190/unsworks/16994>

License:

<https://creativecommons.org/licenses/by-nc-nd/3.0/au/>

Link to license to see what you are allowed to do with this resource.

Downloaded from <http://hdl.handle.net/1959.4/53795> in <https://unsworks.unsw.edu.au> on 2024-05-03

Receiver Autonomous Integrity Monitoring Schemes for Global Navigation Satellite Systems

By

Yiping Jiang

B.Eng. Beihang University, China, 2003-2007

M.Eng. Beihang University, China, 2007-2010

A thesis in fulfillment of the requirements for the degree of
Doctor of Philosophy

School of Civil and Environmental Engineering

Faculty of Engineering

The University of New South Wales

March 2014

PLEASE TYPE

THE UNIVERSITY OF NEW SOUTH WALES
Thesis/Dissertation Sheet

Surname or Family name: Jiang

First name: Yiping

Other name/s:

Abbreviation for degree as given in the University calendar: PhD

School: School of Civil and Environmental Engineering Faculty: Faculty of Engineering

Title: Receiver Autonomous Integrity Monitoring Schemes for Global Navigation Satellite Systems

Abstract 350 words maximum: (PLEASE TYPE)

The accuracy of the navigation solutions can be greatly improved by using modernized GNSS with more visible satellites and multiple civilian frequencies. Another important performance criterion is integrity, which is defined to guarantee the safety of the navigation solution for such applications as civil aviation in which safety is of paramount issue. One of the options of integrity monitoring in civil aviation is Receiver Autonomous Integrity Monitoring (RAIM) with outputs of Vertical Protection Level (VPL), Horizontal Protection Level (HPL). With the modernized GNSS systems and augmentation systems, the number of satellites is increased and the multiple frequency signals are available. Therefore, RAIM can be used for more stringent procedures, such as LPV-200 for vertical guidance on a global scale with two major architectures as feasible choices: Advanced RAIM (A-RAIM) and Relative RAIM (R-RAIM). The algorithms to calculate VPL and HPL are critically important in deciding the final integrity results in both A-RAIM and R-RAIM, which is the focus of this study. With the notion that all current algorithms are expected to be conservative at different levels, the exact PL value is pursued here to improve the service availability, so that RAIM can be used in more stringent services.

With the inequality constrained maximization problem defined as the criterion, an optimization method is applied to obtain the exact VPL within a pre-defined accuracy and to improve the computational efficiency. It is shown that the new method to calculate the exact VPL is more reliable and efficient than the old method. Worldwide simulation results show that the new approach has improved A-RAIM availability from 32%-38% to 74% with GPS and from 44%-43% to 85% with Galileo. With the exact VPL, the conservativeness of all current algorithms can be analyzed with conclusions provided. Similarly, the same approach can be applied to obtain the worst case bias in calculation of HPL with service availability improvement from the 50% ~62% to be around 87% with GPS. Besides, RAIM is generalized with a higher dimensional PL with the separability functionality integrated with A-RAIM results provided.

Declaration relating to disposition of project thesis/dissertation

I hereby grant to the University of New South Wales or its agents the right to archive and to make available my thesis or dissertation in whole or in part in the University libraries in all forms of media, now or here after known, subject to the provisions of the Copyright Act 1968. I retain all property rights, such as patent rights. I also retain the right to use in future works (such as articles or books) all or part of this thesis or dissertation.

I also authorise University Microfilms to use the 350 word abstract of my thesis in Dissertation Abstracts International (this is applicable to doctoral theses only).

Signature

Witness

19/9/2014

Date

The University recognises that there may be exceptional circumstances requiring restrictions on copying or conditions on use. Requests for restriction for a period of up to 2 years must be made in writing. Requests for a longer period of restriction may be considered in exceptional circumstances and require the approval of the Dean of Graduate Research.

FOR OFFICE USE ONLY

Date of completion of requirements for Award:

THIS SHEET IS TO BE GLUED TO THE INSIDE FRONT COVER OF THE THESIS

COPYRIGHT STATEMENT

'I hereby grant the University of New South Wales or its agents the right to archive and to make available my thesis or dissertation in whole or part in the University libraries in all forms of media, now or here after known, subject to the provisions of the Copyright Act 1968. I retain all proprietary rights, such as patent rights. I also retain the right to use in future works (such as articles or books) all or part of this thesis or dissertation.

I also authorise University Microfilms to use the 350 word abstract of my thesis in Dissertation Abstract International (this is applicable to doctoral theses only).

I have either used no substantial portions of copyright material in my thesis or I have obtained permission to use copyright material; where permission has not been granted I have applied/will apply for a partial restriction of the digital copy of my thesis or dissertation.'

Signed *Y - Z*

Date 19/9/2014

AUTHENTICITY STATEMENT

'I certify that the Library deposit digital copy is a direct equivalent of the final officially approved version of my thesis. No emendation of content has occurred and if there are any minor variations in formatting, they are the result of the conversion to digital format.'

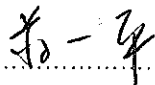
Signed *Y - Z*

Date 19/9/2014

ORIGINALITY STATEMENT

'I hereby declare that this submission is my own work and to the best of my knowledge it contains no materials previously published or written by another person, or substantial proportions of material which have been accepted for the award of any other degree or diploma at UNSW or any other educational institution, except where due acknowledgement is made in the thesis. Any contribution made to the research by others, with whom I have worked at UNSW or elsewhere, is explicitly acknowledged in the thesis. I also declare that the intellectual content of this thesis is the product of my own work, except to the extent that assistance from others in the project's design and conception or in style, presentation and linguistic expression is acknowledged.'

Signed



Date

19/9/2014

The accuracy of the navigation solutions can be greatly improved by using modernized GNSS with more visible satellites and multiple civilian frequencies. Another important performance criterion is integrity, which is defined to guarantee the safety of the navigation solution for such applications as civil aviation in which safety is of paramount issue. Integrity is used to quantify the risky situation when the position error is at a hazardous level with faults in the observations, but the user is not aware of it. Integrity faults can be a consequence of clock anomalies, cycle slips, multipath, etc. One of the popular integrity monitoring methods in civil aviation is Receiver Autonomous Integrity Monitoring (RAIM), which is essentially a consistency check on the GNSS observations by the aircraft. The output is the integrity indicators, such as Vertical Protection Level (VPL) and Horizontal Protection Level (HPL), which is a statistical bound on the position domain with given integrity risk.

With the forthcoming of the modernized GPS system, new constellations and augmentation systems, the number of satellites will be increased and the multiple frequency signals will be available. Therefore, RAIM can be applied in more stringent procedures, such as LPV-200 for vertical guidance on a global scale. Two major RAIM architectures are recognized as feasible choices: Advanced RAIM (A-RAIM) and Relative RAIM (R-RAIM). Currently, there are two positioning methods (the range domain method and the position domain method) available in R-RAIM and two RAIM algorithms (the classic method and the multiple hypothesis solution separation (MHSS) method) available for both A-RAIM and R-RAIM. Based on different implementation methods, all these current choices are analysed by comparing the results within a generalized framework.

The algorithms to calculate VPLs and HPLs are critically important in deciding the final integrity results for both A-RAIM and R-RAIM, which is the focus of this thesis. With the notion that all current algorithms are expected to be conservative at different levels, the exact Protection Level (PL) value within pre-defined accuracy and computational efficiency is pursued to improve the service availability and promoting RAIM in more stringent services in civil aviation.

There are mainly four methods to calculate VPL in literature, among which the ideal VPL method is the least conservative one with the exact value as the ultimate goal. To calculate the ideal VPL with given integrity risk, the bias with the maximum integrity risk, which is a function of the input VPL value, is searched in a boundary. To make sure the maximum integrity risk is equal with the given one, another VPL search loop is added upon the bias search. In this way, the computation becomes complex and the precision of the result is compromised. Therefore, a new procedure is designed with a new worst case search: the maximum VPL is searched among a range to encompass all possible sizes of the bias. VPL is calculated with a given integrity risk for each possible bias size in the search, so that the uncertainty of the arbitrary VPL input in the previous method is avoided. In this way, the calculation is simplified and the computation is faster, but the accuracy is still uncertain. With the inequality constrained maximization problem defined as the criterion, an optimization method can be applied to obtain a solution with a pre-defined accuracy as well as improved the computational efficiency. It is demonstrated that the new method to calculate the exact VPL is more reliable and efficient than the ideal VPL method. Worldwide simulation results show that the new approach has improved A-RAIM availability from 32%-38% to 74% with GPS and from 44%-43% to 85% with Galileo. With the exact VPL, the conservativeness of all current algorithms can be analyzed and conclusions are provided in this thesis.

Similarly, the same approach can be applied to obtain the worst case bias when calculating HPL. Besides the bias search, the calculation of HPL is more complex with

another approximation on the distribution of the two-dimensional position error. There are two types of approximations among current methods: the normal approximation and the chi-squared approximation. Both approximated distributions are analyzed with the exact distribution to determine conservativeness. An approach to calculate the exact distribution with high computational sufficiency is adopted. Together with the optimization method to obtain the worst case bias, the exact HPL is obtained within required accuracy and computational efficiency. In the same way, the conservativeness of current approximated HPLs is also concluded. RAIM is then generalized with a higher dimensional PL, where an example of three-dimensional PL is provided. Results show that the improvement of the service availability is from 50%~62% to around 87% with GPS.

Furthermore, as a component of RAIM, Fault Detection and Exclusion (FDE) is investigated in the background of the classic reliability theory. After analyzing the performance of current FDE methods, theoretical proof on the optimality of test statistics in regard of detectability and separability is made. Plus, the current separability measure is found to be not applicable in one of the test statistics used in navigation, and a new measure is proposed without loss of generality. Results show that the new measure is more consistent with the performance of FDE. Lastly, RAIM is expanded from PL with fault detection only to PL with fault exclusion using the new separability measure. Consequently, a comprehensive framework for RAIM is established here with theoretical and numerical results.

ACKNOWLEDGEMENTS

First of all, I would like to thank my supervisor, Associate Professor Jinling Wang, for his supervision, support and encouragement throughout my PhD study. Only with his consistent supervision, I can finish my research training and achieve these results today. Special thanks also go to Professor Chris Rizos, who is always supportive for me and everyone else in our school.

I would also like to express my thanks to all the staff members, especially Professor Andrew Dempster and Dr Craig Roberts from whom I get sincere suggestions on my PhD study. My colleges: Weidong Ding, Nathan Knight, Tao Li, Xun Li, Ling Yang and Youlong Wu, from whom I have discussions on various research problems.

I would like to acknowledge the Chinese Government for awarding me the Chinese Scholarship Council to pursue my PhD studies at the University of New South Wales.

My gratefulness to my family and Marc-Patrick Zapf for their understanding and support all the way, also my good friends Thomas Gallagher, Yang Xie, Hongliang Xu, Ke Wang and Zhaoyuan Wang, who filled my life with happiness.

TABLE OF CONTENTS

ABSTRACT	I
ACKNOWLEDGEMENTS.....	IV
TABLE OF CONTENTS.....	V
LIST OF TABLES.....	IX
LIST OF FIGURES	XI
LIST OF ABBREVIATIONS.....	XV
CHAPTER 1 INTRODUCTION	1
1.1 BACKGROUND.....	1
1.2 RECEIVER AUTONOMOUS INTEGRITY MONITORING	3
1.2.1 The Development of RAIM	4
1.2.2 Fault Detection and Exclusion	6
1.2.3 Protection Level Computation	8
1.3 FUTURE INTEGRITY MONITORING ARCHITECTURES.....	9
1.4 CRITICAL ISSUES	11
1.5 CONTRIBUTIONS.....	13
1.6 THESIS OUTLINE	15
CHAPTER 2 RAIM AND FAULT DETECTION TECHNIQUES	17
2.1 THE SYSTEM MODEL	17
2.2 FAULT DETECTION AND EXCLUSION	21
2.2.1 The Global Test.....	22
2.2.2 The Local Test	23
2.2.3 The Reliability Measures	26
2.2.4 A Numerical Example.....	28

2.3	RECEIVER AUTONOMOUS INTEGRITY MONITORING SCHEMES..	31
2.3.1	Current Methods to Calculate VPL.....	33
2.3.2	Current Methods to Calculate HPL.....	36
2.3.3	Two Integrity Optimization Methods.....	38
2.4	SUMMARY	44
CHAPTER 3	RELATIVE RAIM	46
3.1	RELATIVE POSITIONING METHODS.....	47
3.1.1	The Range Domain Method.....	49
3.1.2	The Position Domain Method	49
3.2	R-RAIM ALGORITHMS	50
3.2.1	R-RAIM with the Classic Method	50
3.2.2	R-RAIM with the MHSS Method.....	52
3.3	NUMERICAL RESULTS.....	52
3.3.1	R-RAIM VPL.....	53
3.3.2	The Coasting Time.....	57
3.4	SUMMARY	61
CHAPTER 4	ADVANCED RAIM	62
4.1	A-RAIM POSITIONING METHODS.....	63
4.2	A-RAIM ALGORITHMS	64
4.2.1	A-RAIM with the Classic Algorithm.....	64
4.2.2	A-RAIM with the MHSS Algorithm.....	64
4.3	NUMERICAL RESULTS.....	65
4.4	SUMMARY	72
CHAPTER 5	A NEW APPROACH TO CALCULATE THE EXACT VPL	73
5.1	THE IDEAL VPL METHOD.....	73
5.2	THE DESIGN PROCESS OF THE NEW METHOD	75
5.3	NUMERICAL RESULTS.....	79
5.4	SUMMARY	85
CHAPTER 6	THE EXACT HPL AND HIGHER DIMENSIONAL PROTECTION LEVEL	86

6.1	THE EXACT HPL	87
6.1.1	Probability of the Horizontal Position Error	87
6.1.2	A New Approach To Calculate HPL.....	90
6.1.3	Numerical Results	95
6.2	HIGHER DIMENSIONAL PROTECTION LEVELS	104
6.2.1	The Positional Protection Levels	104
6.2.2	Numerical Results	105
6.3	SUMMARY	108
CHAPTER 7	RAIM WITH A NEW SEPARABILITY MEASURE	110
7.1	A NEW CRITERION TO DESIGN TEST STATISTICS	111
7.2	OPTIMALITY IN FAULT DETECTABILITY AND SEPARABILITY ..	112
7.2.1	Detectability	112
7.2.2	Conditions of Best Detection and Separation	113
7.3	A NEW SEPARABILITY MEASURE	114
7.3.1	The Design Process	114
7.3.2	A Numerical Example.....	118
7.4	EXTENDED RAIM WITH SEPARABILITY	123
7.4.1	Extended Risk Definition.....	123
7.4.2	The Extended Protection Level	124
7.4.3	Numerical Results	125
7.5	SUMMARY	130
CHAPTER 8	CONCLUSIONS AND RECOMMENDATIONS	131
8.1	CONCLUSIONS	132
8.2	RECOMMENDATIONS	134
APPENDIX A:	COMPARING TWO MDB SIZE	136
APPENDIX B:	THE SOLUTION SEPARATION STATISTIC	139
APPENDIX C:	CONSERVATIVENESS OF VPL.....	140
APPENDIX D:	CONSERVATIVENESS OF HPL.....	142
REFERENCES	144

PUBLICATIONS DURING PHD STUDIES.....	153
--------------------------------------	-----

LIST OF TABLES

Table 1: MDB with a global test.....	30
Table 2: the separability measure with a local test	30
Table 3: Existing A-RAIM and R-RAIM Mechanisms	63
Table 4: 99% Availability with A-RAIM and R-RAIM	70
Table 5: R-RAIM Range with Different CT	71
Table 6: R-RAIM Position with Different CT	72
Table 7: VPL with two Iterative Methods of different number of steps	79
Table 8: VPL Computational Time per SV in one epoch	81
Table 9: 99% VPL Availability with multiple hypothesis RAIM.....	85
Table 10: The average computational time of P_{HPE} per SV	90
Table 11: Different HPL values in one epoch with various steps.....	95
Table 12: The average computational time of HPL in one epoch.....	97
Table 13: 99% HPL Availability with multiple hypothesis RAIM.....	103
Table 14: 99% PPL Availability with multiple hypothesis RAIM	108
Table 15: the scalar component of MDB	119
Table 16: correlation coefficient with the v-test statistic	119
Table 17: expectation ratio with the v-test statistic.....	120
Table 18: separability with the w-test statistic.....	120
Table 19: separability with the v-test statistic.....	121
Table 20: external reliability of separability with the w-test statistic	121

Table 21: θ_{ij} with two 4m faults on w-statistics	122
Table 22: θ_{ij} with two 4m faults on v-test statistics.....	122
Table 23: 99% Availability with the extended RAIM and 24 GPS	129

LIST OF FIGURES

Figure 1: the Test Statistic in Parity Space	25
Figure 2: the Effect of Noise on Test Statistics in Parity Space	26
Figure 3: the Fault on Test Statistics in Parity Space.....	26
Figure 4: PSD with a global test	29
Figure 5: PCI with a local test.....	29
Figure 6: Risk Distribution in Multiple Hypothesis RAIM	31
Figure 7: Three VPL Calculation Mechanisms.....	35
Figure 8: Slope Parameters before NioRAIM.....	40
Figure 9: Slope Parameters after Nio-RAIM	41
Figure 10: External Reliability after 20 Iterations with Nio-RAIM.....	41
Figure 11: HPL_{BC} with Nio-RAIM	42
Figure 12: VPL_{BC} with risk distribution optimization method.....	44
Figure 13: R-RAIM Positioning Method	47
Figure 14: R-RAIM Position Domain Method	49
Figure 15: Horizontal Accuracy with Position Domain and Range Domain Methods	53
Figure 16: the Vertical Accuracy with Position Domain and Range Domain Methods	54
Figure 17: R-RAIM with the MHSS Method and the Classic Method.....	55
Figure 18: The geometric factors in R-RAIM VPL	56
Figure 19: the statistical parameters in R-RAIM VPL.....	56

Figure 20: Position Domain R-RAIM MHSS VPL with different CT	58
Figure 21: VDOP with CT 8min.....	58
Figure 22: R-RAIM VPL with a dynamic CT	60
Figure 23: the Number of Visible Satellites.....	61
Figure 24: 99% Availability with the Classic Method.....	67
Figure 25: 99% Availability with the Range R-RAIM Classic Method	67
Figure 26: 99% Availability with the Position R-RAIM Classic Method	68
Figure 27: 99% Availability with the MHSS Method	68
Figure 28: 99% Availability with the Range R-RAIM MHSS Method.....	69
Figure 29: 99% Availability with the Position R-RAIM MHSS Method.....	69
Figure 30: Illustration of the exact VPL	74
Figure 31: an Example of the wrong input VPL in VPL_{MO}	75
Figure 32: VPL as a function of Type II error	76
Figure 33: Integrity Risk as a function of Type II error.....	77
Figure 34: VPL as a function of Bias.....	77
Figure 35: Integrity Risk as a function of Bias	78
Figure 36: VPL_{new} and other VPLs	80
Figure 37: New VPL with Risk Distribution Optimization Method.....	81
Figure 38: 99% Availability with VPL PB, 24GPS.....	82
Figure 39: 99% Availability with VPL BC, 24GPS	82
Figure 40: 99% Availability with New VPL, 24GPS	83
Figure 41: 99% Availability with VPL PB, 27Galileo	83
Figure 42: 99% Availability with VPL BC, 27Galileo	84

Figure 43: 99% Availability with New VPL, 27Galileo	84
Figure 44: P_{HPE} as a function of HPL with different distributions.....	89
Figure 45: Illustration of the search method	90
Figure 46: Type II error and Integrity Risk with given HPL	91
Figure 47: Type II error and HPL with given Integrity Risk	92
Figure 48: The uncertainty in iterative methods with the number of steps.....	94
Figure 49: The iterative methods and the optimization approach for the new HPL	96
Figure 50: the new HPL and other approximated HPLs	98
Figure 51: 99% Availability with HPL_{BC1} , 24 GPS	99
Figure 52: 99% Availability with HPL_{BC2} , 24 GPS	100
Figure 53: 99% Availability with HPL_{PB} , 24 GPS.....	100
Figure 54: 99% Availability with the new HPL, 24 GPS	101
Figure 55: 99% Availability with HPL_{BC1} , 27 Galileo.....	101
Figure 56: 99% Availability with HPL_{BC2} , 27 Galileo.....	102
Figure 57: 99% Availability with HPL_{PB} , 27 Galileo	102
Figure 58: 99% Availability with new HPL, 27 Galileo.....	103
Figure 59: probability of the three dimensional position error	105
Figure 60: the new PPL with other approximated PPLs	106
Figure 61: 99% PPL Availability with PPL_{BC1} , 24GPS.....	107
Figure 62: 99% PPL Availability with PPL_{BC2} , 24GPS.....	107
Figure 63: 99% PPL Availability with new PPL, 24GPS	108
Figure 64: the mechanism to calculate the non-centrality parameter ui	116
Figure 65: θ_{ij} and ui with $\rho_{ij} = 0.5$ and varying k	116

Figure 66: θ_{ij} and u_i with $k_{ij} = 0.5$ and varying ρ_{ij}	117
Figure 67: an example of the Observation Geometry	118
Figure 68: VPL_{BC} with FD and VPL_{BC} with FDE.....	126
Figure 69: HPL_{BC1} with FD and HPL_{BC1} with FDE	126
Figure 70 PPL_{BC1} with FD and PPL_{BC1} with FDE.....	127
Figure 71: 99% VPL Availability with VPL_{BC} Exclusion, 24GPS	128
Figure 72: 99% HPL Availability with HPL_{BC1} Exclusion, 24GPS.....	128
Figure 73: 99% PPL Availability with PPL_{BC1} Exclusion, 24GPS	129

LIST OF ABBREVIATIONS

A-RAIM	Advanced Receiver Autonomous Integrity Monitoring
BLUE	Best Linear Unbiased Estimation
CT	Coasting Time
DOP	Dilution of Precision
FD	Fault Detection
FDE	Fault Detection and Exclusion
GBAS	Ground Based Augmentation Systems
GIC	GNSS Integrity Channel
GPS	Global Positioning System
GLT	Generalized Likelihood Test
GNSS	Global Navigation Satellite System
HAL	Horizontal Alert Limit
HPL	Horizontal Protection Level
ISM	Integrity Support Message
LPV-200	Localizer Performance Vertical 200
WLS	Weighted Least Squares
MDB	Minimal Detectable Bias
MHB	Minimal Hazardous Bias
MHSS	Multiple Hypothesis Solution Separation

MSB	Minimal Separability Bias
NPA	Non Precision Approach
PCI	Probability of Correct Isolation
PL	Protection Level
PPL	Positional Protection Level
PSD	Probability of Successful Detection
RAIM	Receiver Autonomous Integrity Monitoring
R-RAIM	Relative Receiver Autonomous Integrity Monitoring
SBAS	Space Based Augmentation Systems
SPS	Standard Positioning Service
SV	Space Vehicle
TDCP	Time-Differenced Carrier Phase
TOA	Time of Arrival
TTA	Time To Alert
UERE	User Equivalent Range Error
UAV	Unmanned Aerial Vehicle
UMP	Uniformly Most Powerful
URA	User Range Accuracy
URE	User Range Error
VAL	Vertical Alarm Limit
VDOP	Vertical Dilution of Precision
VPL	Vertical Protection Level
WCB	Worst Case Bias

WGS

World Geodetic System

CHAPTER 1 INTRODUCTION

Since the first satellite system Transit was developed for the purpose of navigation in 1964, the satellite navigation has progressed very fast in the following years. The optimal system should be able to determine high accuracy three-dimensional position solutions with global coverage under all weather conditions. Under this context, the development of GPS was put on agenda, became fully operationally and met the criteria in the 1960s. With the acceptance of the positioning ability, the application of GPS was expanded every day, from military to civilian, from aviation to road and ships. For example, Global Positioning System (GPS) has revolutionized the way geodetic measurements are made in traditional surveying, mapping and etc. The new developments include the GPS modernization (Macdonald 2002) and new navigation systems including Galileo, Beidou and GLONASS, which will further improve the navigation performance (GEAS 2010; 2012). In the foreseen future, the increasing number of users will continue to raise the impact of Global Navigation Satellite System (GNSS) positioning on a large scale of the economy. However, with the accuracy more or less guaranteed with current systems, the integrity is of a big issue, which will limit the application of GNSS, especially for those where safety is of paramount importance.

In this chapter, GPS and its positioning mechanism are introduced together with current approaches to deal with the integrity issue. With civil aviation as the major application, the integrity monitoring mechanism is also introduced as the starting point of further investigation.

1.1 Background

The GPS system nominally consists of 24 satellites equally distributed in 6 orbital planes with 11h 58min period of rotation. It is comprised of three segments: space segment,

control segment and user segment. The user receiver operates passively, and it is able to receive GPS data anywhere and anytime. The standard service is able to provide accuracy better than 13m (95%) horizontally and 22m (95%) vertically (GPS SPS 2008). The concept of Time of Arrival (TOA) is used for ranging, where highly accurate atomic clock is used on the satellites and clocks on the user side are of varying qualities. Ranging codes and navigation data are broadcast on frequency L1 (1575.42MHz) and L2 (1227.6MHz). Ranging codes including the coarse/ acquisition (C/A) code and the precision P(Y) code are used to identify each satellite with civilian access to the C/A code only. The navigation data is used to determine the location of the satellite at the time of transmission. The earth-centered earth-fixed World Geodetic System (WGS) 84 is applied in GPS ephemeris calculation as the coordination system. With the time difference of signals travelling between satellite and user measured, the range can be determined, which is then applied in nonlinear equations together with the satellite position computed by the navigation data to solve the three-dimensional user position and the clock offset by linearization and estimation techniques (Kaplan and Hegarty 2005).

The basic GNSS observation is the transmitting time between the satellite and the receiver multiplied by the speed of light. There are two types of GNSS observations: the code observation and the carrier phase observation. The pseudorange (code) is defined as the distance between receiver antenna and satellite antenna including receiver and satellite clock offsets, atmospheric delay and other errors. The phase measurement is in whole carrier phase cycles. The code observations are noisy, while the phase observations are more precise but have unknown integer ambiguities. Under the perfect condition, three different GNSS observations would form a unique interception point for the three unknown parameters in the position solution, but the errors in the observations make the unique interception point impossible. The positioning uncertainty caused by errors is dependent on the type of observations and positioning mode with a simple example of stand-alone positioning analyzed as follows.

An error that has major influence on the result is the clock offset, which is caused by the situation when the user receiver clock is not precisely synchronized with the GNSS clock. The clock offset is commonly compensated treated as another unknown parameter to preserve the accuracy by sacrificing the geometry strength. For the stand-alone GPS, these errors include the satellite clock offset, receiver clock offset, ephemeris error, relativistic effects, Ionospheric delay, Tropospheric delay, receiver noise, multipath and etc., which are assumed to be unbiased Gaussian and referred as User Equivalent Range Error (UERE) (Kaplan and Hegarty 2005). Efforts are made to model these errors, which is used in integrity prediction. A geometry factor is defined as the Dilution of Precision (DOP), which represents the amplification of the standard deviation of the observation error onto the position solution error. Therefore, the total position error is a function of both the pseudorange error (UERE) and the user-satellite geometry (DOP).

1.2 Receiver Autonomous Integrity Monitoring

In addition to the predictable UERE, *anomalies* may occur by the satellite, user or the control segment, such as the clock jump in satellites, the software/ hardware issue in the control segment and etc. (Kaplan and Hegarty 2005), which might result in abrupt large range errors above the operational tolerance. These integrity anomalies are rare, but can be critical for safety sensitive applications. In the future navigation system, more visible satellites and the increased burden of the control segment will not necessarily decrease the probability of anomalies occurring, so safety will continue to be a critical issue.

Therefore, besides providing an accurate position and time solution, a navigation system should also be able to generate a valid and timely alerts to the user when the service should not be used. *Integrity* is defined as the measure of trust that can be placed on the correctness of the information supplied by the system (Plan 2008). Civil aviation imposes several requirements including precision, integrity, continuity of service and availability. Integrity is of one of the crucial ones to be satisfied, since the user travelling at high speeds can deviate from the flight plan very fast with any position anomaly, especially if

GPS is used as a primary navigation system. Three integrity architectures have been developed to provide integrity service for aviation users including Receiver Autonomous Integrity Monitoring (RAIM), Space Based Augmentation System (SBAS) and Ground Based Augmentation System (GBAS) (Annex 10 2006). Both SBAS and GBAS utilize differential techniques based on references to improve the positioning performance and generate corrections for the raw pseudorange observations, clock and ephemeris data, integrity data (e.g. satellite should or should not be used) and etc. SBAS uses geostationary satellite to broadcast differential GPS corrections and integrity data, which is used in LPV-200, APV I or II precision approaches. GBAS is an augmented version of GPS Standard Positioning Service (SPS) with a ground reference station, which is used in CAT III operations.

RAIM is a technique that performs consistency checks in the receiver with redundancy in GNSS observations. It utilizes standalone GNSS without dependence on augmentation systems. The detailed introduction on RAIM can be found in Pervan (1996); Ober (2003); Wang and Kubo (2010). RAIM can be used to provide integrity services in en-route, terminal and non-precision/ precision approach phases of flight. It can be implemented in real time integrity monitoring and for predicting integrity outages with the flight plan. Traditional RAIM techniques (Brown and Chin 1997) are consistent of two major parts: *fault detection and exclusion* (FDE) and *protection level* computation (Wang and Ober 2009).

1.2.1 The Development of RAIM

At the first stage, the function of fault detection with single alternative hypothesis was explored with different ways to utilize the redundancy. The redundancy in Lee (1986) is used to form a comparison between estimated and measured values in two basic domains: the range domain and the position domain, which are proved equivalent; the method of range comparison, the least squares residual and the parity method was also proved

equivalent under a unified theory framework in Brown (1992). At the second stage, the function of fault exclusion with multiple alternative hypotheses was pursued. The maximum likelihood estimation method was used to derive the single fault estimation as the test statistic in Sturza (1988); the range residual using full set or subset measurements was used as test statistic in Parkinson & Axelrad (1988). At the third stage, a comprehensive development of the RAIM algorithm comes into sight based on the previous study of fault detection and exclusion in the context of civil aviation. The requirements of different phases of flight (DO-229) were illustrated as the foundation to derive the final results in Kelly (1998).

RAIM can be categorized by the number of hypothesis including RAIM with single alternative hypothesis in the classic method (Brown and Chin 1998) and RAIM with multiple hypotheses proposed by Pervan et. al (1998). The first one is based on fault detection while the latter one is possible to be expanded for fault exclusion. Other technical differences include: 1) the worst case is derived by a geometry parameter - the slope factor in the single alternative hypothesis test under single fault assumption, while it is decided by the final protection level values for each hypothesis in the multiple hypothesis test; 2) the process of allocating total risk onto each hypothesis with a prior probability of each hypothesis only exists in the multiple hypotheses framework. This process introduces uncertainty but also offers a chance to optimize the integrity result with the multiple hypothesis framework. The major advantage of the multiple hypothesis method is the straightforward relationship between the upper bound of the position error (the protection level) and pre-defined risks compared with the classic RAIM method. However, the correlation among multiple hypotheses adds to the ambiguity in the risk distribution process. The multiple hypothesis RAIM is adopted here and the classic method is adapted into this structure.

The basic idea for RAIM with multiple hypotheses (Pervan et. al 1998) is to assume that the real position value is a sum of position values under each hypothesis with independent

probability densities. The position value under each hypothesis is assumed to be the subset position estimation with faulty measurements being removed. The multiple hypotheses method was further developed as the Multiple Hypothesis Solution Separation (MHSS) method in Blanch et al. (2007); Blanch et al. (2010); Blanch et al. (2012) based on risk definitions more relevant to civil aviation where a local continuity risk was defined to replace the global false alarm in Pervan et. al (1998).

The issue in the MHSS method is the definition of the integrity risk, which is defined with one event: the positioning error is outside an upper bound. But the original and most accepted definition for this risk is “the probability of an undetected event where the actual position error is larger than the upper bound for more than Time to Alert (TTA)” (GEAS 2008) which is based on the intersection of two events: the positioning error is outside an upper bound and no alarm is generated in the statistical test. Without loss of consistence, the original definition is adopted in this thesis.

For the current stage, a new RAIM framework is under development with the promising of the modernized GNSS systems. The possibility of providing more stringent services (e.g. LPV-200) with worldwide performance in the near future is explored by researchers in the GNSS Evolutionary Architecture Study (GEAS) group (GEAS I 2008; GEAS II 2010). New RAIM architectures are designed to take advantage of the promising new infrastructures.

1.2.2 Fault Detection and Exclusion

GNSS, like any other systems, is often subject to faults, which may greatly degrade the system performance. It is crucial to maintain the system reliability, especially for some applications where safety and various liabilities are of great concern. Given sufficient geometry, only by detecting faults in time and excluding them from final solutions can we achieve the required integrity level. *Fault* is defined as a deterministic bias (gross error) in an observation that is caused by the integrity anomalies with size big enough to produce

safety risks. The optimal accuracy is guaranteed with current estimation techniques in absence of faults. When a failure occurs, the optimality is lost and integrity is compromised. There are two ways to deal with the fault: designing a robust estimator to compensate the fault or combining the normal estimation with a procedure to detect and exclude the fault. The latter one is adopted here. FDE includes two distinct parts (Van Graas and Farrell 1993; Lee et al. 1996): *fault detection* and *fault exclusion*, with the detection as a consistency check to decide if there is any fault exists in the system in presence of noise, and if the answer is yes, exclusion of the detected fault follows to decide the location of the fault and then remove it from the full set observations. In the statistical test, a test statistic is compared with a threshold to decide between a null hypothesis and an alternative hypothesis. A common assumption in RAIM and FDE algorithms is that only one satellite is failed.

The development of FDE techniques in the Navigation community is integrated in the development of RAIM during 1980s-1990s. The early stage RAIM algorithms (Lee 1986; Brown 1992) strived only to detect the failed satellites, with various methods proved equivalent. Then a geometric factor was defined to prune the satellite resulting in the worst geometry from the all in view solution (Chin et al. 1992; Van Dyke 1993). The maximum residual method can be used for fault exclusion (Banett and Lewis 1994), which was proved equivalent (Kelly 1998) with the standard parity space method (Sturza 1988; Brenner 1990; Pervan et al. 1996) and the single detection method (Parkinson and Axelrad 1988).

In the Geodesy community, FDE is referred as the outlier test with the context of the classic reliability theory with the purpose to control the effect of faults on final results. Based on the number of alternative hypotheses, the fault test can be divided into two categories: the single alternative hypothesis test with single fault (Baarda 1967; 1968) and two faults (Knight et al. 2010); the multiple alternative hypotheses (Förstner 1983; Li 1986; Yang et al. 2013). The design limitation of the outlier test is the assumption on the

knowledge of the number and location of faults (fault mode), which is impossible to be gained before the test in practice. The performance of fault test in RAIM was analyzed by Hewitson and Wang (2006; 2007), and a new separability test was defined as the distance between two statistics (Wang and Knight 2012) to exclude the faulty satellite. It is acknowledged that Baarda's w-test statistic is equivalent to the maximum residual test if there is no correlation among observations, and the solution separation statistic is recognized as equivalent as well.

In the Control community, a popular method is the Generalized Likelihood Test (GLT) (Daly et al. 1979; Potter and Sunman 1977) designed as the ration of two log likelihoods of hypotheses. Based on the Neyman-Pearson Lemma, it is the most powerful test for a given significance level. GLT has an appealing analytic framework and it can partially solve the exclusion problem, whose test statistic can also be proved equivalent with Baarda's w-test statistic. Two steps are defined: residual generation and decision making. The design of residuals with the concept of robustness in parity space is introduced. The optimal residual should be robust with respect to the random errors and sensitive to faults (Patton et al. 1992; Gertler 1991; Lou et al. 1986). A criterion was proposed (Zhang and Patton 1993) to design the optimally robust parity equation with an expanded version designed by Jin and Zhang (1999), which was proved equivalent with the GLT by Zhang et al. (2005).

1.2.3 Protection Level Computation

The RAIM inputs contain standard deviation of noise, geometry and the required performance for certain navigation service including the maximum allowed *probability of a false alarm* (P_{FA}), *probability of a missed detection* (P_{MD}), *alert limit* and TTA. The output is the protection level, e.g. the Vertical Protection Level (VPL) and Horizontal Protection Level (HPL), as an upper bound centered at the real position that is able to ensure the position solution is contained in this bound with given P_{FA} and P_{MD} (Kaplan

and Hegarty 2005). The computed PL is then compared with the given alert limit to decide if the service is available. In some case (GEAS 2008; 2010), *integrity risk* is defined to replace P_{FA} and P_{MD} , which is used in Section 2.3. Therefore, PL is a statistical error bound to guarantee *the probability of position error* exceeding this bound is within the required integrity risk. If the computed PL is larger than the given alert limit, an alert within required TTA should be generated by the system. This definition is an adaption based on the standard one (Annex 10 2006) (DO-229 2006).

Current algorithms to compute the VPL and the HPL are introduced as follows. When calculating the VPL with the conventional algorithms, there are mainly three options: *the classic method* (Brown and Chin 1998), *the Stanford method* (Walter and Enge 1995) and *the solution separation method* (Brenner 1996). Different sizes of the unknown bias when calculation VPL were recognized in Ober (2003) including Minimal Detectable Bias (MDB), Minimal Hazardous Bias (MHB) and Worst Case Bias (WCB). MDB is used in the classic method, and WCB as the bias size between MHB and MDB is used to derive the exact value of VPL (Milner and Ochieng 2011; Milner and Ochieng 2010a). Also, the solution separation method is adapted in a multiple hypothesis structure as the MHSS method (Pervan et al. 1998; Blanch et al. 2007; 2010). The advantages of the multiple hypothesis structure include a) the ability to accommodate a complete set of failure modes; b) the flexibility of risk allocation onto each hypothesis; c) flexibility to define the prior probability of any fault mode according to the environment. Similarly, various methods are also proposed to compute HPL (Brown and Chin 1998; Walter and Enge 1995; A-RAIM report 2012).

1.3 Future Integrity Monitoring Architectures

With the modernized GPS and GLONASS, as well as the new GNSS systems (Compass, GALILEO) underway, the number of satellites is to be increased and the multiple frequency signals are available. With double civilian frequencies being transmitted, the ionosphere error can be measured, and therefore removed from the error source which

will improve the precision. It is therefore reasonable to pursue the possibility of using RAIM in civil aviation for more stringent procedures, such as LPV-200 for vertical guidance on a global scale. This possibility was explored by US Federal Aviation Administration under the panel of GEAS, which has attracted attention of researchers thereafter.

Currently, there are three technologies that can observe the faulty situation for civil aviation including RAIM, GBAS and SBAS. The integrity monitoring task is designed in the aircraft receiver, ground station and satellites separately. The tendency in the near future is to put the integrity monitoring responsibility in the satellite itself with dual frequency diversity, new constellation, build-in integrity function in the constellation, etc.

Within the GEAS panel, the design of the integrity monitoring architecture, all the integrity information is centralized as the Integrity Support Message (ISM), which contains the error model (fault rate, error distribution etc.) information from all kinds of augmentation and monitoring systems that needs to be provided to the user. Together with the GNSS measurements, it is possible to output the integrity monitoring results as the indicator of service availability.

Two major architectures have been identified as feasible choices to meet the LPV-200 requirement: A-RAIM and R-RAIM. A-RAIM is the preferred choice and R-RAIM is only used when A-RAIM is unavailable. The major difference between these two architectures is in the positioning method such that only the code measurements are used in A-RAIM, and both code and Time-Differenced Carrier Phase (TDCP) measurements are used in R-RAIM to ensure higher precision without the necessity of integer ambiguity resolution. Examples of TDCP applications can be found in Serrano et al. (2004a; 2004b); van Grass and Soloviev (2004); Ding and Wang (2011). R-RAIM is further divided by the location where observations from two time epochs

are combined together as the range domain R-RAIM and the position domain R-RAIM, which results in different errors and projection matrices. With advantages in R-RAIM, the trade-off is more complicated errors and projection matrices, and therefore a more complicated process to transfer these errors with given risks in RAIM.

To make the service available, the following requirements must be met: VPL, Effective Monitoring Threshold EMT and the vertical positioning accuracy. With VPL as the most difficulty to satisfy requirement, the algorithm to calculate VPL results is of major interest. By the number of alternative hypotheses, there are two types of RAIM algorithms for both A-RAIM and R-RAIM: the classic method with single alternative hypothesis (Brown and Chin 1998), and the Multiple Hypothesis Solution Separation (MHSS) method (Pervan et al. 1998; Blanch et al. 2007; 2008; 2010; 2012a). A brief comparison of these two RAIM algorithms within the A-RAIM context is provided in Blanch et al. (2008).

In the latest A-RAIM report (2012) from the joint EU-US study, further details are provided on the performance requirements, user algorithm and fault modes, making the A-RAIM design more mature. Future works were recognized to be on the following aspects: evaluation of RAIM algorithms with the ISM messages, validation with GNSS observations, further development of the GNSS fault characterization, allocation and migrations of fault modes, definition of ISM requirements and etc.

1.4 Critical Issues

a) The A-RAIM structure for future integrity monitoring

As the preliminary design for future integrity monitoring architecture, uncertainties exist in A-RAIM, which need further investigation and validation. For the structure design, there are many technical details need to be clearly defined, such as the ISM; the distribution of the integrity monitoring burden on space systems, ground systems and aircraft; the modeling of errors for future GNSS and augmentation systems; the FDE

procedure design including with the accommodation of the constellation fault; the distribution of the total risk onto each fault mode; the optimization method to improve integrity performance, and etc. (GEAS 2008; 2010; Blanch et al. 2012b).

b) Conservativeness of current approximated protection levels

There are two parts involving heavy computational burden to obtain the exact PL with given integrity risk: the probability of position error and the determination of the worst case to accommodate all possible bias values. To simplify the calculation, two approximated distributions of the horizontal position error were used in the conventional methods including the normal approximation (Lee 1995) and the chi-squared approximation (Ober 1997). The first one has the disadvantage of underestimating the probability in some cases and the latter one is an overestimate (Ober 1997). Approximations were also used on the second part to fasten the process. Without a search for the worst case, specific formulas were given in the conventional methods (Brown and Chin 1998; Walter and Enge 1995). These approximations are fast, but they are designed to be conservative with higher protection level than the exact one. The exact PL value can achieve higher service availability, which is pursued by computing these two parts without approximation but at the same time fast enough to be implemented in real time applications.

These current algorithms (Brown and Chin 1998; Walter and Enge 1995) to calculate PLs are supposed to be conservative, so that they are safe to be used. But there is no specific proof of the conservativeness in current RAIM literatures. With the theoretical exact PL obtained, conservativeness of current methods is analyzed by comparing it with the exact value with numerical examples. To be more convincing, the theoretical proof is provided without loss of generality.

c) Higher dimensional PL

The PL is generally used in the form of the two-dimensional HPL or the one-dimensional VPL. In this way, the three-dimensional position is separated into the horizontal domain and the vertical domain, and the positional bound is separated as the horizontal bound within a two-dimensional ellipse and a vertical bound along the one-dimensional line. Also, the total integrity risk needs to be divided into the horizontal part and the vertical part. But in some applications, e.g. the Unmanned Aerial Vehicle (UAV) positioning, the position error might need to be bounded by a three-dimensional bound, which is named as the Positional Protection Level (PPL) in this thesis. Consequently, the calculation algorithms for VPL and HPL need to be generalized into three-dimensional and multiple dimensional PL.

d) Optimality of test statistics and its influence on RAIM

With existing test statistics designed from different perspectives, the reason to choose certain statistic is not justified yet. Therefore, the quality measures of detectability and separability are used to derive the criterion for optimal test statistics and its influence on RAIM, where separability is defined as the quality measure of the performance to distinguish between two alternative hypotheses in fault exclusion.

e) The fault separability issue

The current measure for separability in fault exclusion is the correlation coefficient. But it is observed that this measure is not general enough, which is only applicable to the case when observations are not correlated. Therefore, a more general measure is desirable.

1.5 Contributions

- a) Current RAIM algorithms are applied and compared in A-RAIM with comprehensive numerical results for worldwide availability distribution.

- b) A new approach to compute the exact VPL within required efficiency is proposed. In this method, a criterion is defined to search the worst case and solved by an interior point algorithm to optimize the calculation, which has higher precision and computational efficiency than the iterative search method used before.
- c) A new efficient approach to compute the exact HPL is proposed. First, current methods with approximations in both the probability of horizontal position error and the search for the worst case are recognized. The approaches to compute the exact value of both the probability and the worst case are proposed within required precision and computational efficiency.
- d) Conclusions on conservativeness of current RAIM algorithms are provided for both HPL and VPL. It is found that the method in Brown and Chin (1998) is conservative for both HPL and VPL with theoretical proof. The method in Walter and Enge (1995) is not safe for both HPL and VPL. The method in A-RAIM report (2012) is conservative for HPL and the solution separation method in Pervan et al. (1998) and Blanch et al. (2010) is conservative for VPL.
- e) RAIM is expanded with higher dimensional PL. PPL as the three dimensional PL is established based on the approach to calculate the exact HPL. Higher dimensional PL is easy to be derived based on PPL.
- f) Conclusions of the test statistics' optimality on detectability and separability are made with theoretical proof on the minimum MDB with best detectability.
- g) A new sparability measure in the range domain is proposed with more generality than the old measure.
- h) RAIM is expanded with the risk and the non-centrality parameter obtained based on the new separability measure.

1.6 Thesis Outline

This thesis consists of eight chapters and the organization of the following chapters is outlined as follows:

In Chapter 2, the basic RAIM technique is introduced. The basic model is defined followed by the least squares estimation, least squares residuals and parity vectors. FDE is regarded as a component of RAIM, which is illustrated by introducing the global test and local test with different test statistics, the robustness issue and the reliability theory. The RAIM technique is then followed by first defining the requirements and integrity risks, and then providing current algorithms to compute VPL and HPL, together with two current integrity optimization methods.

In Chapter 3, one of the future integrity monitoring structure R-RAIM is studied with two positioning methods including the range domain method and the position domain method, and two RAIM algorithms including the classic method and the MHSS method. The two positioning methods are shown to have very close precision, but the RAIM results are different with different projection matrices for errors. The position domain method with the MHSS RAIM algorithm is used as an example to further analyze the details. The two influencing factors on the final VPL results including the geometric factor and the statistical one are studied, followed by the analyze on the influence of different Coasting Time (CT)s on final results with a new dynamic CT tested.

In Chapter 4, the other structure for the future integrity monitoring A-RAIM is studied with two RAIM algorithms including the classic method and the MHSS method. A-RAIM results are compared with the R-RAIM results with 99.9% service availability worldwide. The conclusions are obtained with precision and integrity results influenced by different positioning methods, RAIM algorithms and integrity monitoring structures.

In Chapter 5, a new approach to calculate the exact VPL is proposed to generate results with a predefined accuracy and improved computational efficiency. The disadvantages in

the previous iterative method are analyzed followed by a new faster iterative method. An optimization method is then applied and results show that the accuracy is within control and it is much faster than other two iterative methods. With the exact VPL, the service availability worldwide is used to quantify the improvements. Also, the conservativeness of current methods is analyzed with both theoretical proof and numerical results.

In Chapter 6, a similar approach is applied for HPL computation. The difference is that the distribution of the two-dimensional positional error is more complicated than the single dimensional one in VPL. Therefore, current approximation methods and a latest method are studied to obtain results within required accuracy and computational efficiency. Then the approach to obtain the worst case bias used in VPL computation is applied for HPL. Results are used to show different computational efficiency and accuracy with various methods. The conservativeness of current methods is analyzed with both theoretical proof and numerical results. Also, this method is generalized for multiple dimensional protection level with an example of three-dimensional PPL provided.

In Chapter 7, the performance of FDE in detectability and separability is generalized in the form of theorems and proofs. A new criterion is proposed for the separability between two alternative hypotheses to fill in the gap of current reliability measures for fault exclusion. Then RAIM is generalized with the new separability measure with given definition of the Type III error.

In Chapter 8, conclusions and suggestions for future study are provided based on this thesis.

CHAPTER 2 RAIM AND FAULT DETECTION TECHNIQUES

There are several requirements to be met in civil aviation for a navigation service to be available including precision, availability, integrity and continuity. Integrity is defined as the capability of providing timely warnings to users when the navigation solution is hazardous, which is used to guarantee the safety of different services in civil aviation. The integrity of the GNSS solutions is determined by performing integrity monitoring inside the aircraft receiver without any dependent on external augmentation systems. Redundancy in the available observations is taken advantage of for consistency check and a boundary is calculated with given integrity risk to indicate if the solution is outside certain safety level or not. Conventional RAIM algorithms follow three steps: fault detection, exclusion of the faulty satellite and protection level computation. At least five satellites are needed to provide integrity with possible faults detected. Six or more satellites enable the receiver to detect and perform the exclusion. The conventional RAIM technique is introduced here together with FDE for current constellations as the basis for further introduction on future integrity monitoring architectures.

2.1 The System Model

After linearization, the GNSS observation is expressed with a functional model and a stochastic model,

$$y = Ax + \varepsilon + b; D(\varepsilon) = Q_y \quad (2.1)$$

where:

y is the observation vector whose elements are the difference between the measured ones and predicted ones with dimension $m \times 1$ and m is the number of observations.

x is the unknown position vector with elements as the incremental deviations from the nominal state during linearization. The dimension is $n \times 1$ and $n=4$ is used for GPS positioning with the first three elements as the east, north and up position components and receiver clock bias as the last one.

A is the design matrix with the first three columns as the user-space vehicle (SV) line of sight unit vector and the fourth column is a vector of ones.

ε is the random error in observations, which is assumed to be of centred Gaussian distribution.

Q_y is the covariance matrix of the random error.

b is the deterministic error in observations.

With Q_y^{-1} as the weight matrix, the Weighted Least Squares (WLS) estimator is the Best Linear Unbiased Estimation (BLUE) for the navigation solution estimation. The WLS criterion is the minimization of the sum of squares of the weighted residuals,

$$\min_x \{(y - A\hat{x})^T Q_y^{-1} (y - A\hat{x})\} \quad (2.2)$$

The estimated position solution \hat{x} is,

$$\hat{x} = (A^T Q_y^{-1} A)^{-1} A^T Q_y^{-1} y = Sy \quad (2.3)$$

where $\hat{x} = [\hat{x}_E \ \hat{x}_N \ \hat{x}_U \ \hat{x}_T]^T$ with \hat{x}_E , \hat{x}_N , \hat{x}_U as the east north and up estimation, and \hat{x}_T as the clock estimation. $S = [S_E \ S_N \ S_U \ S_T]^T$ is the corresponding solution estimation matrix.

The position error is the difference between the estimated value and the true value, which

also contains four elements with \tilde{x}_E , \tilde{x}_N , \tilde{x}_U as the east north and up error and \tilde{x}_T as the clock error,

$$\tilde{x} = \hat{x} - x = S\nabla y \quad (2.4)$$

With Q_y^{-1} as the weight matrix, the variance of the position error is minimal (Teunissen 2004). The standard deviation of the position error $\sigma_x = [\sigma_E \ \sigma_N \ \sigma_U \ \sigma_T]^T$ is the square root of the diagonal elements of the covariance matrix,

$$Q_x = (A^T Q_y^{-1} A)^{-1} \quad (2.5)$$

RAIM is based on consistency check and the least squares residual is commonly used as a measure of consistency, which is defined as the difference between the real observations and the estimated ones,

$$v = y - A\hat{x} = [I - A(A^T Q_y^{-1} A)^{-1} A^T]y \quad (2.6)$$

The covariance of the least squares residual is,

$$Q_v = Q_y - A(A^T Q_y^{-1} A)^{-1} A^T \quad (2.7)$$

Since the range residual is based on estimation, it is required that there are at least four observations. The parity vector p can be formed by a transformation matrix P , which is more general than the residuals as the measure of consistency without constraint of the four observations (Lou et al. 1986),

$$p = Py \text{ subject to } PA = 0 \quad (2.8)$$

To establish a valid parity vector for consistency check, it is required that the parity space is the orthogonal complement of the observation space to completely decouple the unknown vector x . There are various choices for the parity matrix P . A popular choice is the standard parity matrix P_s (Potter and Sunman 1977), which satisfies two conditions

at the same time: $P_s P_s^T = I_{m-n}$ and $P_s A = 0$.

In this way, the matrix in least squares residuals $I - A(A^T Q_y^{-1} A)^{-1} A^T$ can be regarded as a special case of P . The connection between the least squares residuals and parity vectors is expressed by the following equation,

$$P^T (P Q_y P^T)^{-1} P = Q_y^{-1} Q_v Q_y^{-1} \quad (2.9)$$

The proof is as follows: According to the Cholesky decomposition, if Q_y is symmetric and positive definite and has real entries, then it can be decomposed as,

$$Q_y = q q^T \quad (2.10)$$

where q is a lower triangular matrix with strictly positive diagonal entries.

The orthogonal condition can be expressed as,

$$P q q^{-1} A = 0 \quad (2.11)$$

Therefore, the following equation can derived,

$$q^T P^T (P q q^T P^T)^{-1} P q = I - q^{-1} A [A^T (q^{-1})^T q^{-1} A]^{-1} A^T (q^{-1})^T \quad (2.12)$$

Multiply q on the left side and q^{-1} on the right side of the parameters on both sides of the equation, and left multiply Q_y^{-1} on both sides of the equation, the following equation is derived,

$$P^T (P Q_y P^T)^{-1} P = Q_y^{-1} - Q_y^{-1} A (A^T Q_y^{-1} A)^{-1} A^T Q_y^{-1} \quad (2.13)$$

With equation (2.7), the conclusion of eq. (2.9) is derived.

2.2 Fault Detection and Exclusion

Least squares estimation is optimal under the no fault assumption, but the estimation would deviate from the true value greatly if there is any fault. FDE is then needed to reduce the effect of faults on final solutions. Fault Detection (FD) requires at least five visible satellites to detect the presence of an unacceptable large position error. An alarm is sent to the cockpit if a failure is detected to warn the pilot that GPS should not be used for navigation. If it is required that not only the failed satellite is detected but also excluded from the observations for generating navigation solutions, the RAIM should be extended with the fault exclusion operation, which requires at least six visible satellites.

The FDE procedure is based on statistical hypothesis testing where the null hypothesis is tested against the alternative hypothesis by comparing with a pre-defined level of significance (P_{FA}), which is the probability of incorrectly rejecting the null hypothesis, also known as the probability of false alarm. The power of the test ($1-P_{MD}$) is the probability of correctly rejecting the null hypothesis with P_{MD} known as the probability of missed detection. Normally the null hypothesis indicates there is no fault, while the alternative one is used for the faulty situation. P_{FA} and P_{MD} are also referred as Type I error and Type II error respectively. With the power of test as a performance measure of the test, GLT is Uniformly Most Powerful (UMP) with the Neyman-Pearson lemma.

In the GLT (Daly et al. 1979; Potter and Sunman 1977), a chi-squared statistic is used to decide if there is any fault in the system. If the fault is detected, the exclusion of the fault should be considered, where two statistics with normal distribution are used. These two statistics are expressed with parity vectors without consideration of the covariance matrix (Patton et al. 2000),

$$T_{FD} = p^T (PP^T)^{-1} p \quad (2.14)$$

$$T_{FEi} = \frac{e_i^T P^T (PP^T)^{-1} P y}{\sqrt{e_i^T P^T (PP^T)^{-1} P e_i}} \quad (2.15)$$

where $e_i \in R^{m \times 1}$ is a zero vector with an one indicating the location of the fault.

There are no statistical characteristics described in the GLT test statistics. To generalize the test with random error of any normal distribution, further generalization is pursued in the following parts with a division of global test and local test. In the global test, there is a single alternative hypothesis, while in the local test, there are multiple alternative hypotheses. The procedure for detection is simple with one decision to make between the null hypothesis and the single alternative hypothesis. With all the redundancy information used in the test statistics in a global test, it is able to decide if there is any fault exist in the whole observations. However, since the statistic is projected on the direction of the i th fault in a local test for a single alternative hypothesis, a single detection test is not able to decide if there is fault in the whole observations, and only if there is fault in the i th observation can be decided. With these characteristics, a local test can be used in the exclusion procedure, which is more complicated and uncertain without prior knowledge of the number and location of faults than the detection test. It is commonly assumed that there is only one fault existing in the system. In GLT, the maximum test statistics among all alternative hypotheses is the one that is most likely to have a failure. A more comprehensive statistical procedure is also defined for multiple alternative hypotheses (Förstner 1983; Li 1987).

2.2.1 The Global Test

The chi-squared statistic with $m-n$ degree of freedom is (Brown and Chin 1998),

$$C = v^T Q_y^{-1} v \sim \chi_{m-n}^2 \quad (2.16)$$

In the statistical test, test statistic C is compared the threshold T to decide which of the following hypotheses to accept

$$H_0: E(C) = 0; H_a: E(C) = \delta \quad (2.17)$$

where H_0 is the fault free hypothesis and H_a is the faulty hypothesis indicating there is fault existing in the observations; δ is the non-centrality parameter of C .

Consequently, Type I error α and Type II error β with the global test are,

$$\alpha = P\{C > T|H_0\} \quad (2.18)$$

$$\beta = P\{C < T|H_a\} \quad (2.19)$$

2.2.2 The Local Test

The fault mode for H_i is defined as follows: the direction of the fault vector is $e_i \in R^{m \times 1}$ as a zero vector with the element of one indicating the location of the fault; the magnitude of the fault is ∇S_i .

Two commonly used test statistics for the data-snooping test are the w-test statistic (Baarda 1967; 1968) based on the mean shift model, and the studentized residual (Kelly 1998), which is referred as the v-test statistic here. The w-test statistic under H_i is (Baarda 1967; 1968),

$$w_i = \frac{\nabla \hat{S}_i}{\sqrt{Q_{\nabla \hat{S}_i}}} = \frac{e_i^T Q_y^{-1} v}{\sqrt{e_i^T Q_y^{-1} Q_v Q_y^{-1} e_i}} \quad (2.20)$$

where the estimation of the fault term $\nabla \hat{S}_i$ and its covariance $Q_{\nabla \hat{S}_i}$ are,

$$\nabla \hat{S}_i = (e_i^T Q_y^{-1} Q_v Q_y^{-1} e_i)^{-1} e_i^T Q_y^{-1} v \quad (2.21)$$

$$Q_{\nabla \hat{S}_i} = (e_i^T Q_y^{-1} Q_v Q_y^{-1} e_i)^{-1} \quad (2.22)$$

The v-test statistic under H_i is (Kelly 1998),

$$v_i = \frac{e_i^T v}{\sqrt{e_i^T Q_v e_i}} \quad (2.23)$$

The test statistic used in A-RAIM (GEAS 2010) is referred as the vertical solution separation statistic here. The subset solution estimation \hat{x}_i is obtained with the i^{th} observation removed from the full set. The vertical subset position estimation \hat{x}_{Ui} is the third element in \hat{x}_i . With the vertical solution separation as $\hat{x}_U - \hat{x}_{Ui}$ and its standard deviation as σ_{Uss} , the standardized solution separation is used as the test statistic for failure mode i,

$$ss_i = \frac{\hat{x}_U - \hat{x}_{Ui}}{\sigma_{Uss}} \quad (2.24)$$

The relationship between the solution separation statistic and other test statistics is not clearly defined (Young and McGraw 2003). Assuming there is an unknown bias in the measurements, \hat{x}_{Ui} was proved to be equivalent with the unbiased vertical position estimation (Deggelen and Brown 1994). Further proof based on this conclusion is provided in the Appendix B with the conclusion that the vertical solution separation test statistics is equivalent with the w-test statistic when all the measurements are uncorrelated, which is the case for GNSS RAIM.

In the hypothetical test, test statistic ts_i (w_i, v_i, ss_i) is compared the threshold T_i to decide which hypothesis to accept

$$H_0: E(ts_i) = 0; H_i: E(ts_i) = \delta_i \quad (2.25)$$

where H_i hypothesizes a single fault in observation i and H_0 hypothesize that there is no fault in observation i. δ_i is the non-centrality parameter of ts_i .

Therefore, Type I error α_i and Type II error β_i with the local test are,

$$\alpha_i = P\{|ts_i| > T_i | H_{0i}\} \quad (2.26)$$

$$\beta_i = P\{|ts_i| < T_i | H_i\} \quad (2.27)$$

With the magnitude of the parity vector as the test statistic for detecting faults (Kaplan and Hegarty 2006), these two statistics can also be expressed with the parity matrix. The

parity matrix in the w-test statistic is $P_w = P_s^T (P_s Q_y P_s^T)^{-1} P_s$, and in the v-test statistic it is $Q_y P_w$. There are also other examples of parity matrix, like $P_s^T (P_s W_i Q_y W_i P_s^T)^{-1} P_s$ with W_i as a unit matrix with the i^{th} diagonal element as zero. If and only if the observations are of the same variance without correlation, this statistic is equivalent with others. With the notion that different choices of parity matrix produce different test statistics, parity space is regarded as a general framework for the design of test statistics here. The geometric illustration of the test statistic in parity space is shown in Figure 1.

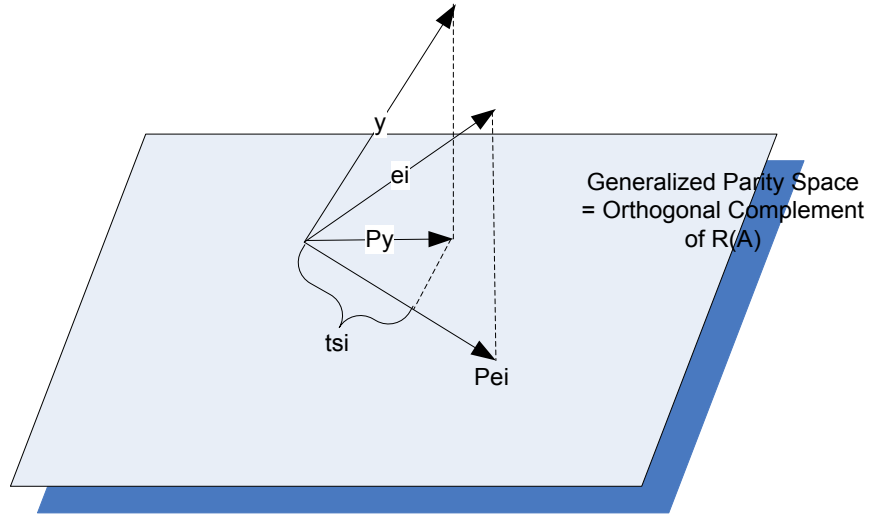


Figure 1: the Test Statistic in Parity Space

Based on the mechanism of statistical tests, a good test statistic should be easily distinguishable among different hypotheses to optimize the performance, and therefore, the effect of fault on test statistics should be strengthened and the uncertainty induced by other errors should be repressed. This is defined as the robustness issue in generation of test statistics. Under the mechanism of hypothetical test, the basic principle for generation of test statistics is the maximization of the effect of any fault and minimization of the effect of other errors that may disturb the performance in a bad way as shown in Figure 2 and Figure 3.

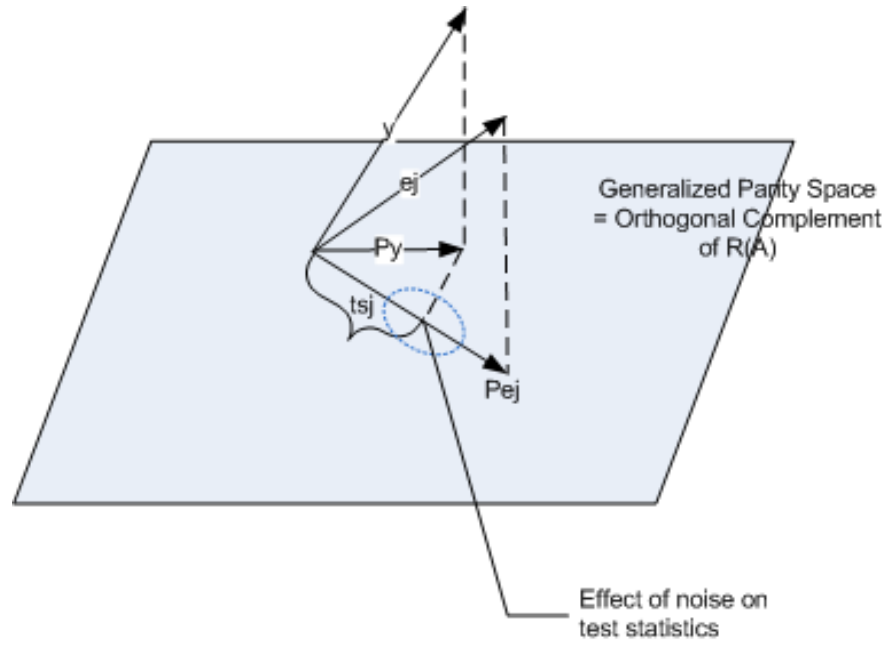


Figure 2: the Effect of Noise on Test Statistics in Parity Space

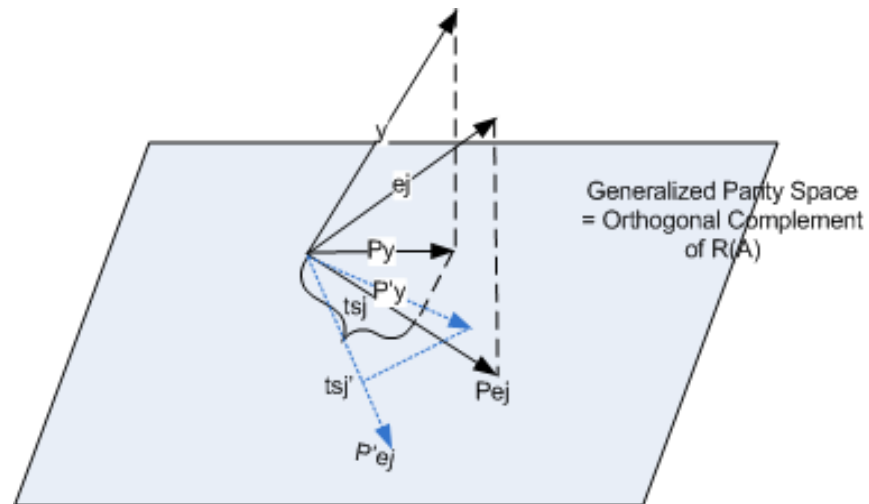


Figure 3: the Fault on Test Statistics in Parity Space

2.2.3 The Reliability Measures

With the test procedure defined, the performance of the test in terms of the power of detecting and excluding the fault also needs to be known due to the presence of random noise. Both the Type I error and the Type II error are used to quantify the reliability level of the navigation solution with quality measures such as internal reliability and external reliability in Geodesy. The internal reliability is also known as MDB, which is the fault

magnitude that can be detected with given significance level and the power of the test (Baarda 1968; Förstner 1985; Teunissen 1990; Wang and Chen 1994a; Wang and Chen 1994b; Schaffrin 1997; Li and Yuan 2002). MDB is derived by the non-centrality parameter of the test statistic with given Type I error and Type II error. Therefore, MDB based on the chi-squared statistic is,

$$MDB_{ci} = \sqrt{\frac{\delta}{e_i^T Q_y^{-1} Q_v Q_y^{-1} e_i}} \quad (2.28)$$

MDB based on the the v-test statistic is,

$$MDB_{vi} = \frac{\delta_i \sqrt{e_i^T Q_v e_i}}{|e_i^T Q_v Q_y^{-1} e_i|} \quad (2.29)$$

MDB based on the w-test statistic is,

$$MDB_{wi} = \frac{\delta_i}{\sqrt{e_i^T Q_y^{-1} Q_v Q_y^{-1} e_i}} \quad (2.30)$$

It can be proved that $MDB_{vi} \geq MDB_{wi}$, which can be found in Appendix A. Also, it is concluded that if and only if there is no correlation among observations, they are equal with each other.

The external reliability is used to assess the effect of MDB on the position error (Baarda 1967; Prószyński 1994; Teunissen 2006) with an example of the w-test expressed as,

$$ER_i = \frac{|Se_i| \delta_i}{\sqrt{e_i^T Q_y^{-1} Q_v Q_y^{-1} e_i}} \quad (2.31)$$

Also, the test statistics and reliability measures were generalized with multiple outliers (Knight et al. 2010).

Separability is a quality measure for the performance of fault exclusion. It conveys the capability of the test to distinguish the faulty observation with the correlation among all test statistics. The separability was studied in previous research (Hewitson and Wang

2007; Zhao 1990; Patton et al. 2000) with the correlation coefficient between two test statistics ρ_{ij} as a commonly accepted measure. An equivalent measure was used as angle between two parity vectors in a geometric term in the parity space (Patton et al. 2000),

$$\sin \alpha_{ij} = 1 - \rho_{ij} \quad (2.32)$$

As explained in Patton et al. (2000), the best case is when two parity vectors are orthogonal with each other with $\sin \alpha_{ij} = 1$, and the worst case is when the angle between two parity vectors is zero, which means it is impossible to separate these two faults and in this case $\sin \alpha_{ij} = 0$.

2.2.4 A Numerical Example

A single epoch example is shown below with the design matrix given,

$$A = \begin{bmatrix} -0.7728 & -0.2978 & -0.5605 & 1.000 \\ 0.7780 & -0.5562 & -0.2922 & 1.000 \\ 0.8738 & -0.4086 & -0.4846 & 1.000 \\ -0.4216 & 0.6079 & -0.6728 & 1.000 \\ 0.3766 & -0.4249 & -0.8232 & 1.000 \\ -0.3415 & -0.3625 & -0.8671 & 1.000 \end{bmatrix}$$

The random error is assumed to be of the standard normal distribution with unit variance and no correlation. Type I error and Type II error are given as 10^{-5} and 10^{-3} separately. With the two conditions satisfied, the standard parity space matrix is,

$$P_s = \begin{bmatrix} 0.0208 & 0.3495 & -0.6448 & 0.0742 & 0.5671 & -0.3668 \\ 0.4184 & 0.4723 & -0.3773 & 0.0824 & -0.3398 & 0.5808 \end{bmatrix}$$

The global test is used for FD and the local test for fault exclusion. This test was based on 10,000 Monte Carlo experiments with simulated random error and determinant faults. With different fault sizes from 0m to 200m on each satellite, results of Probability of

Successful Detection (PSD) and Probability of Correct Isolation (PCI) are provided below.

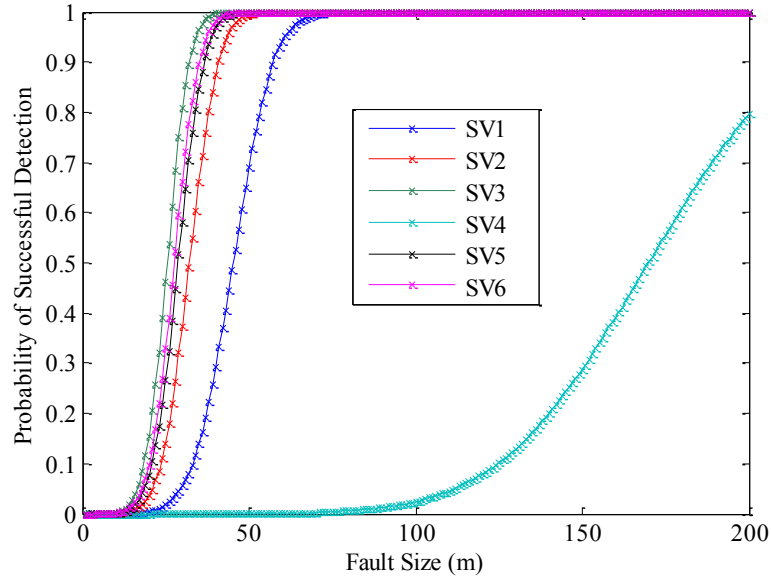


Figure 4: PSD with a global test

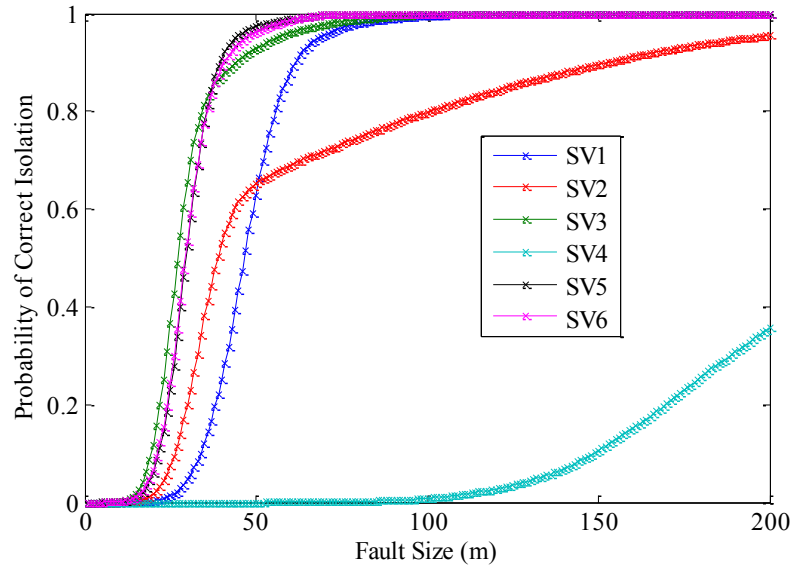


Figure 5: PCI with a local test

Based on the results in Figure 4, if there is a fault less than 200m on satellite 4, it is very hard to detect it, while other satellites have much better performance with fault size close

to 50m easily detected. From the results of Figure 5, the fault on satellite 2 and satellite 4 is difficult to be excluded even when the fault is growing big, while all others are easily excluded when fault size is larger than 50m.

The performance in the above two figures can be explained by the reliability measures including the MDB and $\sin \alpha_{ij}$ with results shown in the tables below.

Table 1: MDB with a global test

	1	2	3	4	5	6
MDB(m)	43.4142	22.0696	13.6508	619.6476	17.4317	16.1460

Table 2: the separability measure with a local test

$\sin \alpha_{ij}$	1	2	3	4	5	6
1	0	0.6340	0.8871	0.7052	0.8312	0.4913
2	0.6340	0	0.3934	0.0959	0.9953	0.9322
3	0.8871	0.3934	0	0.3034	0.8768	0.9994
4	0.7052	0.0959	0.3034	0	0.9814	0.9626
5	0.8312	0.9953	0.8768	0.8768	0	0.4508
6	0.4913	0.9322	0.9994	0.9994	0.4508	0

With big MDB size on SV 4 in Table 1, the corresponding detection performance is also poor as shown in Figure 4. Also, a too small $\sin \alpha_{ij}$ value 0.0959 in Table 2 indicates small angle between SV4 and SV2, and therefore more difficulties to separate them,

which explains the poor performance of exclusion with these two SVs in Figure 5.

2.3 Receiver Autonomous Integrity Monitoring Schemes

The inputs to RAIM include the covariance of the observation noise, the user-satellite geometry and the required risks. The snapshot RAIM algorithm in support of RTCA SC-159 (Lee et al. 1996) to generate HPL for Non-Precision Approach (NPA) and the A-RAIM structure used to generate VPL for LPV-200 are introduced in this section.

The multiple hypothesis structure in A-RAIM is adopted here to calculate both HPL and VPL, and therefore the local test is used. Two risks are defined in this structure including the integrity risk and the continuity risk. The continuity risk is defined as the probability of any alarm generated during an approach. Therefore, the continuity risk under fault free hypothesis can be used to derive P_{FA} . The integrity risk is the probability of the navigation system failing to protect against the hazardous situation within the TTA, which is caused by faults producing undetected navigation errors greater than a VAL (GEAS 2008; 2010).

With the multiple hypothesis structure (Pervan et al. 1998; Blanch et al. 2010) adopted for VPL and HPL computation in the following sections, the first step is to distribute the total risk onto each different fault modes as shown in Figure 6.

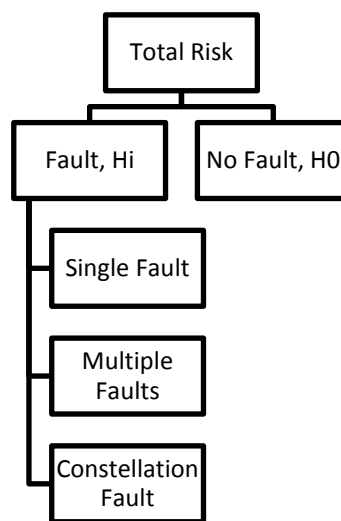


Figure 6: Risk Distribution in Multiple Hypothesis RAIM

The integrity risk for the single failure mode IR is distributed onto each hypothesis as IR_i with the local test as,

$$IR = \sum_{i=0}^m IR_i \quad (2.33)$$

For the global test, IR is divided by the fault free mode IR_0 and faulty mode IR_a ,

$$IR = IR_0 + IR_a \quad (2.34)$$

Then, each local risk is divided into the horizontal one and vertical one,

$$IR_i = IR_{Hi} + IR_{Vi} \quad (2.35)$$

With the vertical one as an example, the vertical integrity risk under failure mode i IR_{Vi} is defined as follows, where P_{H_i} is the prior probability of the failure mode i , (GEAS 2008),

$$IR_{Vi} = P\{|\tilde{x}_U| > VPL \cap |ts_i| < T_i | H_i\} P_{H_i} \quad (2.36)$$

With the un-correlation among measurements in GNSS A-RAIM and the multivariate normal distribution of the position error and test statistic, the independence of these two is concluded (Milner and Ochieng 2010b). Therefore, the integrity risk can also be expressed as,

$$IR_{Vi} = P\{|\tilde{x}_U| > VPL | H_i\} P\{|ts_i| < T_i | H_i\} P_{H_i} \quad (2.37)$$

where the integrity risk IR_i is a function of the probability of the vertical position error $P_{VPE} = P\{|\tilde{x}_U| > VPL | H_i\}$, the prior probability of H_i hypothesis P_{H_i} and β_i .

Similarly, the horizontal one is defined as,

$$IR_{Hi} = P\{|\tilde{x}_H| > HPL | H_i\} P\{|ts_i| < T_i | H_i\} P_{H_i} \quad (2.38)$$

where \tilde{x}_H is the horizontal position error as a two dimensional vector with east and north position errors $[\tilde{x}_E \quad \tilde{x}_N]$.

2.3.1 Current Methods to Calculate VPL

The risk definition in A-RAIM for LPV-200 is defined as follows. The total integrity risk 2×10^{-7} was divided into the horizontal and vertical case evenly. Within the vertical case, the multiple fault modes were excluded, leaving the single fault and fault free hypotheses with the integrity risk as 8.7×10^{-8} . The integrity risk was distributed evenly onto each hypothesis. The prior probability of each single fault mode was 1×10^{-5} . The probability of the null hypothesis was approximated as 1. The continuity risk under the fault free and single fault modes was 4×10^{-6} separately. Again, the continuity risk was distributed evenly onto each hypothesis.

Two current methods that can be adopted for calculation of VPL in A-RAIM are studied and compared with R-RAIM in Jiang and Wang (2014a). VPL is then compared with Vertical Alert Limit (VAL) as one of the conditions to decide service availability. However, the application of other methods to calculate VPL under this framework is very limited. Efforts are made in this study to integrate all popular methods in this framework.

Under the faulty mode, there is an unknown bias in both the position error and the test statistic, and the P_{MD} under faulty mode is not given. Therefore, the straightforward derivation of VPL is impossible. There are algorithms aimed to obtain conservative VPLs with higher efficiency of computation, where the conservative VPL is able to guarantee a lower than given integrity risk.

When calculating the VPL with the conventional algorithms, there are mainly three options: the classic method (Brown and Chin 1998), the weighted RAIM method (Walter and Enge 1995) and the solution separation method (Brenner 1996). There are also different ways to fix the size of the unknown bias in calculation of VPL (Ober 2003) including MDB, MHB and WCB. The WCB that produces the maximum integrity risk is

searched within the range of MHB and MDB. The MDB is used in the classic method, and the WCB was used to derive the ideal VPL with the exact value of VPL satisfying the required integrity risk (Milner and Ochieng 2011), which is also applied in the A-RAIM structure (Milner and Ochieng 2010a).

Three current algorithms in the A-RAIM framework are listed below.

In Brown and Chin (1998), the bias is fixed with given P_{FA} , $\frac{IR_{Vi}}{P_{Hi}}$ and the noise is bounded by $\frac{IR_{Vi}}{P_{Hi}}$ (Angus 2007), which is referred as the classic method with its VPL noted as VPL_{BC} ,

$$VPL_{BCi} = \delta_i \cdot Vslope_i + K(1 - \frac{IR_{Vi}}{2P_{Hi}})\sigma_U \quad (2.39)$$

where $K()$ is the inverse of the cumulative distribution function of a Gaussian random variable with zero mean and unit variance; δ_i can be derived by given α_i and $\beta_i = \frac{IR_{Vi}}{P_{Hi}}$ with the following procedure: 1) With the normal distribution of the test statistics, a threshold value is determined by a central normal distribution with given α_i ; 2) The non-centrality parameter is then determined by the non-central normal distribution with given threshold and β_i ; The slope parameter $Vslope_i$ is defined as the project matrix from the test statistic domain to the position domain, which was proved equivalent with standard deviation of the vertical solution separation (Blanch et al. 2010),

$$Vslope_i = \frac{|S_U e_i|}{\sqrt{e_i^T Q_y^{-1} Q_v Q_y^{-1} e_i}} = \sigma_{Uss} \quad (2.40)$$

The final VPL is the maximum one among all faulty hypotheses, and this maximization process is applied in all RAIM algorithms, which will be omitted later.

$$VPL_{BC} = \max(VPL_{BCi}) \quad (2.41)$$

Instead of the bias, the threshold with given P_{FA} is projected into the position domain in the weighted RAIM method (Walter and Enge 1995) with the VPL for each hypothesis defined as,

$$VPL_{WEi} = K(1 - \frac{\alpha_i}{2})Vslope_i + K(1 - \frac{IRv_i}{2P_{H_i}})\sigma_U \quad (2.42)$$

The total position error is separated into the solution separation and the subset position error without the necessarily of projecting from the test statistic domain in Pervan et al. (1998); Blanch et al. (2010), which is referred as the MHSS method. The VPL based on this method is noted as VPL_{PB} ,

$$VPL_{PBi} = K(1 - \frac{\alpha_i}{2})\sigma_{ss,Ui} + K(1 - \frac{IRv_i}{2P_{Hi}})\sigma_{Ui} \quad (2.43)$$

These three different methods to calculate VPL are illustrated in Figure 7.

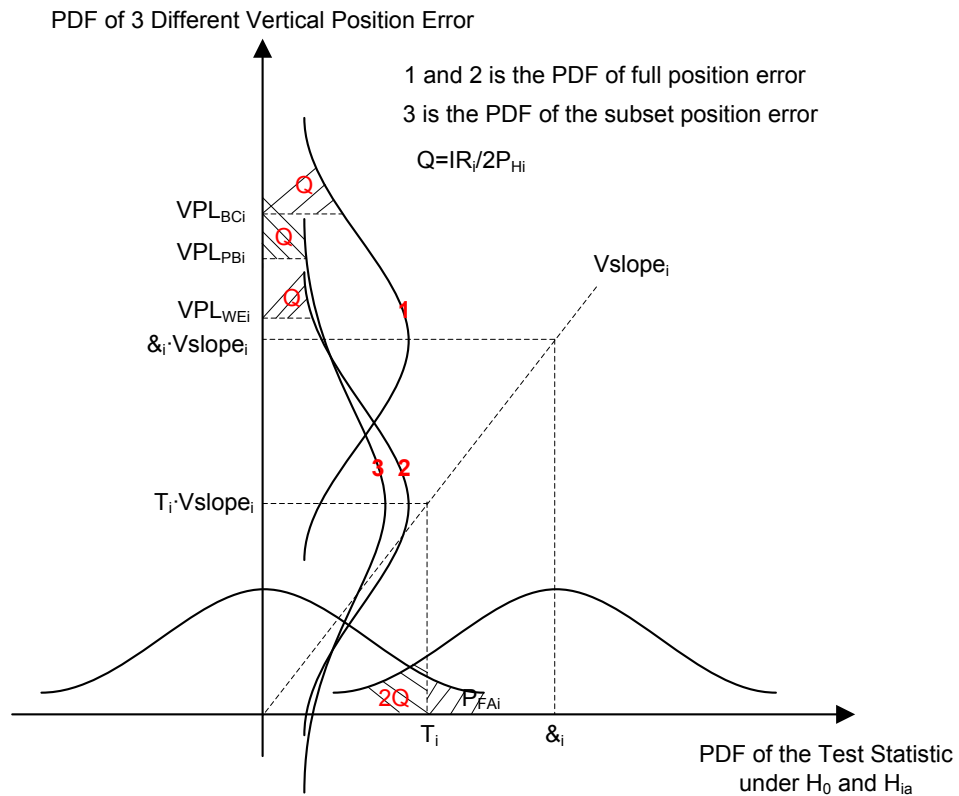


Figure 7: Three VPL Calculation Mechanisms

2.3.2 Current Methods to Calculate HPL

The original risk definition for NPA is based on the chi-squared test. With the multiple hypothesis structure, the risk for each hypothesis is set as (Brenner 1995; Kelly 1998): $\alpha_i = 3.33 \times 10^{-7}/m$, $IR_{Hi} = 10^{-7}$, $P_{Hi} = 10^{-4}$, and therefore the given value of $\frac{IR_{Hi}}{P_{Hi}}$ is 10^{-3} .

The integrity risk for the horizontal domain is,

$$IR_{Hi} = P\{|\tilde{x}_H| > HPL|H_i\}P\{|ts_i| < T_i|H_i\}P_{Hi} \quad (2.44)$$

where the horizontal position error $\tilde{x}_H = [\tilde{x}_E \ \tilde{x}_N]^T$ is a vector with the east position error and the north position error. $P\{|\tilde{x}_H| > HPL|H_i\} = P_{HPE}$ is the probability of horizontal position error.

Current methods to calculate HPL are approximated with simplified distributions, due to the complicated calculation process to gain the exact probability, including the external reliability method (Brown and Chin 1998), the weighted RAIM method (Walter and Enge 1995) and the solution separation method (A-RAIM report 2012)

The external reliability method (Brown and Chin 1998) was expanded with a random part (Angus 2007) with its HPL noted as HPL_{BC} . Two approximated distributions can be used to calculate the P_{HPE} . With the normal approximation, $\sqrt{\|\tilde{x}_H\|^2}$ is approximated as a one degree Taylor series (Lee 1995),

$$\sqrt{\nabla \tilde{x}_E^2 + \nabla \tilde{x}_N^2} + \frac{\nabla \tilde{x}_E}{\sqrt{\nabla \tilde{x}_E^2 + \nabla \tilde{x}_N^2}}(\tilde{x}_E - \nabla \tilde{x}_E) + \frac{\nabla \tilde{x}_N}{\sqrt{\nabla \tilde{x}_E^2 + \nabla \tilde{x}_N^2}}(\tilde{x}_N - \nabla \tilde{x}_N) \quad (2.45)$$

where $\nabla \tilde{x}_E$ and $\nabla \tilde{x}_N$ are the non-centrality parameters of \tilde{x}_E and \tilde{x}_N ; The approximated variance is of normal distribution $N(\sqrt{\nabla \tilde{x}_E^2 + \nabla \tilde{x}_N^2}, \sigma_{\nabla i})$. The variance $\sigma_{\nabla i}^2 = S_2 Q_H S_2^T$ is projected on the direction of the faulty observation i with $S_2 = \begin{bmatrix} \frac{S_E e_i}{\sqrt{(S_E e_i)^2 + (S_N e_i)^2}} & \frac{S_N e_i}{\sqrt{(S_E e_i)^2 + (S_N e_i)^2}} \end{bmatrix}$ and Q_H as the covariance matrix of \tilde{x}_H .

With the normal approximation, HPL_{BC} under H_i is (Angus 2007),

$$HPL_{BC1i} = Hslope1_i \cdot \delta_i + K(1 - \frac{IR_{Hi}}{2P_{Hi}})\sigma_{\nabla i} \quad (2.46)$$

where δ_i is derived by given α_i and $\beta_i = \frac{IR_{Hi}}{P_{Hi}} = 10^{-3}$; The horizontal slope parameter is defined as the project matrix from the i th observation domain to the horizontal position error domain (Brown and Chin 1998) with $S_{EN} = [S_E \ S_N]^T$, which is equivalent to the standard deviation of the horizontal solution separation as proved in Appendix B,

$$Hslope1_i = \sqrt{\frac{e_i^T S_{EN}^T S_{EN} e_i}{e_i^T Q_y^{-1} Q_v Q_y^{-1} e_i}} = \sigma_{HSS} \quad (2.47)$$

The second approximation is the chi-squared approximation, which is derived by the following inequality (Ober 1997),

$$\sqrt{\|\tilde{x}_H\|^2} \leq \sqrt{\frac{1}{\lambda_m} \tilde{x}_H^T Q_H^{-1} \tilde{x}_H} \quad (2.48)$$

where $\tilde{x}_H^T Q_H^{-1} \tilde{x}_H \sim \chi^2(2, \delta_c)$ has 2 degree of freedom with δ_c as the non-centrality parameter; λ_m is the minimum eigenvalue of Q_H^{-1} . With the above inequality, it can be concluded that the chi-squared approximation is always safe (Ober 1997).

In a similar way, HPL_{BC} under H_i with the chi-squared approximation is derived as,

$$HPL_{BC2i} = \sqrt{\frac{1}{\lambda_m}} [Hslope2_i \delta_i + \sqrt{\chi^2(2, 1 - \frac{IR_{Hi}}{P_{Hi}})}] \quad (2.49)$$

where δ_i is also derived by given α_i and $\beta_i = \frac{IR_{Hi}}{P_{Hi}} = 10^{-3}$; $\chi^2(2, 1 - \frac{IR_{Hi}}{P_{Hi}})$ represents the value at probability $1 - \frac{IR_{Hi}}{P_{Hi}}$ with the central chi-squared inverse cumulative distribution function and 2 degrees of freedom. The slope factor for each hypothesis with the chi-squared approximation is,

$$Hslope2_i = \sqrt{\frac{e_i^T S_{EN}^T Q_H^{-1} S_{EN} e_i}{e_i^T Q_y^{-1} Q_v Q_y^{-1} e_i}} \quad (2.50)$$

Another popular method is the weighted RAIM method (Walter and Enge 1995) designed for precision approach with its HPL noted as HPL_{WE} ,

$$HPL_{WEi} = Hslope1_i T_i + K(1 - \frac{IR_{Hi}}{2P_{Hi}}) \sqrt{\sigma_E^2 + \sigma_N^2} \quad (2.51)$$

The solution separation method was proposed by Brenner (1996) and applied in a multiple hypothesis structure (Pervan et al. 1998), which is referred as the MHSS method in A-RAIM (A-RAIM report 2012) for service LPV-200. The MHSS HPL defined in A-RAIM is,

$$HPL_{PBi} = \sqrt{HPL_{Ei}^2 + HPL_{Ni}^2} \quad (2.52)$$

where the east HPL is defined as,

$$HPL_{Ei} = \sigma_{ssE} T_i + K(1 - \frac{IR_i}{2P_{Hi}}) \sigma_{iE} \quad (2.53)$$

where σ_{ssE} as the standard deviation of the east solution separation, which is equivalent to the east slope parameter $\frac{|S_E e_i|}{\sqrt{e_i^T P Q_v P e_i}}$ (Blanch et al. 2010); σ_{iE} is the standard deviation of the subset position error \tilde{x}_{iE} , which is derived with the i th observation removed in the estimator. The HPL for the north HPL_{Ni} can be derived in a similar way.

2.3.3 Two Integrity Optimization Methods

a) The Nio-RAIM Method

The general idea of the Nio-RAIM method (Hwang and Brown 2005) is to update the weight matrix in the WLS estimator by a predicted PL value. The weight with the bigger PL value gets decreased after iterations. In this way, the satellite that is most sensitive to undetected fault will be suppressed in the WLS estimator. In this way, the

position accuracy is improved with any fault existing in observations. But the sacrifice is the increased computational burden with induced the correlation between the position error and the test statistic. The diagonal element of the new diagonal weight matrix W for each iteration is designed as,

$$w_i(k+1) = \frac{(\prod_{i=1}^m PL_i)^{\frac{1}{m}}}{PL_i} w_i(k) \quad (2.54)$$

Therefore, the covariance matrix of the position error with the new weight matrix is

$$Q_{nio} = (A^T W A)^{-1} A^T W Q_y W A (A^T W A)^{-1} \quad (2.55)$$

The covariance between the estimation error and the test statistic is,

$$cov(\tilde{x}, ts_i) = \frac{(A^T W A)^{-1} A^T W Q_y P^T (P Q_y P^T)^{-1} P e_i}{\sqrt{e_i^T P^T (P Q_y P^T)^{-1} P e_i}} \quad (2.56)$$

With correlation between the position error and the test statistic, the old way to calculate VPL is not valid any more. Therefore, the bivariate normal distribution function for integrity risk should be used to search for the new PL value,

$$\frac{IR_i}{P_{Hi}} = \int_{PL_i}^{+\infty} \int_{-T_i}^{T_i} \frac{1}{2\pi\sigma_{nio}\sqrt{1-\rho_{nio}^2}} \exp f_{xy} dx dy + \int_{-\infty}^{-PL_i} \int_{-T_i}^{T_i} \frac{1}{2\pi\sigma_{nio}\sqrt{1-\rho_{nio}^2}} \exp f_{xy} dx dy \quad (2.57)$$

where $f_{xy} = -\frac{1}{2(1-\rho_{nio}^2)} \left[\frac{(x-u_x)^2}{\sigma_v^2} + (y-u_y)^2 - \frac{2\rho_{nio}(x-u_x)(y-u_y)}{\sigma_v} \right]$, σ_{nio} is the standard deviation of the position error with new weight matrix, and $\rho_{nio} = \frac{cov(\tilde{x}, ts_i)}{\sigma_{nio}}$ is the correlation coefficient; u_x and u_y are the non-centrality parameters.

Since the search for the PL value with above equation is too complex to be used in real time applications, there is a search table defined in Hwang and Brown (2005) to speed up the calculation. The calculation process is: all PL values are decided by a RAIM method; all these values are used as inputs to compute a new weight, which is used to

decide the standard deviation and the correlation coefficient; The PL value is then searched in a table with these values.

The performance of Nio-RAIM is shown with an example in the following figures with $Q_y = I$ and design matrix as

$$A = \begin{bmatrix} -0.8342 & -0.3263 & -0.4446 & 1.000 \\ -0.2324 & -0.5703 & 0.7879 & 1.000 \\ -0.8742 & 0.4846 & 0.0394 & 1.000 \\ 0.3074 & -0.9110 & -0.2749 & 1.000 \\ 0.2882 & -0.5574 & 0.7786 & 1.000 \\ -0.5023 & -0.7792 & -0.3749 & 1.000 \end{bmatrix}$$

It is depicted that the slope parameters are more evenly distributed in Figure 8 and Figure 9, and therefore the worst case PL is reduced in Figure 10.

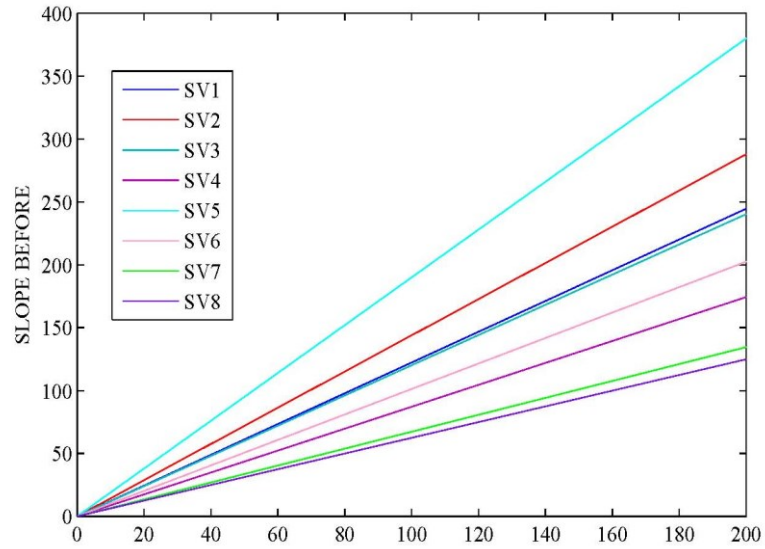


Figure 8: Slope Parameters before NioRAIM

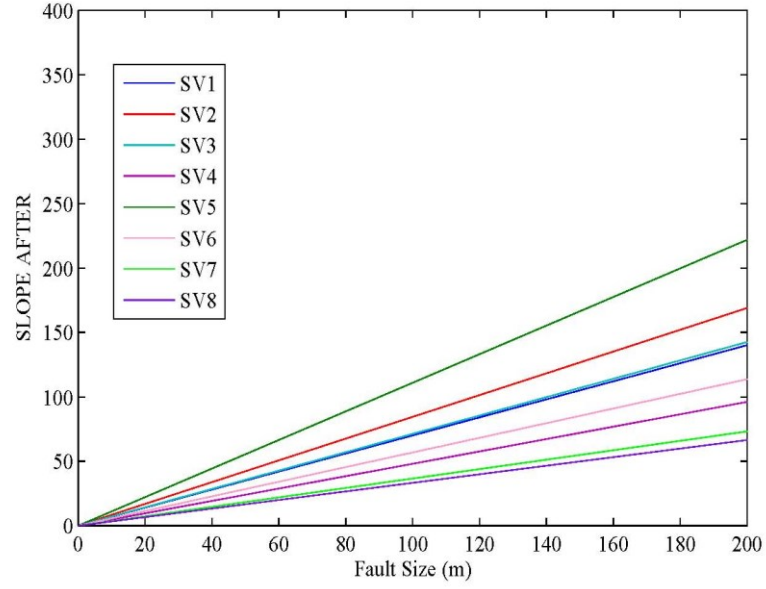


Figure 9: Slope Parameters after Nio-RAIM

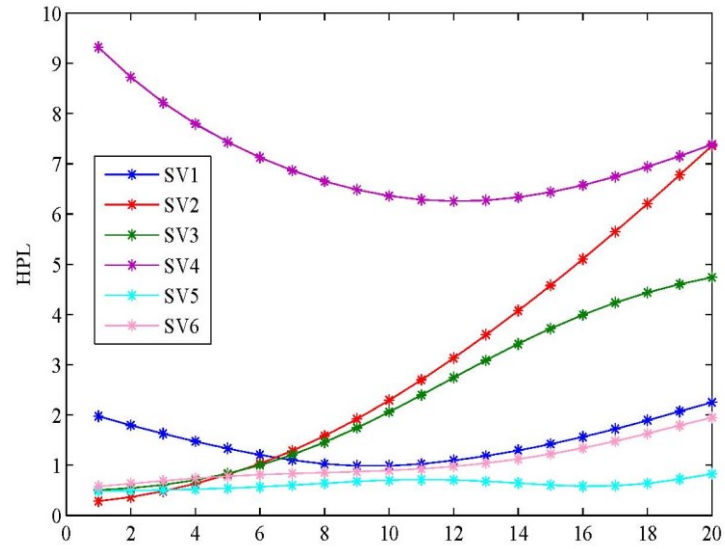


Figure 10: External Reliability after 20 Iterations with Nio-RAIM

Numerical results with HPL_{BC} are shown in Figure 11 with improvements after 5 iterations.

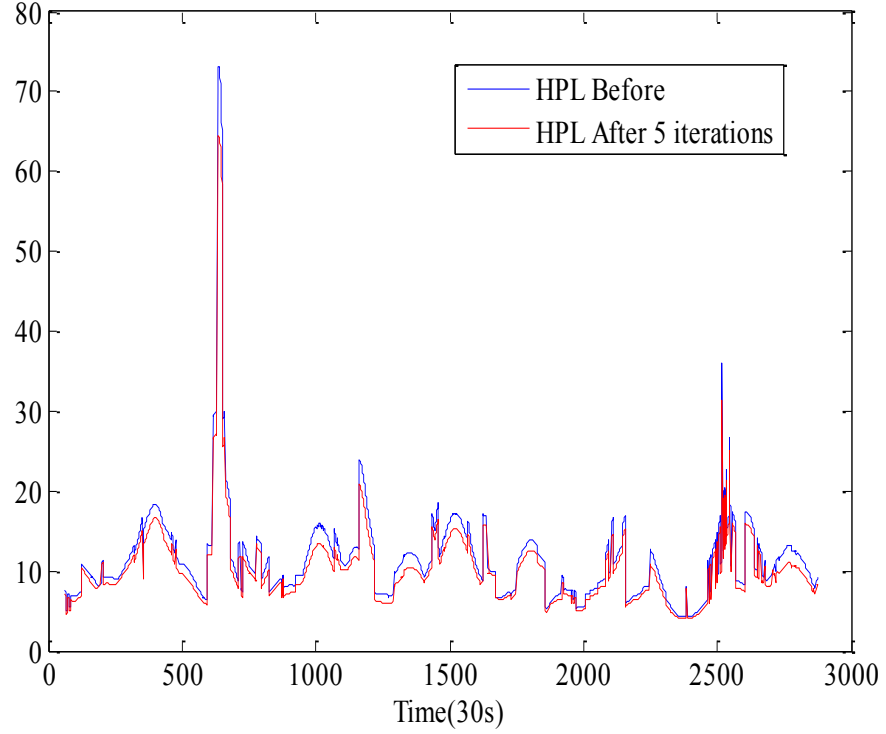


Figure 11: HPL_{BC} with Nio-RAIM

It is shown in Figure 11 that the optimized HPL value is reduced from the original value by around 1.5m. The averaged computational time per epoch is increased from 1.71×10^{-4} s with the conventional method to 0.214s.

It can be seen from Figure 11 that the improvement after 5 iterations is not impressive and the computational time is too large. Plus, there are several disadvantages within the implementation of this method: 1) There is uncertainty and complexity involved in designing a search table; 2) It is shown in Figure 10 that there is an optimal step of iteration with the lowest PL value, and after that step, the PL value would increase. But this optimal step varies with different geometry, which increases the difficulty in implementation; 3) It can only be applied in one of the current RAIM algorithms of HPL_{BC}, where the non-centrality parameter is fixed; 4) the compromised precision of the position estimation might beyond the required level with increase of the integrity level, which means a monitor of precision might be necessary.

b) Risk Distribution Optimization Method

This optimization method takes advantage of the flexibility in the allocation of the faulty integrity risk onto each hypothesis (Lee 2008; Lee and McLughlin 2008; Blanch et al. 2010). With given IR_i as the total integrity for faulty cases, the optimal PL (PL_{opt}) is obtained by the risk distribution that is able to generate same PL for each H_i . The following equation is used to derive the optimal value,

$$\sum_{i=1}^m 2P_{H_i} \cdot N(PL_{opt}) = IR \quad (2.58)$$

where $N()$ is the cumulative distribution function of a Gaussian random variable with zero mean and unit variance. Two examples are shown with the VPL_{BC} and VPL_{PB} ,

$$\sum_{i=1}^m 2P_{H_i} \cdot N\left(-\frac{VPL_{BC,opt}-\delta_i Vslope_i}{\sigma_U}\right) = IR_V \quad (2.59)$$

$$\sum_{i=1}^m 2P_{H_i} \cdot N\left(-\frac{VPL_{PB,opt}-K(1-\frac{\alpha_i}{2})\sigma_{ss,Ui}}{\sigma_{Ui}}\right) = IR_V \quad (2.60)$$

This method is simpler to implement than the Nio-RAIM method and its performance is shown below with VPL_{BC} ,

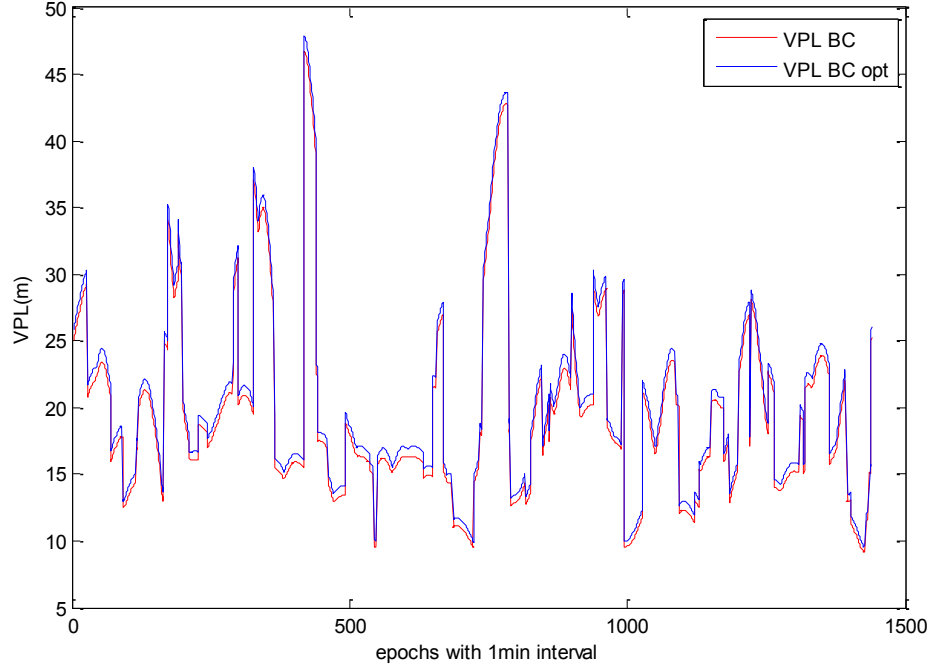


Figure 12: VPL_{BC} with risk distribution optimization method

It is shown in Figure 12 that the optimized VPL value is reduced from the original value with around the scale of 1m. The averaged computational time per epoch is increased from 1.71×10^{-4} s for the conventional method to 0.0159s. In this example, the improvements on integrity with these two methods are both not impressive. The risk distribution optimization method is faster and has less uncertainty compared with the Nio-RAIM method for the multiple hypothesis RAIM algorithms.

2.4 Summary

The navigation model and current algorithms for FDE and RAIM are introduced together with two integrity optimization methods as the basis for further study. The FDE test results are shown with the probability of successful detection and correct isolation, together with the two reliability measures for detectability and separability. Results with current RAIM methods will be shown in the next few chapters together

with new methods for comparison. Also, integrity improvements are shown with two available optimization methods.

CHAPTER 3 RELATIVE RAIM

In the architectures proposed by the GEAS panel including GNSS Integrity Channel (GIC), R-RAIM and A-RAIM (GEAS 2008) for airborne navigation integrity monitoring to provide world-wide LPV-200 service, several important factors are considered to obtain a balance of geometry and latency, such as the distribution of integrity monitoring burden among aircraft satellite and ground, the delay caused by transmitting the corrections from ground stations to aircraft to satisfy the TTA requirement and etc. GIC is the one that relies least on aircraft and most on outside augmentation systems, and therefore it is the most difficult one to satisfy the TTA requirement, but least demanding on the constellation geometry. A-RAIM is the one that is very similar with current RAIM methods except that dual-frequency is considered in A-RAIM and ionosphere delay can be removed. It performs the integrity monitoring mostly in avionics, and therefore it is more influenced by the constellation geometry. R-RAIM is the one in middle with integrity monitoring task shared among the aircraft, GNSS constellations and external monitors. The positioning and integrity monitoring functionality are performed by the user aircraft with relative carrier phase observations and code observations that have been validated by corrections from GIC. Therefore, there are a few seconds and perhaps even a few minutes for GIC information to age before being used, and it is more relaxing with the TTA requirement, which would facilitate the implementation of this method world-wide. With the code observations protected, fault detection is only necessary for TDCP used for relative positioning, which relaxes the TTA requirement as well. The positioning and integrity monitoring mechanisms in R-RAIM are introduced in this Chapter.

3.1 Relative Positioning Methods

The positioning scenario for R-RAIM is shown in Figure 13. Depending on the different domain when merging the initial measurement and the delta range, there are two methods: the range domain method and the position domain methods. The range domain method merges these two types of ranges in the range domain and the position domain method merges them in the position domain. There are no obvious differences between these two different positioning methods with numerical results demonstrated in Ding and Wang (2011). The difference between these two methods for integrity monitoring reflects in the different ways of error propagation.

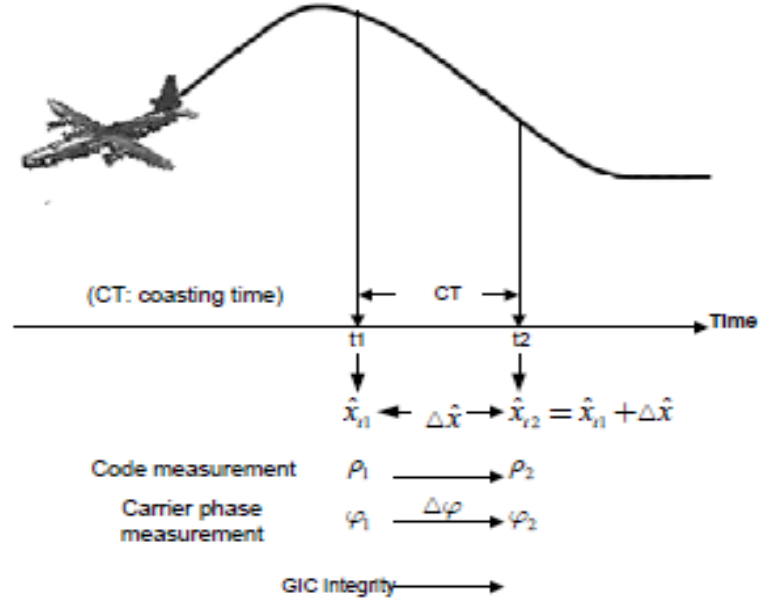


Figure 13: R-RAIM Positioning Method

The basic equation after linearization for positioning at the initial time $t-T$ is,

$$y_0 = A_0 x_0 + \epsilon_0 + b_0 \quad (3.1)$$

where:

A_0 is the design matrix at the initial time $t-T$ with t as the current time and T as the coasting time.

y_0 is the carrier phase smoothed code measurement vector at the initial time $t-T$ with SV Doppler effect adjustment (Van Graas 2005).

x_0 is the user position at the initial time $t-T$.

ϵ_0 is the random error of the code measurement for the initial position estimation with distribution $N \sim (0, Q_0)$. The statistical model is adopted from GEAS (2008) to determine the standard deviation of the initial position error.

b_0 is the bounded bias error vector to account for faults of small size undetected by the GIC or errors that cannot be modelled with Gaussian distribution.

The basic equation after linearization for positioning at the current time t is,

$$\Delta y = Ax - A_0 x_0 (\epsilon_\Delta + f_\Delta) \quad (3.2)$$

where:

Δy is the relative carrier phase measurement vector at time $t-T$ and t with SV Doppler effect adjusted.

ϵ_Δ is the random error of the TDCP measurement for the relative position estimation with distribution $N \sim (0, Q_\Delta)$. The statistical model is adopted from GEAS (2008) to determine the standard deviation of the relative position error.

f_Δ is the fault vector in the TDCP measurement. The code measurements with GIC integrity information are used for initial position estimation at the initial time $t-T$ to guarantee the integrity. Therefore, it is assumed that no fault exists in the initial position error. With the difference of carrier phase measurement between two epochs, the bias is eliminated in the TDCP measurement.

3.1.1 The Range Domain Method

The measurements from two time epochs are added together before position estimation in the range domain R-RAIM method. With the covariance matrix of the final solution error as $Q_r = Q_0 + Q_\Delta$, the position error is expressed as,

$$\tilde{x}_r = (A^T Q_r^{-1} A)^{-1} A^T Q_r^{-1} (\epsilon_0 + \epsilon_\Delta + b_0 + f_\Delta) \quad (3.3)$$

3.1.2 The Position Domain Method

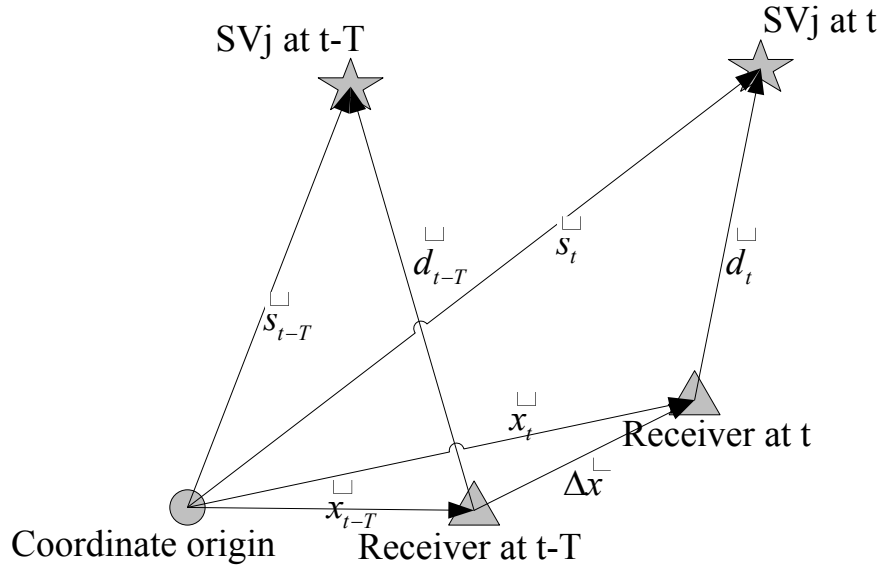


Figure 14: R-RAIM Position Domain Method

In the position domain method, two measurements from two epochs are estimated individually before being combined together with the geometric illustration shown in Figure 14. The code measurements with GIC integrity information are used for initial position estimation at the initial time $t-T$ to guarantee the integrity. Therefore, it is assumed that no fault exists in the initial position. With the projection matrix as $S_0 = (A_0^T Q_0^{-1} A_0)^{-1} A_0^T Q_0^{-1}$, the initial position error is,

$$\tilde{x}_0 = S_0(\epsilon_0 + b_0) \quad (3.4)$$

The TDCP measurements are used to estimate the relative position between the initial time $t-T$ and the current time t with assumption that no bias term exists in this position error, which is expressed as,

$$\begin{aligned}\tilde{x}_\Delta &= S_\Delta(\epsilon_\Delta + f_\Delta - \Delta A \tilde{x}_0) \\ &= S_\Delta[\epsilon_\Delta + f_\Delta - \Delta A S_0(\epsilon_0 + b_0)]\end{aligned}\tag{3.5}$$

where $\Delta A = A - A_0$ is the geometry change during the coasting time T . Only satellites in view in common at $t-T$ and t are used here; $W_\Delta = (Q_\Delta + Q_{\Delta A})^{-1}$ with $Q_{\Delta A} = \Delta A(A_0^T W_0 A_0)^{-1} \Delta A^T$; the projection matrices $S_\Delta = (A^T W_\Delta A)^{-1} A^T W_\Delta$.

The final position error is the sum of two estimation errors at two epochs,

$$\tilde{x}_p = \tilde{x}_0 + \tilde{x}_\Delta\tag{3.6}$$

The covariance is,

$$D(\tilde{x}_p) = (A_0^T Q_0^{-1} A_0)^{-1} + (A^T W_\Delta A)^{-1} - (A_0^T Q_0^{-1} A_0)^{-1} \Delta A^T S_\Delta^T - S_\Delta \Delta A (A_0^T Q_0^{-1} A_0)^{-1}\tag{3.7}$$

3.2 R-RAIM Algorithms

Based on these two positioning methods, two current RAIM methods can be applied in R-RAIM including the classic method and the MHSS method.

3.2.1 R-RAIM with the Classic Method

VPL with the range domain method under H_a with the classic method is (GEAS 2008; Gratton et al. 2010),

$$VPL_{R,r,a} = \delta \cdot \sigma_{r,ss,a} + K(1 - \frac{IR_a}{2P_{Ha}}) \sigma_r + |R_0| b_{max}\tag{3.8}$$

where:

$\sigma_r = \sqrt{[(A^T Q_r^{-1} A)^{-1}]_{v,v}}$ is the standard deviation of the vertical position error.

IR_a , is the integrity risk of H_a under the global test.

P_{H_a} is the prior probability of H_a under the global test.

δ is derived with given α and $\beta = \frac{IR_a}{P_{H_a}}$.

$b_{max} = b_m E$ is the bias vector with b_m used for integrity.

$\sigma_{r,ss,a} = \max\{\sigma_{r,ss,i}\}$ where $\sigma_{r,ss,i} = \sqrt{[(R_i - R_0)Q_r(R_i - R_0)^T]_{v,v}}$ is the standard deviation of the vertical solution separation with $R_i = [(A_i^T Q_{r,i}^{-1} A_i)^{-1} A_i^T Q_{r,i}^{-1}]_v$, $Q_{r,i}$ as Q_r with i th row and column eliminated, $R_0 = [(A^T Q_r^{-1} A)^{-1} A^T Q_r^{-1}]_v$ as the projection matrix for the bias vector. The notation $[\]_{v,v}$ stands for the 3rd column and row of the matrix, and the notation $[\]_v$ means the 3rd row of the matrix in this Chapter and the next Chapter.

VPL with the position domain method under H_a with the classic method is (Gratton et al. 2010),

$$VPL_{R,p,a} = \delta \cdot \sigma_{p,ss,a} + K(1 - \frac{IR_a}{2P_{H_a}})\sigma_p + |P_0|b_{max} \quad (3.9)$$

where:

$P_0 = [S_0 - S_\Delta \Delta A S_0]_v$ is the projection matrix for the bias vector.

$\sigma_p = \sqrt{D[\tilde{x}_p]_{v,v}}$ is the standard deviation of the position error.

$\sigma_{p,ss,a} = \max\{\sigma_{p,ss,i}\}$ and $\sigma_{p,ss,i} = \sqrt{D(\hat{x}_{\Delta,i} - \hat{x}_\Delta)_{v,v}}$, $D(\hat{x}_{\Delta,i} - \hat{x}_\Delta) = (S_{\Delta,i} - S_\Delta)(Q_\Delta + Q_{\Delta A})$ and $S_{\Delta,i} = (A^T W_{\Delta,i} A)^{-1} A^T W_{\Delta,i}$, $W_{\Delta,i}$ is W_Δ with the i th row and column eliminated.

3.2.2 R-RAIM with the MHSS Method

VPL with the range domain method under H_i with the MHSS method is,

$$VPL_{R,r,i} = K(1 - \frac{\alpha_i}{2})\sigma_{r,ss,i} + |R_{ss,i}|b_{nom} + K(1 - \frac{IR_i}{2P_{H_i}})\sigma_{r,i} + |R_i|b_{max} \quad (3.10)$$

where:

$R_{ss,i} = R_0 - R_i$ is the projection matrix for bias vector.

$\sigma_{r,i} = \sqrt{[A_i^T Q_{r,i}^{-1} A_i]_{v,v}^{-1}}$ is the standard deviation of the vertical subset position error.

VPL with the position domain method under H_i with the MHSS method is (Lee 2008; GEAS 2010),

$$VPL_{R,p,i} = K(1 - \frac{\alpha_i}{2})\sigma_{p,ss,i} + |P_{\Delta,i}|b_{nom} + K(1 - \frac{IR_i}{2P_{H_i}})\sigma_{p,i} + |P_i|b_{max} \quad (3.11)$$

where:

$P_i = (S_0 - S_{\Delta,i}\Delta A S_0)_v$ is the projection matrix for maximum bias vector;

$P_{\Delta,i} = (S_{\Delta,i}\Delta A S_0 - S_{\Delta}\Delta A S_0)_v$ is the projection matrix for the nominal bias;

$\sigma_{p,i} = \sqrt{D(\tilde{x}_{\Delta,i} + \tilde{x}_0)_{v,v}}$ is the standard deviation is with $D(\tilde{x}_{\Delta,i} + \tilde{x}_0)$ as

$$(A_0^T Q_0^{-1} A_0)^{-1} + (A^T W_{\Delta,i} A)^{-1} - (A_0^T Q_0^{-1} A_0)^{-1} \Delta A^T S_{\Delta,i}^T - S_{\Delta,i} \Delta A (A_0^T Q_0^{-1} A_0)^{-1}.$$

3.3 Numerical Results

The error model for range measurements are combined with the random error and the bias with characteristics carried in the ISM. Error models are defined for different errors in the range error for evaluation of continuity and integrity purpose in the GEAS report. There are two types of bias magnitudes in the GEAS report for the error model. One is designed for the nominal condition b_{nom} used for evaluation of the continuity

performance. One is the maximum bias magnitude b_{max} used for evaluation of the integrity performance.

3.3.1 R-RAIM VPL

Test data was collected in the IGS station ABPO on 23 March 2009 for 24 hour with 30 seconds sampling rate. The input of the simulation process is the number of visible satellites and geometry at each epoch from real data and the observation error model (Lee and McLaughlin 2008). First, the standard deviation of the horizontal and vertical position error with the range domain method the position domain method are shown in Figure 15 and Figure 16 respectively.

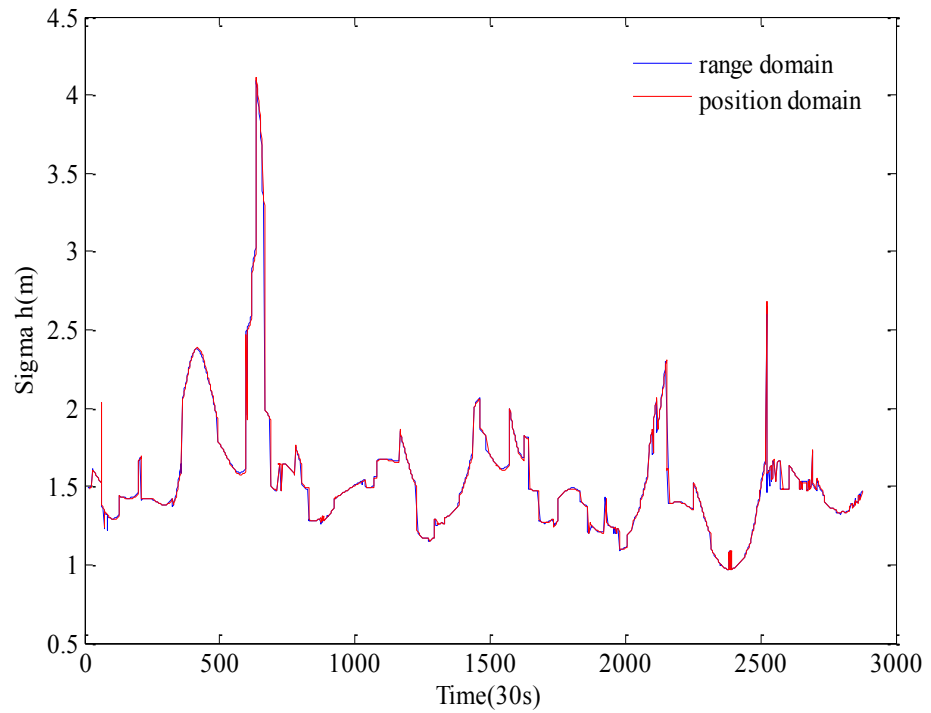


Figure 15: Horizontal Accuracy with Position Domain and Range Domain Methods

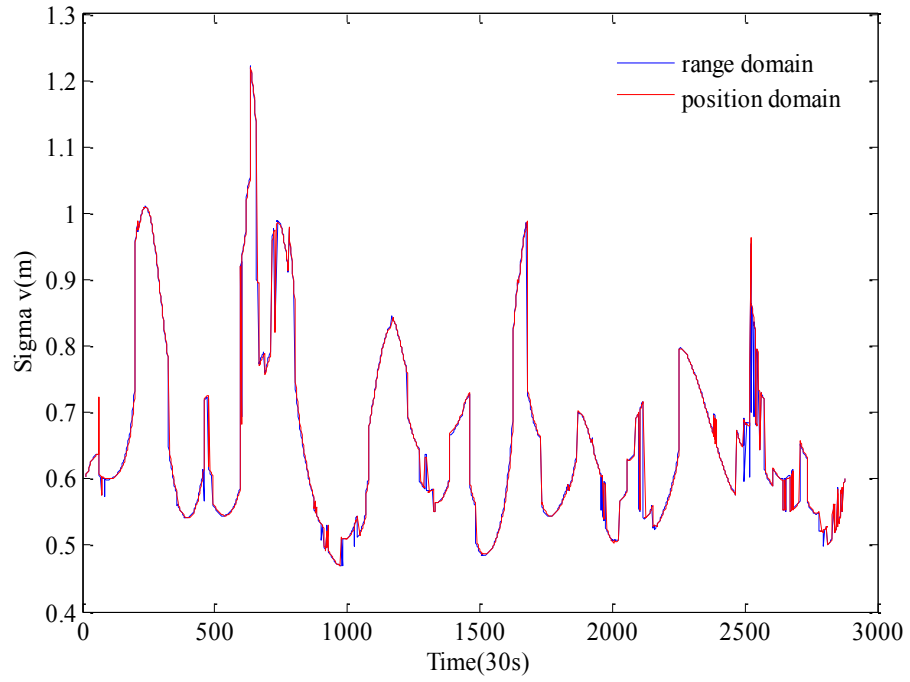


Figure 16: the Vertical Accuracy with Position Domain and Range Domain Methods

As shown in the figures above, both accuracies with these two positioning methods is very close with each other. Similar conclusion can be found in Ding and Wang (2011). But the VPL results based on two positioning methods are different due to the different projection matrices for different errors, which will be shown with numerical results in Chapter 4.

The R-RAIM results of CT 5min with two RAIM algorithms: the MHSS method and the classic method are shown in Figure 17, where the first one has worst results than the latter one.

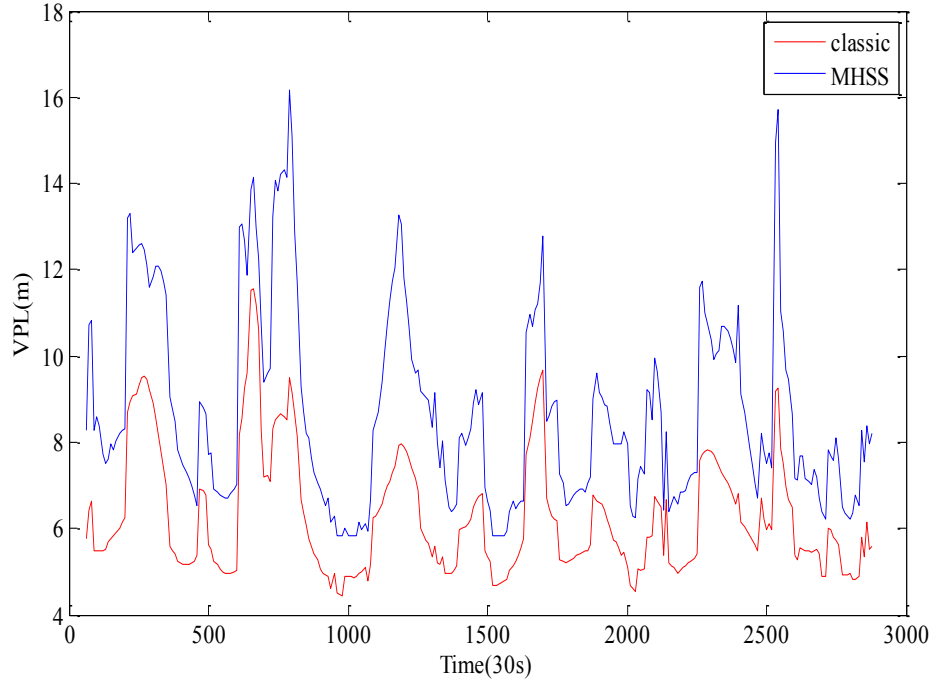


Figure 17: R-RAIM with the MHSS Method and the Classic Method

As defined in Section 3.2, the VPL difference with these two methods are caused by: 1) the adoption of different tests, the local test for the MHSS method and the global test for the classic method, and therefore the different integrity risk distribution from the total risk; 2) different VPL formulas as a conservative bound for the given integrity risk with two methods. Further comparison of these two methods is provided in Chapter 4 with both A-RAIM and R-RAIM structures. Also to test the difference of RAIM algorithms without the influence of different risk distributions, the classic method is adapted in the multiple hypothesis structure with the local test in Chapter 5, and compared with the MHSS method, so that the RAIM algorithms can be further studied in a unified structure.

The position domain method and the MHSS RAIM algorithm are used as an example to further examine the VPL results. Test data collected from IGS station BRFT is used to analyse the influence of geometry and precision on final result of the position domain MHSS VPL with CT 30s in Figure 18 and Figure 19.

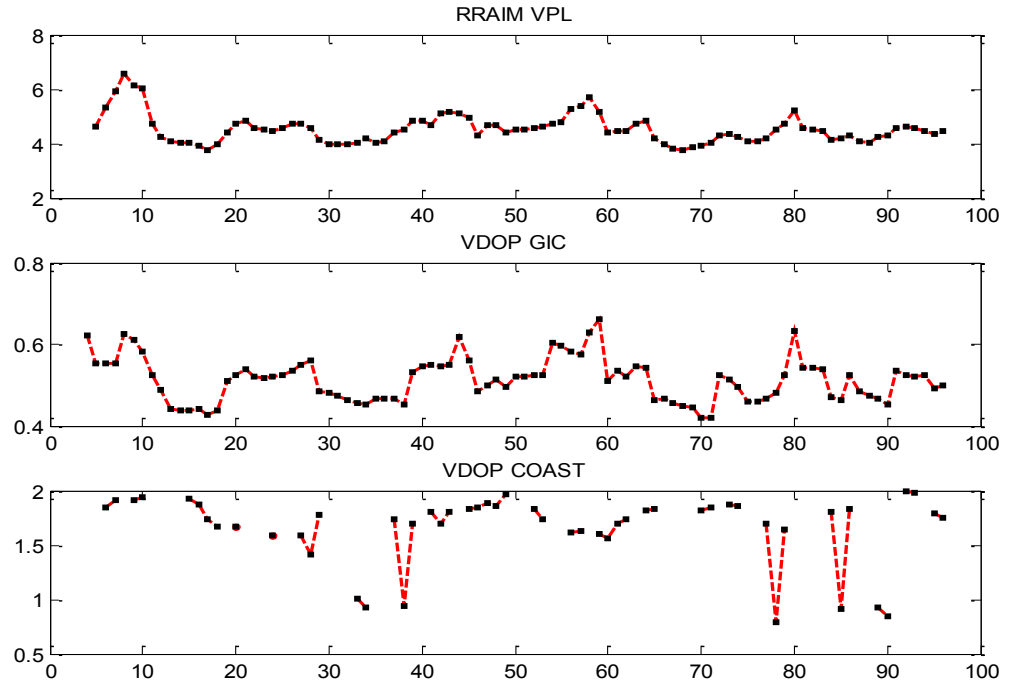


Figure 18: The geometric factors in R-RAIM VPL

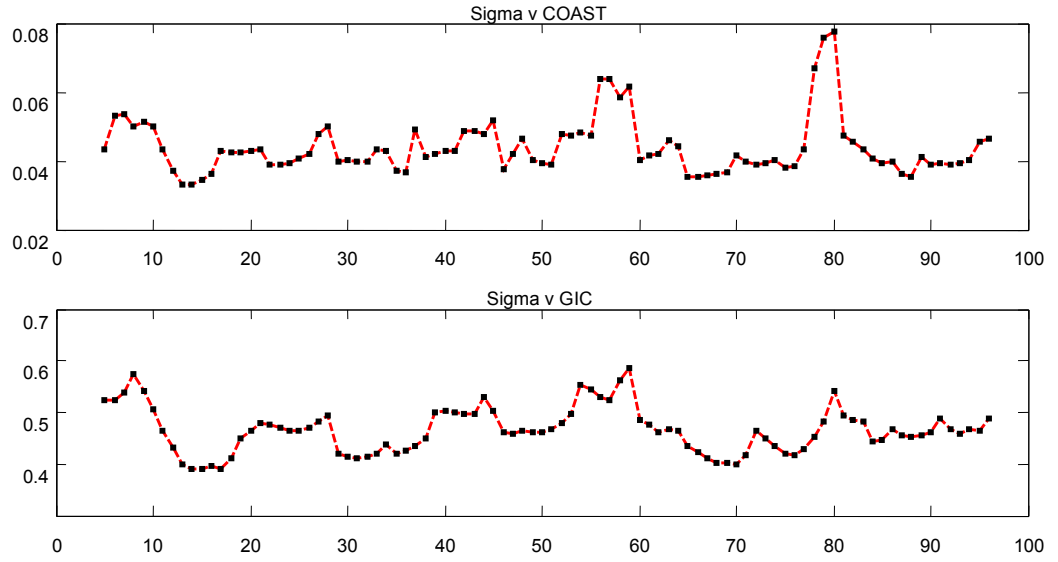


Figure 19: the statistical parameters in R-RAIM VPL

As shown in the two figures above, the final VPL has similar dynamics with the geometry at the initial time, which means the initial geometry parameter largely

influences the VPL dynamics. As for the geometry change during the CT represented by Vertical Dilution of Precision (VDOP) coast, the value is bigger than the VDOP at initial values (VDOP GIC), which means a smaller standard deviation of observations would cause bigger positional precision degradation during the CT. Also, VDOP coast is more stable which means the DOP of the geometry change within constant CT is more stable than the DOP at the initial geometry. Therefore, the geometry during the coast time is more influencing on the final VPL value. The VDOP coast is not as continuous as the VDOP GIC as shown in Figure 18. This is caused by satellite lost if the CT is set large, since only the common satellite from current epoch to the last epoch were used. In the situation when there is less than 4 satellites, the VDOP is set as null.

As for the two precision parameters at the initial time and during the CT, the latter one has higher precision than the first one, mainly due to the use of the relative carrier phrase observations.

3.3.2 The Coasting Time

The ABPO data is used to study the influence of the CT on the position domain MHSS VPL, which is shown in Figure 20.

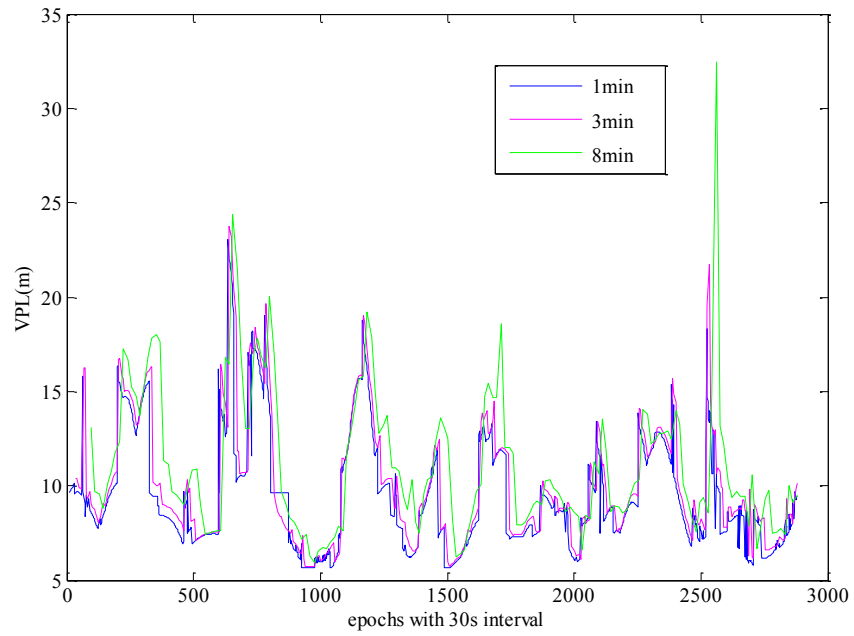


Figure 20: Position Domain R-RAIM MHSS VPL with different CT

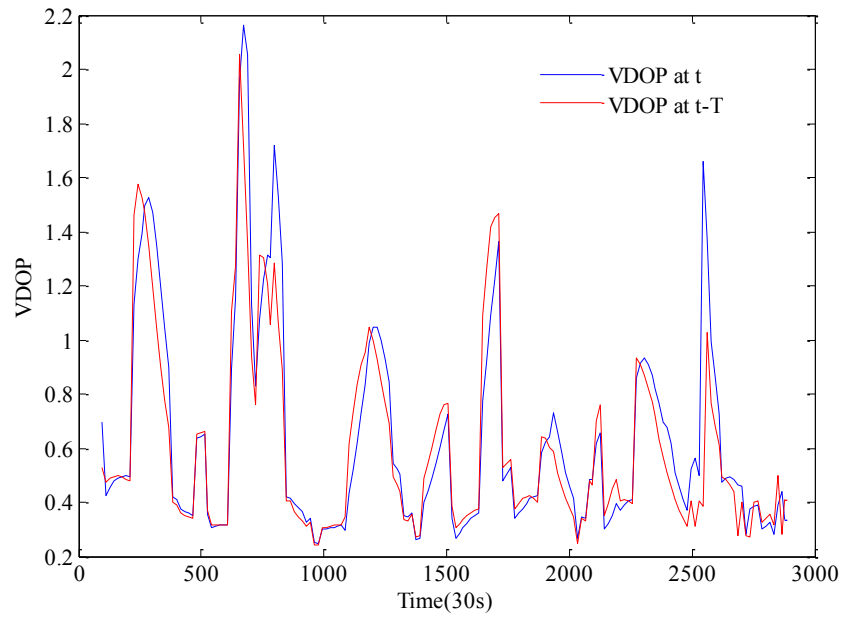


Figure 21: VDOP with CT 8min

It is noted in Figure 20 with CT increased from 1min, 3min to 8min, the whole figure dynamics is shifted rightwards with the geometric shift shown in Figure 21. This is

caused by the bigger delay with bigger time interval, which means the geometry change is reflected in the result slower. Also, the VPL value is increased with larger CT, and therefore there is an optimal CT value for better integrity performance and in this situation 1min is the best choice.

In R-RAIM, positioning solutions at the current time is influenced by geometry both at the initial time and the current time with position error projected by geometry change matrix. With a lot of dynamics in geometry, it is hard to get a definite measure on the effect of geometry change. But in the above cases, where the CT was set to be 1min and 3min, geometry change was very small and the projected error terms was small enough to be ignored compared with other error terms. However with the CT set as 8min, the geometry change is bigger and the error induced by the geometry change stays more dominant.

As shown in the above figure, VPL with the CT set to be 3min is generally bigger than VPL of 1min. The reason is mainly due to the satellite lost during the CT. With the CT increased, the possibility of some satellites becoming invisible is also increased and weak geometry is propagated and exaggerated. With the position domain positioning method, only the satellites visible lasting from the initial time to the current time can be used in the delta range solution. Comparing R-RAIM with CT 1min and 3min, we can see if CT is increased, there is a small tendency of right shift. The reason is that VPL of the current time is related to the information (error and geometry) at the initial time within the CT. With a larger CT, results of the current time are related with the older information.

There is not a dominant criterion to decide a fixed value for the CT. However, the choice of the CT can influence a lot of things, e.g., geometry change to project initial error to current time, probability of cycle slips and other faults happening during the CT, error covariance matrix with errors collected during the CT, etc. The risk caused by the

CT is accounted for in the covariance matrix and the prior probability of any fault exist in the system.

As for the choice of a constant CT, if it was set to be too large, there would be unexpected big geometry changes. If it is too small, there is not enough time for the GIC integrity information to be transmitted. To account for the above problems, we try to use a dynamic CT, which is the longest time during which the number of satellite keeps stable. By using a dynamic CT, we can make the best use of all visible satellites and compensate for the effect of geometry change during the CT. Also in implementation, the effort to examine if satellites are lost during CT is saved.

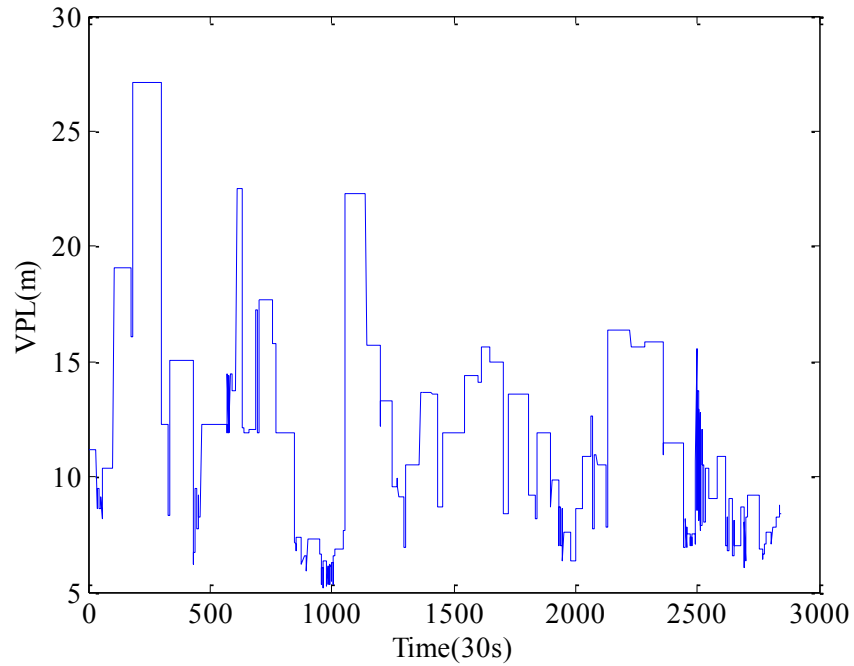


Figure 22: R-RAIM VPL with a dynamic CT

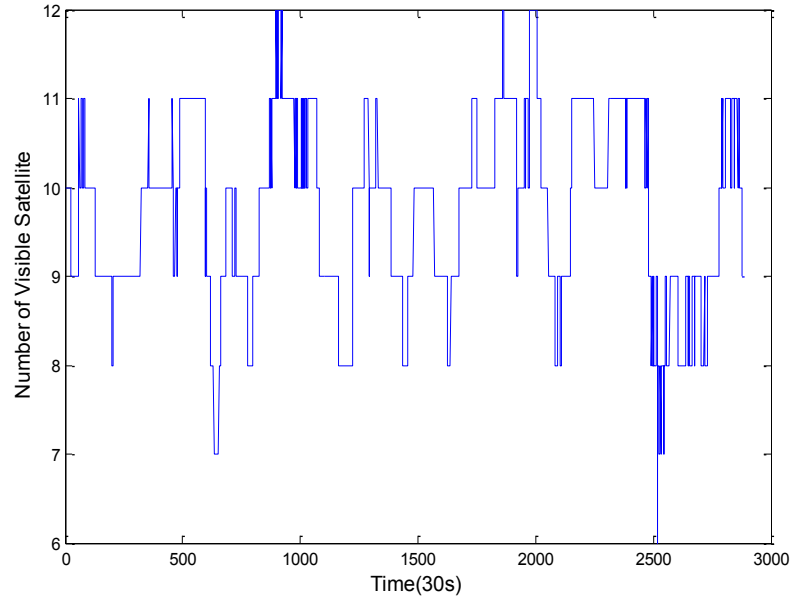


Figure 23: the Number of Visible Satellites

Comparing Figure 22 and Figure 20, VPL at some point is improved but it is worse at other points. Therefore, the issue with a dynamic CT is that CT value is not under control as shown with the number of visible satellites in Figure 23 with the possibility of causing too big a geometric change to propagate the precision.

3.4 Summary

The R-RAIM structure is studied with the focus on two positioning methods and two RAIM algorithms. The precision based on two positioning methods is observed to be close, while the difference on RAIM algorithms will be shown in the next chapter together with the A-RAIM results. The influencing factors both geometric and statistical ones on final VPL results are shown with the conclusion that the geometry at initial time is dominant. Weak geometry is identified to be the main reason for service unavailability in R-RAIM. CT is the unstable element in the R-RAIM design without any mature method to fix an optimal value. A dynamic CT is designed and tested on R-RAIM with unsatisfactory results. Further work on an optimal CT in a relative positioning and RAIM scenario is needed.

CHAPTER 4 ADVANCED RAIM

A-RAIM is adopted as the main architecture in GEAS panel (GEAS 2010) with the advantages that it is not demanding on ground monitoring TTA requirement, since all faults would be detection and the integrity be monitored on the user aircraft. One of the roles of the ground and space monitoring is to maintain a priori fault rate that is later used as an input in the A-RAIM algorithm. With longer allowable TTA, the integrity information can be broadcast with the GNSS satellites, such as the L5 navigation message in modernized GPS. A-RAIM has simpler positioning method with the carrier smoothed code observations used compared with R-RAIM. There are two algorithms used to calculate the VPL including the classic method and the MHSS method, which are introduced in this Chapter.

Also, a study is conducted to compare A-RAIM and R-RAIM with different positioning and RAIM algorithms. In GEAS (2008), the classic RAIM method is used in the range domain R-RAIM, and the MHSS method is used in A-RAIM. The MHSS method for the position domain R-RAIM is developed and optimized in Lee (2008); Lee and McLaughlin (2008). GEAS (2010) reported updated results with A-RAIM adopted as the major method and the position domain R-RAIM was only used when A-RAIM was not available. The MHSS method was applied on both architectures. Also, the optimization method developed for the MHSS (Blanch et al. 2010) can be applied on A-RAIM. Recent studies on A-RAIM with the MHSS method can be found in Milner and Ochieng (2010); Rippl et al. (2011); Wu et al. (2013) with a validation study in Choi et al. (2011a; 2011b).

The comparison of the range domain and the position domain R-RAIM methods with the classical RAIM method is conducted in Gratton et al. (2010). Another comparison of A-RAIM and position domain R-RAIM is provided in Jiang and Wang (2011) with the MHSS algorithm, where the difference in the integrity results is caused by both the position precision and propagation of the errors. These comparisons are conducted with only one or two existing algorithms under an un-unified framework. All existing studies on A-RAIM and R-RAIM are listed in Table 3. This study fills in the gaps of the existing studies and provides a comprehensive comparison with all candidates of RAIM architectures (A-RAIM, range domain R-RAIM, position domain R-RAIM) with both RAIM algorithms applied (the classical method and the MHSS method). The advantages and disadvantages of each candidate are to be pointed out for further study.

Table 3: Existing A-RAIM and R-RAIM Mechanisms

Architectures	Measurements	Positioning	Algorithms
A-RAIM	Code	Stand-Alone	MHSS
R-RAIM	Code	Range	Classic
Range	&Carrier-Phase	Domain	
R-RAIM	Code	Position	MHSS,
Position	&Carrier-Phase	Domain	Classic

4.1 A-RAIM Positioning Methods

The normal snapshot positioning method is used for A-RAIM where position estimation is obtained using code measurements for the current time. The position error with A-RAIM is expressed as,

$$\tilde{x}_A = (A^T Q_A^{-1} A)^{-1} A^T Q_A^{-1} (\epsilon_A + b_A + f_A) \quad (4.1)$$

where:

$A \in R^{m \times n}$ is the design matrix;

$\epsilon_A \in R^{m \times 1}$ is the random error of the code measurement used in A-RAIM with distribution $N \sim (0, Q_A)$;

$b_A = bE$ is the bias term with the scalar component as b and the vector component as the matrix of ones $E \in R^{m \times 1}$;

f_A is the unknown fault vector.

4.2 A-RAIM Algorithms

4.2.1 A-RAIM with the Classic Algorithm

VPL under H_a with the classic RAIM method is,

$$VPL_{A,a} = \delta \cdot \sigma_{A,ss,a} + K(1 - \frac{P_{HML,a}}{2P_{Ha}})\sigma_A + |S_A|b_{max} \quad (4.2)$$

where:

$\sigma_A = \sqrt{[A^T Q_A^{-1} A]_{v,v}^{-1}}$ is the standard deviation of the vertical position error;

$S_A = [(A^T Q_A^{-1} A)^{-1} A^T Q_A^{-1}]_v$ is the projection matrix for bias .

$\sigma_{A,ss,a} = \max(\sigma_{A,ss,i})$ where $\sigma_{A,ss,i} = \sqrt{[(S_{A,i} - S_A)Q_A(S_{A,i} - S_A)^T]_{v,v}}$ is the standard deviation of the vertical solution separation with $S_{A,i} = [(A_i^T Q_{A,i}^{-1} A_i)^{-1} A_i^T Q_{A,i}^{-1}]_v$ and A_i and $Q_{A,i}$ are the design matrix and covariance matrix with ith observation removed.

4.2.2 A-RAIM with the MHSS Algorithm

VPL under H_i with the MHSS method is (GEAS 2008; 2010),

$$VPL_{A,i} = K(1 - \frac{P_{cont,0}}{2P_{H_0}})\sigma_{A,ss,i} + |S_{A,ss,i}|b_{nom,i} + K(1 - \frac{P_{HML,i}}{2P_{H_i}})\sigma_{A,i} + |S_{A,i}|b_{max,i} \quad (4.3)$$

where:

$S_{A,ss,i} = S_A - S_{A,i}$ is the projection matrices for the bias vector.

$\sigma_{A,i} = \sqrt{[A_i^T Q_{A,i}^{-1} A_i]_{v,v}^{-1}}$ is the standard deviation of the vertical subset position error.

$b_{nom,i} = b_n E_i$ and $b_{max,i} = b_m E_i$, E_i is a unit vector E with i th element as zero and b_n is used for calculation of accuracy.

4.3 Numerical Results

Generally, the difference between A-RAIM and R-RAIM is caused by different positioning methods. A comparison is made as follows: 1) Only code measurements are used for A-RAIM, while both code and carrier phase measurements are used for R-RAIM; 2) In R-RAIM, both the TDCP during the CT and the initial time observations are used to obtain the current position, while in A-RAIM, the current position is obtained by current code measurements directly; 3) Taylor expansion can be used for linearization for both methods, while a geometric relationship can also be used in R-RAIM for delta-range positioning (Van Graas 2005); 4) A-RAIM VPL is only a function of current time and location, while R-RAIM is related not only to current time and location but also to the initial time and location.

With the same RAIM algorithm, the difference between these architectures when the calculating the upper bound is in the error model and the error projection matrix. The differences were tested on two RAIM algorithms with different mechanism to allocate risks onto the position error. To get explicit numerical results for LPV-200, the following numerical example was designed.

All RAIM methods are shown with numerical results on A-RAIM and R-RAIM with the worldwide distribution for the availability of service LPV-200 around the world

within 24 hours. The definition of the error model for both architectures can be found in GEAS (2008; 2010). The nominal bias is 0.1m and the maximum bias is 0.75m. URE is 0.25m and URA is 0.5m. The total integrity risk is 2×10^{-7} which is evenly divided into the horizontal and vertical cases. Within the vertical case, the multiple fault modes are excluded, leaving the single fault and fault free hypotheses with total integrity risk as 8.7×10^{-8} . The integrity risk is distributed evenly onto each hypothesis. The prior probability for each single fault mode is 1×10^{-5} . The prior probability for null hypothesis is approximated as 0. The total continuity risk is 9.2×10^{-6} and the probability of the fault free and single fault modes is 8×10^{-6} .

The almanac data from the standard GPS constellation with 24 satellites is used to decide the geometry at each location with 5 x 5 degree grid on the world map at 50m altitudes. With the error model described above, VPL at each location is decided with 1min interval for A-RAIM or different CT for R-RAIM within a 24 hour time span. The availability is computed by comparing each VPL value with the VAL to decide the final availability for each location. The percentage of over 99% availability over this time is shown worldwide. The software is based on the MATLAB Algorithm Availability Simulation Tool by Stanford University. The result is the LPV-200 availability from different methods with VAL set at 35m.

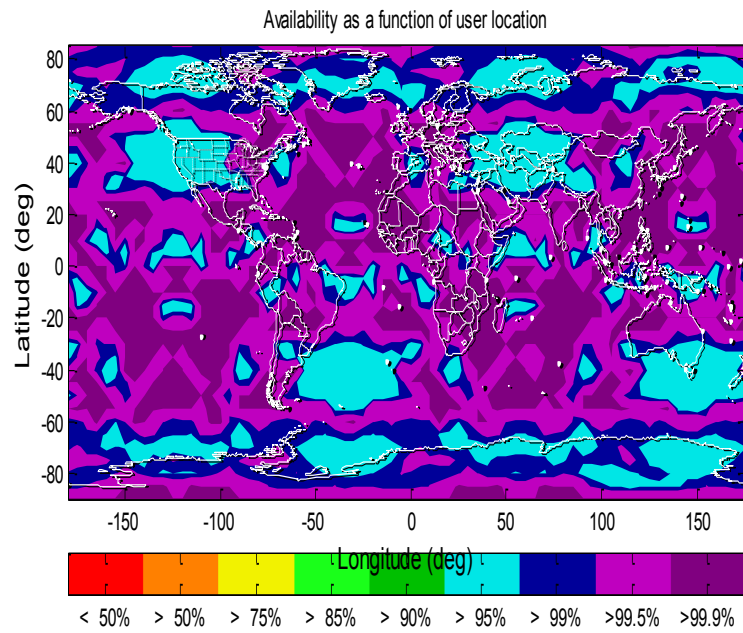


Figure 24: 99% Availability with the Classic Method

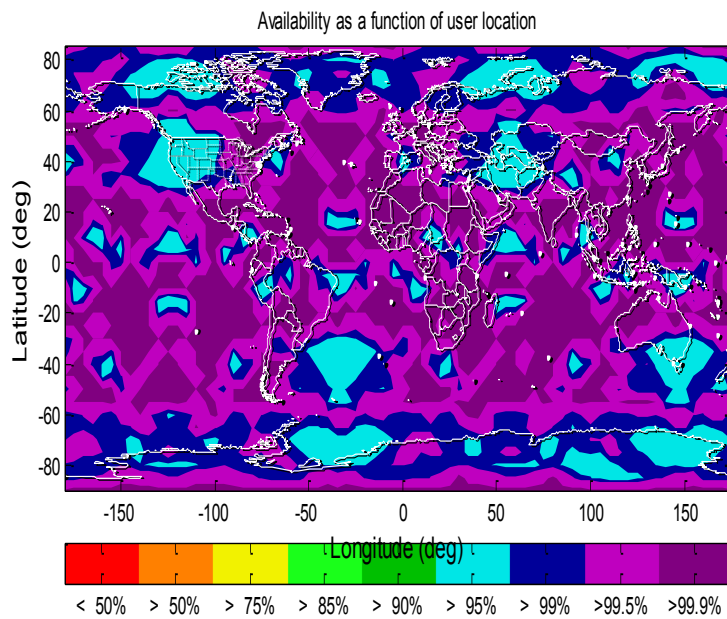


Figure 25: 99% Availability with the Range R-RAIM Classic Method

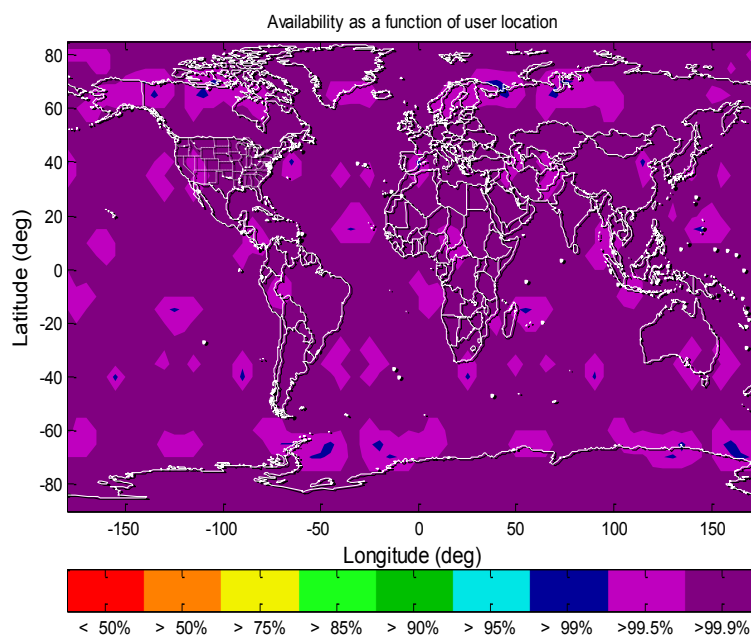


Figure 26: 99% Availability with the Position R-RAIM Classic Method

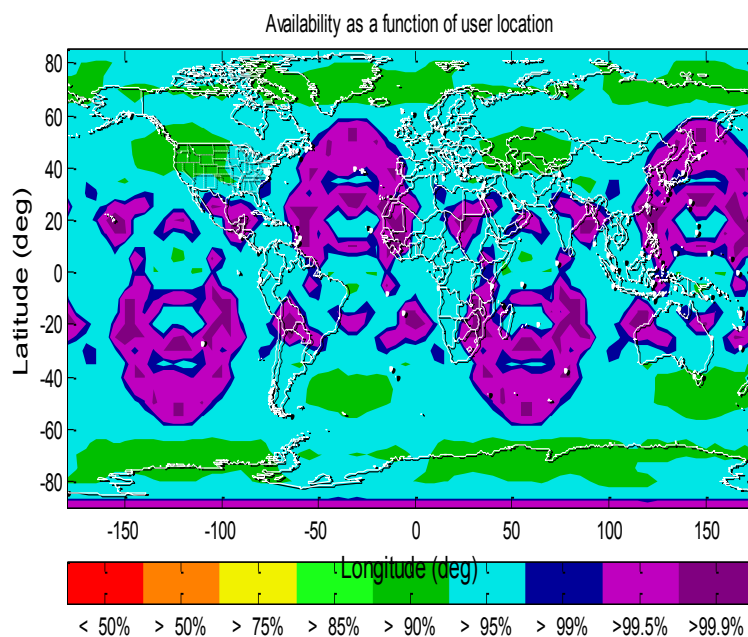


Figure 27: 99% Availability with the MHSS Method

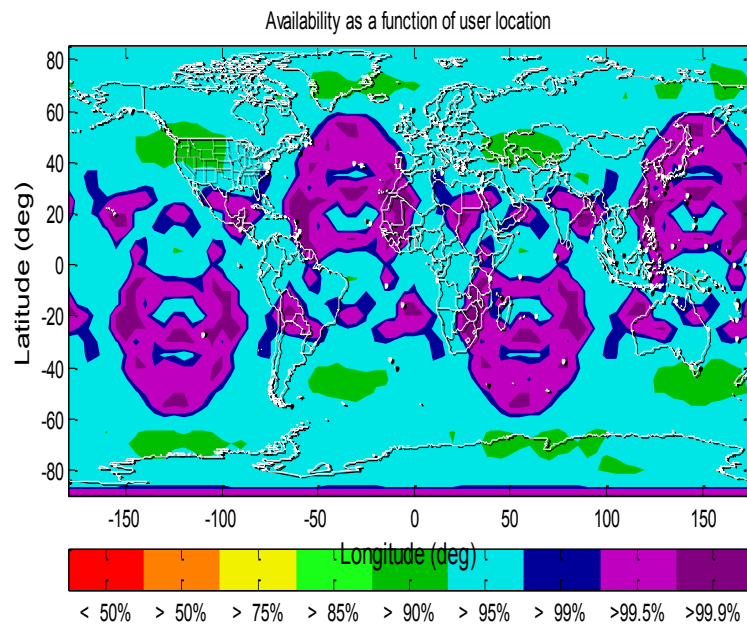


Figure 28: 99% Availability with the Range R-RAIM MHSS Method

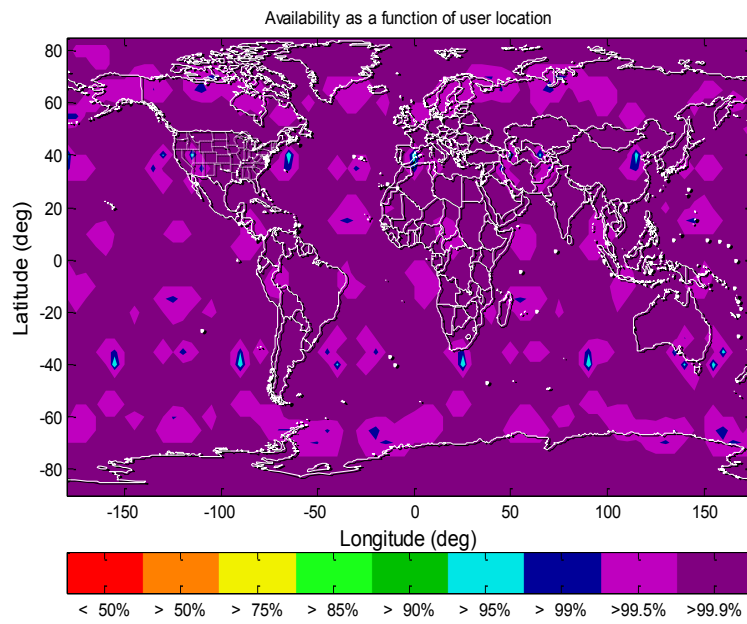


Figure 29: 99% Availability with the Position R-RAIM MHSS Method

Table 4: 99% Availability with A-RAIM and R-RAIM

Availability Coverage	A	B1	C1
Vertical Precision <2 m	63.8%	75.54%	75.71%
Classic RAIM VPL<35m	78.46%	85.68%	100%
MHSS RAIM VPL<35m	31.46%	35.57%	99.03%

***A:** A-RAIM; **B1:** R-RAIM\ Range Domain\ CT 1min;

***C1:** R-RAIM\ Position Domain\ CT 1min.

The influence of different positioning methods on different RAIM architectures can be seen from comparing the columns A/B1/C1 in Table 4 and the influence of different RAIM algorithms from the rows of classic and MHSS RAIM. Based on the results in Table 4, conclusions may be drawn as follows:

- R-RAIM has better integrity results compared with A-RAIM, and R-RAIM with CT 1min has better precision results compared with A-RAIM. The precision results with two R-RAIM positioning methods are very close, but the position domain method has better integrity results than the range domain one.
- The classic method has better integrity results than the MHSS method that can be explained by a more relaxed integrity requirement for the alternative hypothesis. With same integrity risk for the faulty case and assumption of even allocation on each hypothesis, the faulty VPL with the classic method is derived by the integrity risk m times the one used in the MHSS method.
- R-RAIM using the position domain method has a big advantage with the MHSS method compared with the other options. It is the best choice with the classic method, but the difference with the MHSS method is more obvious.

The reason for better integrity results with the R-RAIM position domain method is as follows. It is assumed that there is only fault in the delta carrier phase and no fault in the code measurement in the initial time. With the capability to separate the delta range positioning and initial time positioning in the position domain method, the continuity risk is only allocated to the delta range position error in the position domain method instead of the total position error in the other two methods. With much better precision of the delta range position from the delta carrier phase, the standard deviation with the continuity risk allocated is much smaller, resulting in lower VPL and better availability.

The uncertainty in the R-RAIM architecture is the choice of coasting time, which will influence the results by the sampling rate (Jiang et al. 2010). If it is too small, there is not enough time for the integrity information to transfer. Three different choices of CT are tested in the following tables with both range and position domain methods.

It can be seen in Table 5 and Table 6 that with the increase of the CT for the R-RAIM method, both the precision and the integrity results degraded, which is caused by the loss of visible satellites and errors accumulated during the CT.

Table 5: R-RAIM Range with Different CT

99% Availability Coverage	B1	B2	B3
Vertical Precision <2 m	75.54%	69.71%	49.49%
Classic RAIM VPL<35m	85.68%	78.78%	67.87%
MHSS RAIM VPL<35m	35.57%	31.74%	25.12%

Table 6: R-RAIM Position with Different CT

99% Availability Coverage	C1	C2	C3
Vertical Precision <2 m	75.71%	72.7%	56.63%
Classic RAIM VPL<35m	100%	97.83%	92.45%
MHSS RAIM VPL<35m	99.03%	96.5%	91.7%

***B2:** R-RAIM\ Range Domain\ CT 2min; **B3:** R-RAIM\ Range Domain\ CT 3min

***C2:** R-RAIM\ Position Domain\ CT 2min; **C3:** R-RAIM\ Position Domain\ CT 3min

4.4 Summary

With the same definition of integrity risk and continuity risk, the classic RAIM method has better integrity results than the MHSS method with architectures of A-RAIM and R-RAIM. However, MHSS has the potential to accommodate more complicated failure modes with the multiple hypothesis structure. With the same RAIM algorithm, the R-RAIM position domain method has the best integrity results. The advantage of using this method is most obvious with the MHSS method. Coasting time for R-RAIM in this simulation is found to be best around 1min. With a longer coasting time period, the results deteriorate with lost satellites and accumulated errors. With better integrity results, the disadvantages of R-RAIM include the uncertainty of the coasting time and heavier computation burden.

CHAPTER 5 A NEW APPROACH TO CALCULATE THE EXACT VPL

When calculating the VPL with the conventional algorithms, there are mainly three options: the classic method (Brown and Chin 1998), the method in Walter and Enge (1995) and the solution separation method (Brenner 1996). There are also different ways to fix the size of the unknown bias for calculation of VPL (Ober 2003): MDB, MHB and WCB. The MDB is used in the classic method. The WCB has been used to derive the ideal VPL with the exact value of VPL satisfying the required integrity risk (Milner and Ochieng 2011), which is also applied in A-RAIM (Milner and Ochieng 2010). The WCB that produces the maximum integrity risk is searched within the range of MHB and MDB. However the disadvantage of this procedure is that WCB is highly dependent on the input VPL, which reduces the reliability and accuracy of the results. A new procedure to calculate the exact VPL value is presented to overcome this problem with the following procedure. First, the search bias is defined in the domain of Type II error, which has a one-to-one relationship with the bias size with a given Type I error. And then the VPL corresponding to each Type II error in the search domain is calculated. The maximum VPL is the desired result that is able to protect the user against all possible bias. Also, an optimization algorithm is adopted to reduce the computational time and improve the accuracy of the result.

5.1 The Ideal VPL Method

The exact VPL value that is able to prevent user against all possible bias is illustrated in Figure 30. What is worth noted is that the different β_i in VPL_{BC} and the exact VPL,

example in Figure 31 is used to show this situation. The black horizontal line represents the given integrity risk which was used to derive the MHB and MDB. The integrity risk on the vertical axis is calculated with the bias on the horizontal axis and the VPL_{MO} derived by the correct VPL input (red line) and the wrong VPL input (green line).

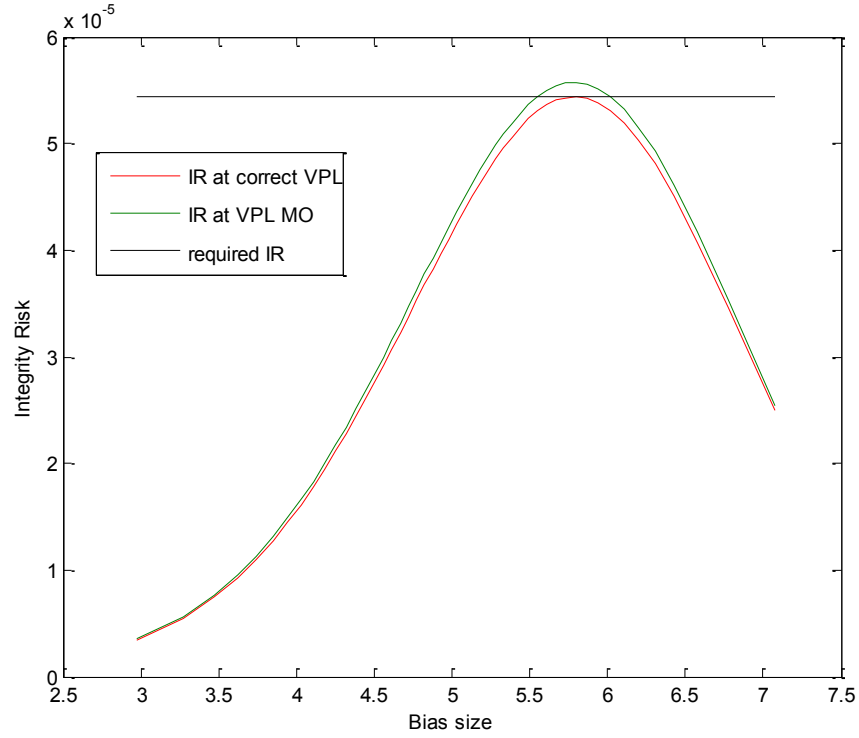


Figure 31: an Example of the wrong input VPL in VPL_{MO}

Therefore another search loop of VPL is added to guarantee the correct VPL input. Thus, the computation process becomes complex and the accuracy of result is uncertain depending on the number of steps in these two loops. This method is referred as the *iterative A* method.

5.2 The Design Process of the New Method

To simplify the *iterative A* method, the following new procedure is proposed. Firstly, β_i and the bias have a one-to-one relationship with the bias derived by β_i and α_i in eqs.

(2.22) and (2.23). When β_i is larger, the bias is smaller. Therefore, the search boundary is defined in the β_i domain as follows,

$$\frac{IR_{VI}}{P_{Hi}} < \beta_i < 1 - \alpha_i \quad (5.1)$$

The relationship between the β_i and VPL with a given integrity risk is shown in Figure 32, and the relationship between the β_i and the integrity risk with a given VPL is shown in Figure 33. β_i is changed to the bias, and similar relationship is shown in Figure 34 and Figure 35. The input integrity risk in Figure 32 and Figure 34 is derived by the input VPL value in Figure 33 and Figure 35. The maximum β_i depicted in Figure 32 and Figure 33 and the maximum bias shown in Figure 34 and Figure 35 are the same respectively. Therefore, the worst case is defined as the maximum VPL in the new procedure instead of the maximum integrity risk. The integrity risk with the maximum VPL is guaranteed to be not bigger than required one among the bias range. In this way, the uncertainty of the input VPL is avoided.

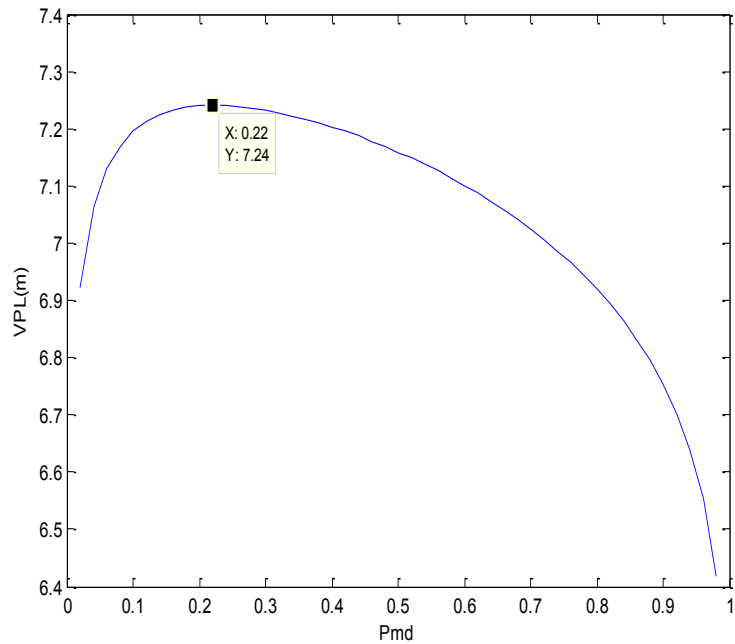


Figure 32: VPL as a function of Type II error

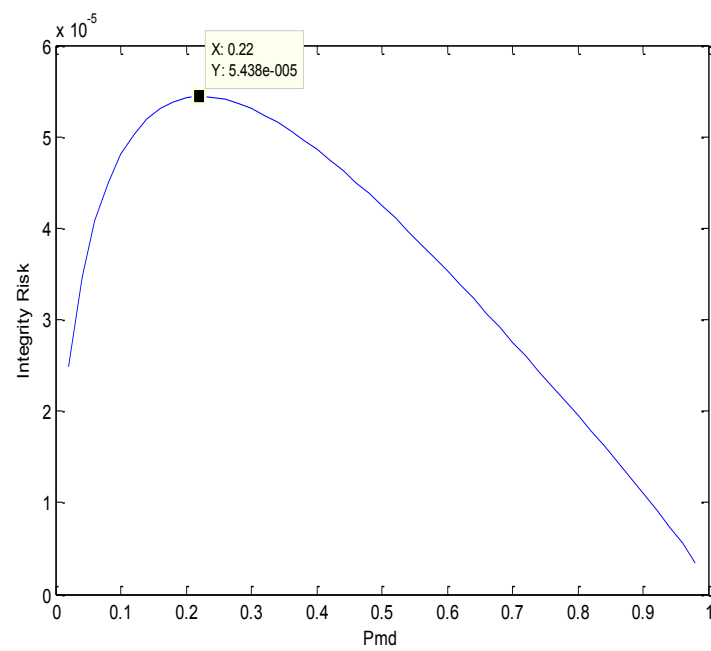


Figure 33: Integrity Risk as a function of Type II error

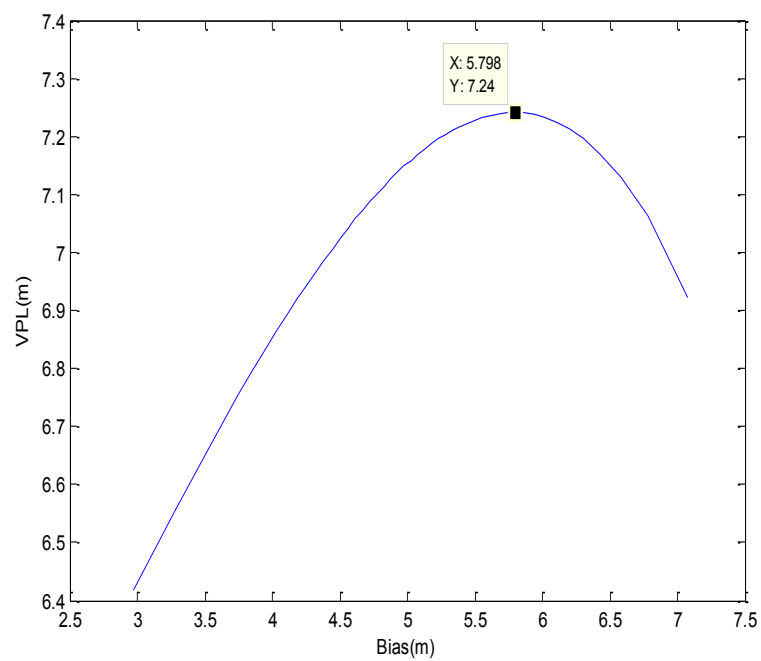


Figure 34: VPL as a function of Bias

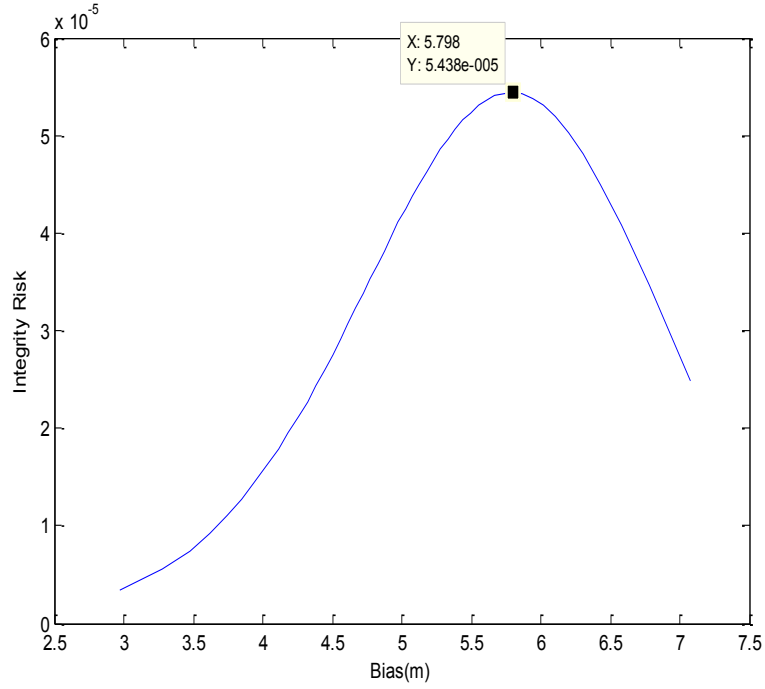


Figure 35: Integrity Risk as a function of Bias

In this method, the β_i range is first divided by pre-defined total number of steps. Within each step, the β_i value is then determined, and the VPL value satisfying defined conditions are calculated. The maximum VPL is the desired result. This is referred as the *iterative B* method with the criterion described as,

$$\max f_{VPL}(\beta_i), \text{ subject to } \frac{IR_{Vi}}{P_{H_i}} < \beta_i < 1 - \alpha_i \quad (5.2)$$

where $f_{VPL}(\beta_i)$ stands for VPL as a function of β_i derived by the equation $\int_{-\infty}^{-VPL} f(x)dx + \int_{VPL}^{+\infty} f(x) dx = \frac{IR_{Vi}}{P_{H_i}\beta_i}$, and $f(x)$ is the probability density function of \tilde{x}_v .

The computational efficiency is improved with one search loop in the *iterative B* method. But it is still not able to control the accuracy of the result. Therefore, an *optimization method* is applied to find the maximum of a single-variable function within a fixed interval. There are two MATLAB implementations that can be used to obtain result with pre-defined accuracy and higher computational efficiency: *fminbnd* and *fmincon*. The

fminbnd algorithm is based on the Golden Section search and parabolic interpolation, and the fmincon algorithm is based on an interior point method. It is found out that the latter one is faster but is more complicated in implementation since it is designed for more general and complex problem. The first one is slower but simpler and more reliable for this problem. It is tested that the fmincon algorithm can be used for VPL with higher efficiency, but it is not able to be used for HPL. The fminbnd algorithm will be used for HPL computation in Chapter 6. The VPL within pre-defined accuracy is noted as VPL_{new} . Based on the definition of the exact VPL, the theoretical proof of conservativeness for current VPLs is provided in the Appendix B.

5.3 Numerical Results

The accuracy of the result is uncertain with two iterative methods as shown in Table 7 with the new VPL result as 7.2404, the accuracy with iterative A is constrained by the VPL number of steps 5000 with 0~50 range. Also, it is shown that the accuracy is not necessarily better with more steps in the results with the iterative B method. Therefore, the iterative method is not reliable with possibility that the result is lower than the exact value, causing integrity outages.

Table 7: VPL with two Iterative Methods of different number of steps

Steps	10	30	50	100	300
Iterative A(m)	7.24	7.24	7.24	7.24	7.24
Iterative B(m)	7.2394	7.2402	7.2404	7.2403	7.2404

The VPL_{new} determined by the analytical method together with other VPLs are shown in Figure 36 with GPS observations collected on UNSW campus within a 24 hour time span. The mask angle of GPS was 5° . The prior probability for each local hypothesis is 1×10^{-5} . The integrity risk under the faulty case is 2.175×10^{-8} . The P_{FA} of each hypothesis

is 4×10^{-6} . The measurements are assumed to follow standard normal distribution without correlation among each other. It was found that after around 150 steps, the accuracy stays stable. Therefore, 150 steps were used. To ensure convergence in the analytical method, the initial values were chosen by using the search method.

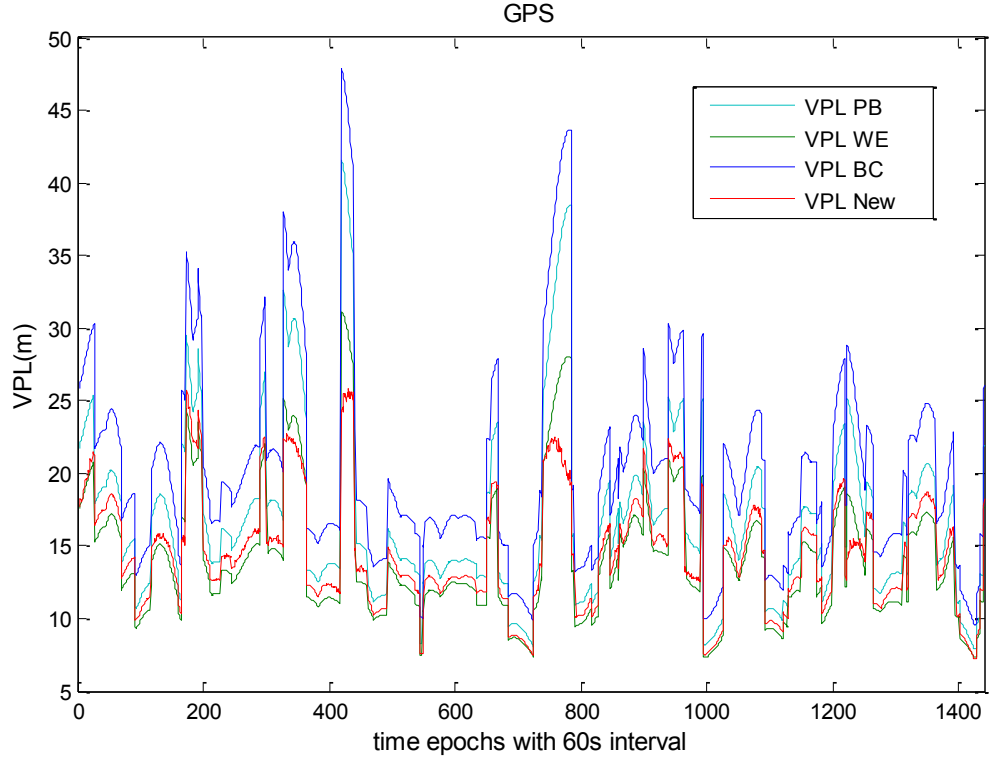


Figure 36: VPL_{new} and other VPLs

VPL_{BC} and VPL_{PB} were always bigger than VPL_{new} with different levels of conservativeness, which is consistent with the proof in Appendix C. There were situations where VPL_{WE} was smaller than VPL_{new} in this experiment, which is evidence that VPL_{WE} is not safe to be used. The computation time with the all methods are listed in Table 8, where the β_i search use 150 steps and the VPL search use 200 steps in the *Iterative A* method.

Table 8: VPL Computational Time per SV in one epoch

	Conventional	Iterative A	Iterative B	New
Time (s)	1.71×10^{-4}	3.56	0.7514	0.05

The risk distribution optimization method for multiple hypothesis RAIM method is applied on the new VPL with the improvement shown in Figure 37.

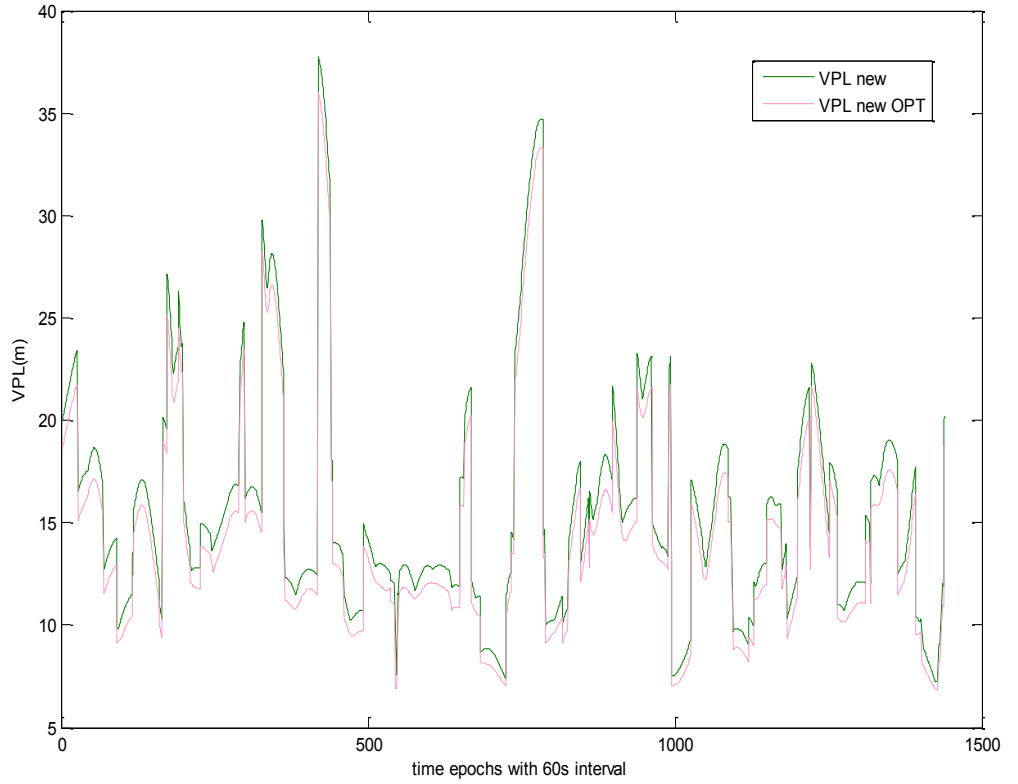


Figure 37: New VPL with Risk Distribution Optimization Method

Also the A-RAIM results with availability distribution worldwide are shown with setting as above.

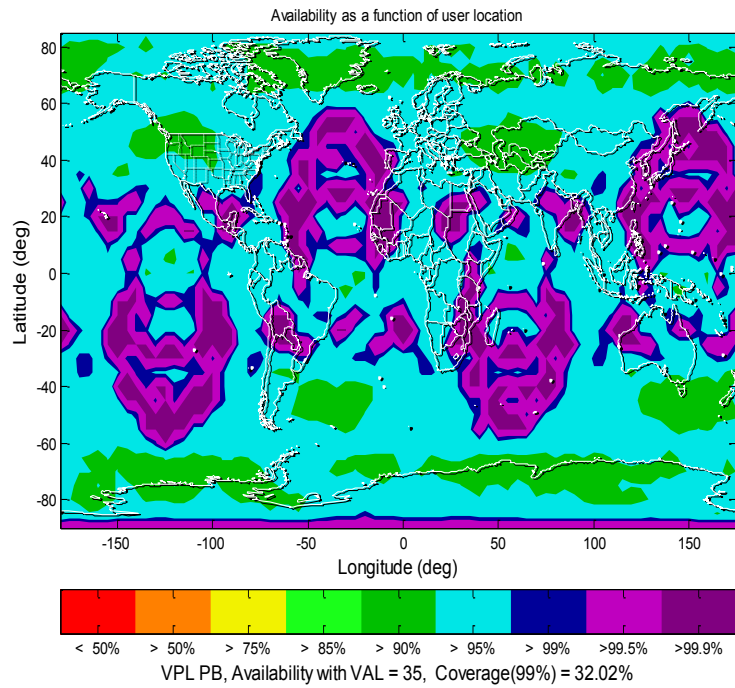


Figure 38: 99% Availability with VPL PB, 24GPS

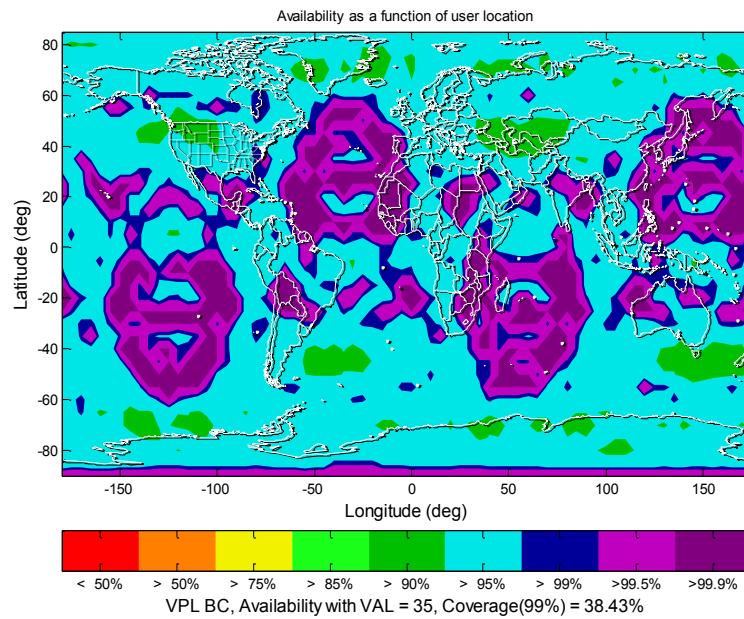


Figure 39: 99% Availability with VPL BC, 24GPS

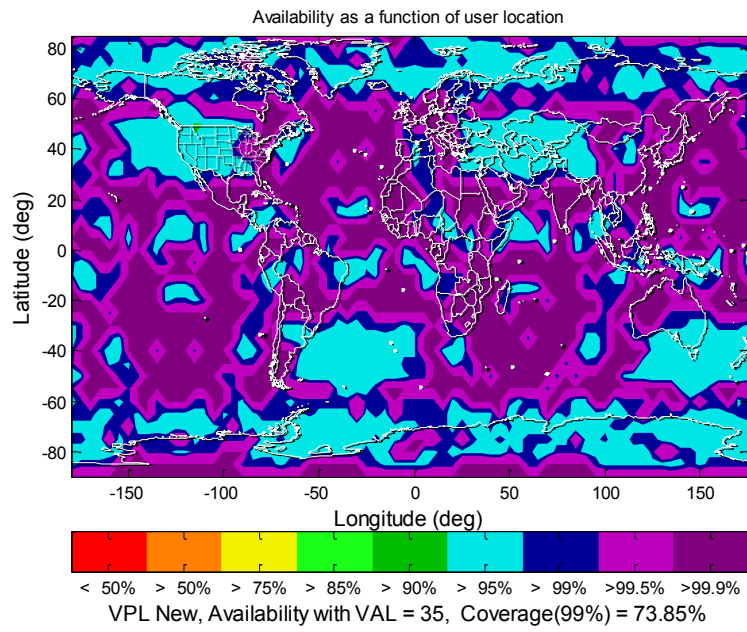


Figure 40: 99% Availability with New VPL, 24GPS

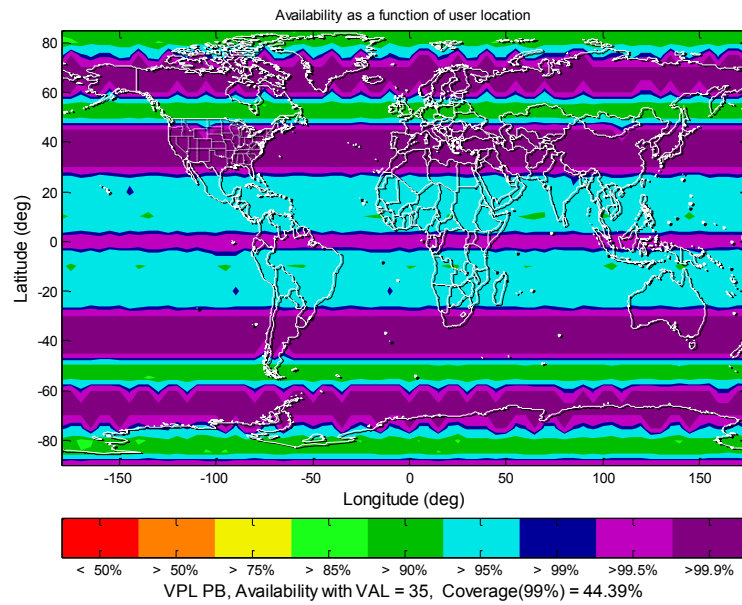


Figure 41: 99% Availability with VPL PB, 27Galileo

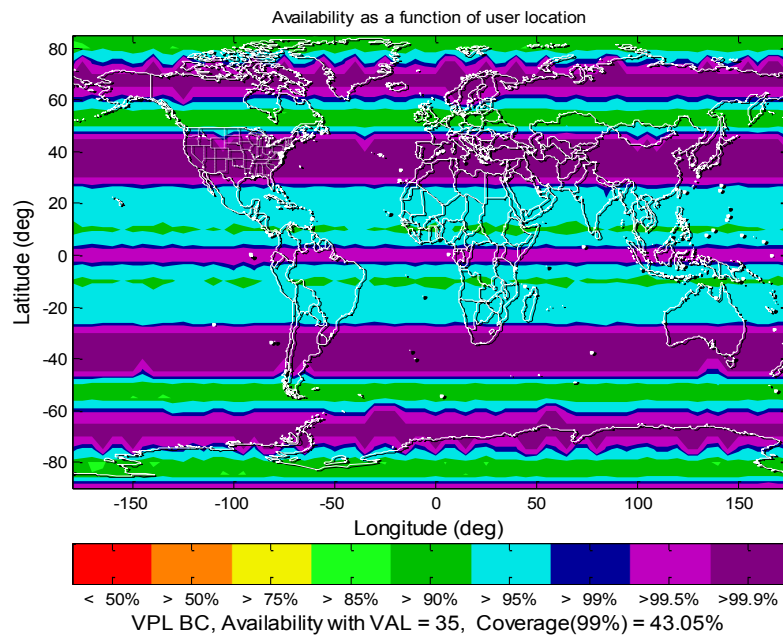


Figure 42: 99% Availability with VPL BC, 27Galileo

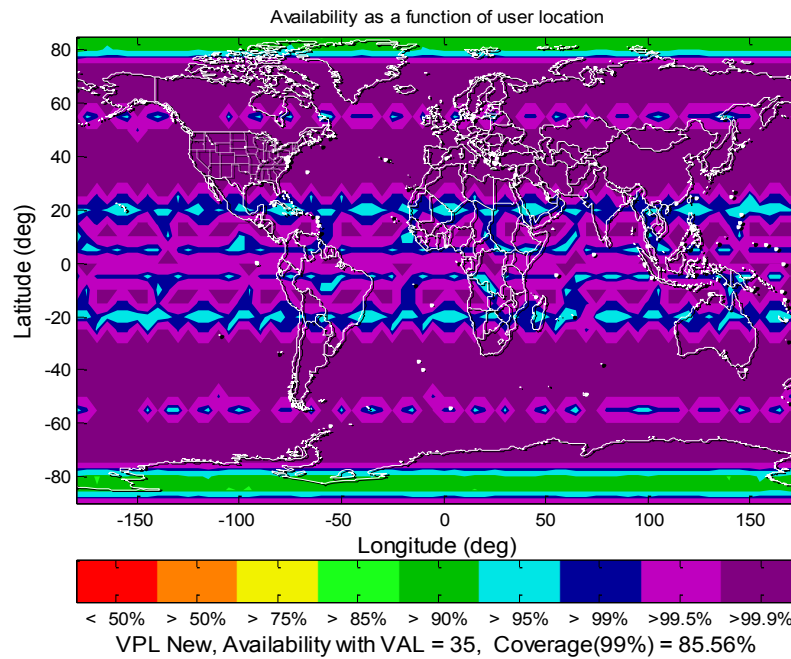


Figure 43: 99% Availability with New VPL, 27Galileo

Table 9: 99% VPL Availability with multiple hypothesis RAIM

RAIM Algorithms	VPL_{PB}	VPL_{BC}	VPL_{new}
24 GPS	32.02%	38.43%	73.85%
27 Galileo	44.39%	43.05%	85.56%

It has been shown that A-RAIM performance is greatly improved using the new VPL with both GPS and Galileo. It should also be noted that the new VPL took around 100 times more time to calculate than the other two methods. Also, VPL_{PB} showed worse A-RAIM performance than VPL_{BC} with GPS, but better performance with Galileo. Therefore, it is concluded that there is no definite conclusion comparing the size of VPL_{PB} and VPL_{BC} , which is influenced by geometry.

Comparing the classic method with classic method in a global test 78%, the MHSS method with a local test 31% from Table 4 and the multiple hypothesis results with a local test 38% in Figure 39, it is concluded that risk distribution plays a major role in the final results. With the total integrity risk same, the global test only has one alternative hypothesis to be distributed the integrity risk, while the local test has multiple alternative hypotheses with each one distributed smaller integrity risk and therefore higher VPL.

5.4 Summary

The new procedure is demonstrated to be simpler, more reliable and more computational efficient than the ideal VPL to gain the exact value within the required integrity risk. A-RAIM performance is greatly improved with the new VPL compared with the conventional ones from 32%-38% to 74% with GPS and from 44%-43% to 85% with Galileo. Also, the VPL_{BC} and VPL_{PB} methods are proved to be safe regardless of the size of the bias, while the other method is not.

CHAPTER 6 THE EXACT HPL AND HIGHER DIMENSIONAL PROTECTION LEVEL

There are two major issues to calculate the exact HPL with given integrity risk. First, the distribution of the horizontal position error is too complicated to calculate the probability of position error for real time applications. Second, the determination of the worst case is also not straightforward to accommodate all possible bias values. Various methods were proposed to simplify the calculation, resulting in approximated HPLs. Two approximated distributions of the horizontal position error are used in the conventional method including the normal approximation (Lee 1995) and the chi-squared approximation (Ober 1997). The first one has the disadvantage of underestimating the probability in some cases and the latter one is an overestimate (Ober 1997). Approximations are also made on the second issue to speed up the process. Without a search for the worst case, specific formulas were given in the conventional methods (Brown and Chin 1998; Walter and Enge 1995; Brenner 1996). These approximations can speed up the HPL computation, but they are designed to be conservative with higher protection level than the exact one. The exact HPL value can achieve higher service availability, which is pursued by solving the two major issues.

A Monte Carlo simulation is commonly used to calculate the probability of position error, which is very time-consuming. Two ways to calculate the exact position error probability are identified to be equivalent (Johnson and Kotz 1970; Ober 1997; Ober 1998): 1) the integration of the distribution for 2D position error in a quadratic form; 2) the integration of the bivariate normal distribution over a circle. Several implementations are studied and

compared for the first approach (Duchesne and Lafaye de Micheaux 2010) and the one in Imhof (1961) showing reliable results is used here. The latter one is applied with a method (DiDonato and Jarnagin 1961) to speed up the calculation, which was first used in navigation integrity monitoring by Milner and Ochieng (2010). These two implementations to calculate the probability can achieve a pre-defined accuracy, and they are both referred as the “exact distribution” in this paper.

For the second issue, an iterative search was designed in Milner and Ochieng (2011) to search the worst case bias with the maximum integrity risk. But it is shown that the iterative method is not able to control the accuracy of the results with uncertainty caused by the number of steps, and computationally heavy with two search loops (Jiang and Wang 2014b). A new approach was developed here to improve these two performance criteria for the VPL computation (Jiang and Wang 2014b). A similar approach is applied here for HPL. A new iterative method with one search loop is shown to have higher computational efficiency, while the accuracy of the results is still uncertain. An optimization method is then used to generate results within a pre-defined accuracy, and also the computation is much faster than the other methods.

6.1 The Exact HPL

6.1.1 Probability of the Horizontal Position Error

Two implementations to calculate the exact probability P_{HPE} are studied: Imhof approach (Imhof 1961), DJ approach (DiDonato and Jarnagin 1961; Milner and Ochieng 2010b). They are chosen in consideration of the ability to control error tolerance for high accuracy, which is set at 10^{-9} for both implementations.

The Imhof approach is introduced as follows. With the correlation between the east and north error, $\|\tilde{x}_H\|^2$ is not of chi-squared distribution, but a sum of independent chi-squared variables (Ober 1997),

$$\|\tilde{x}_H\|^2 = \tilde{y}^T S_{EN}^T S_{EN} \tilde{y} = \sum_{j=1}^2 \lambda_j \|q_j^T \tilde{y}\|^2 \quad (6.1)$$

where $\tilde{y} = y - A\hat{x}$ is the observation error vector, which is the difference between the real value and the estimated value; The eigen-decomposition of the symmetric matrix $S_{EN}^T S_{EN}$ is $D^T \Lambda D$ with Λ as the diagonal matrix, λ_j as the non-zero diagonal elements, q_i as the corresponding eigen-vector, which is the columns of the orthogonal matrix D . Therefore, $\|\tilde{x}_H\|^2$ is a linear composition of independent chi-squared variables $\|q_j^T \tilde{y}\|^2$ with 1 degree of freedom and non-centrality parameter δ_j . The probability of P_{HPE} can be computed with the Imhof method,

$$P\{\|\tilde{x}_H\|^2 > HPL^2 | H_i\} = 0.5 + \frac{1}{\pi} \int_0^\infty \frac{\sin \theta(u)}{u \rho(u)} du \quad (6.2)$$

where $\theta(u)$ and $\rho(u)$ are,

$$\theta(u) = 0.5 \sum_{j=1}^2 [\tan^{-1}(\lambda_j u) + \delta_j \lambda_j u (1 + \lambda_j^2 u^2)^{-1}] - 0.5 HPL^2 u \quad (6.3)$$

$$\rho(u) = \prod_{j=1}^2 [(1 + \lambda_j^2 u^2)^{\frac{1}{4}} \exp\left(\frac{\delta_j \lambda_j^2 u^2}{2 + 2\lambda_j^2 u^2}\right)] \quad (6.4)$$

With given error tolerance E_U , the upper bound of the upper limit U of the integral in eq. (6.2) can be derived by,

$$E_U = \pi U \prod_{j=1}^2 [\lambda_j^{\frac{1}{2}} \exp\left(\frac{\delta_j \lambda_j^2 U^2}{2 + 2\lambda_j^2 U^2}\right)] \quad (6.5)$$

With the east and north de-correlated (Milner and Ochieng 2010b), the DJ approach was applied, where a rectangular bound was defined to replace the cross area between an ellipse and a circular to reduce the computational load (DiDonato and Jarnagin 1961). The center position of the circular is the absolute value of the bias position after rotation of the correlation system. The given error tolerance is used to adjust the rectangular bound. Both implementations and the two approximated ones (Chi-squared, Normal) are compared with the exact one in Figure 44 with a single epoch example of 7 visible

satellites and a 12m outlier on the first observation. The value obtained by the integration of cross area between the ellipse with the bivariate normal distribution and a circle is used as a reference which is referred as the Bivariate Normal.

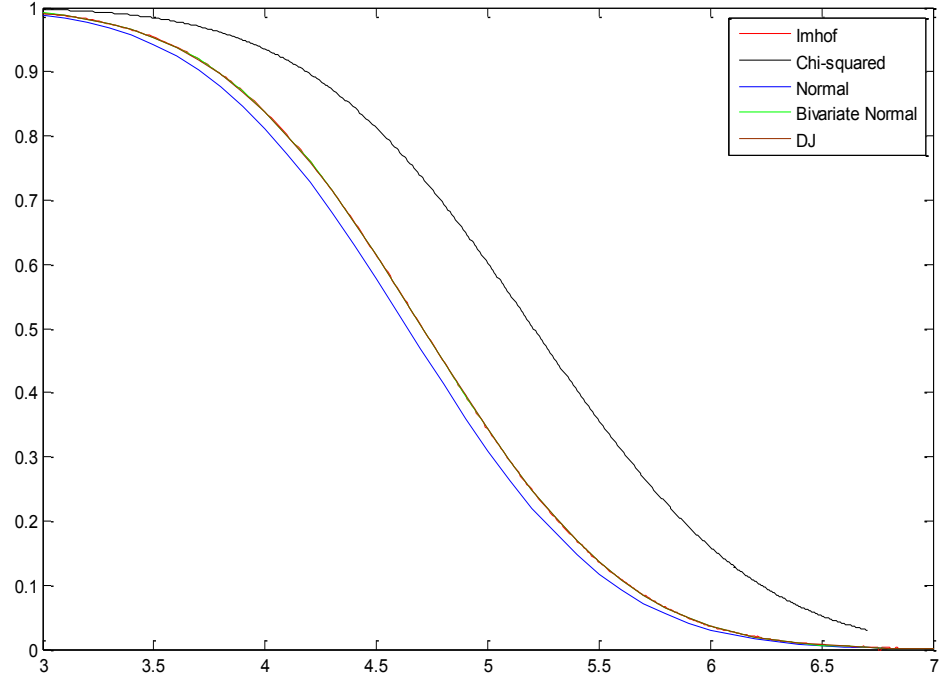


Figure 44: P_{HPE} as a function of HPL with different distributions

As shown in Figure 44, the probabilities based on the Imhof and DJ approaches with 10^{-9} error tolerance are almost the same with the Bivariate Normal one. The chi-squared approximation is conservative with larger P_{HPE} , while the normal approximation is not. Similar conclusion can be found in Ober (1997). With the Intel Core 2 Duo Processor E8400, the computational time per SV to calculate the P_{HPE} with different approaches is shown in Table 10.

Therefore, the DJ approach should be used with the higher accuracy and computational efficiency. It should be also noted that the Imhof approach is more general and can be used for higher dimensional cases.

Table 10: The average computational time of P_{HPE} per SV

per SV	<i>Bivariate Normal</i>	<i>Imhof</i>	<i>DJ</i>	<i>Chi-squared</i>	<i>Normal</i>
Time (ms)	100	85	0.5	0.79	0.35

6.1.2 A New Approach To Calculate HPL

The second issue is about the search of the worst case in a boundary. The boundary can be in the β_i domain as $\frac{IR_{Hi}}{P_{Hi}} \sim 1 - \alpha$ with $\frac{IR_{Hi}}{P_{Hi}}$ given as 10^{-3} , or equivalently in the bias range from 0 to MDB in Milner and Ochieng (2010b). With a closed boundary, it is guaranteed that there is always an extreme value. The mechanism is shown in Figure 45, with the decrease of β_i in the range, the non-centrality parameter is increased from δ_a to δ_c . The corresponding HPL increases from $HPLa$ to $HPLb$ and then decrease to $HPLc$. Therefore, a search is needed to obtain the worst case.

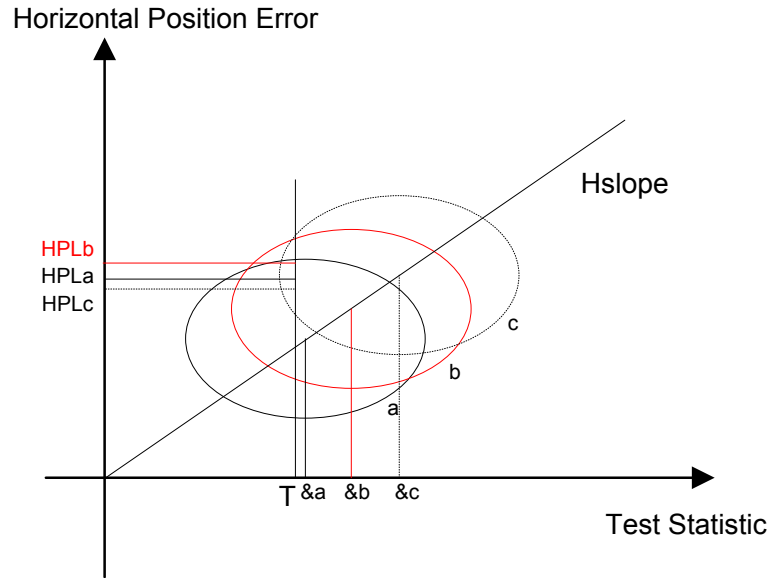


Figure 45: Illustration of the search method

To search the worst bias among the β_i range, it is necessary to define the worst case first. Both the maximum HPL with a given integrity risk and the maximum integrity risk with a

given HPL can be used as shown in Figure 46 and Figure 47. Both the maximum values are obtained at the same β_i value point 0.1501, which means both produce the same HPL values. Therefore, two ways can be used to search two worst cases with the maximum integrity risk and maximum HPL respectively.

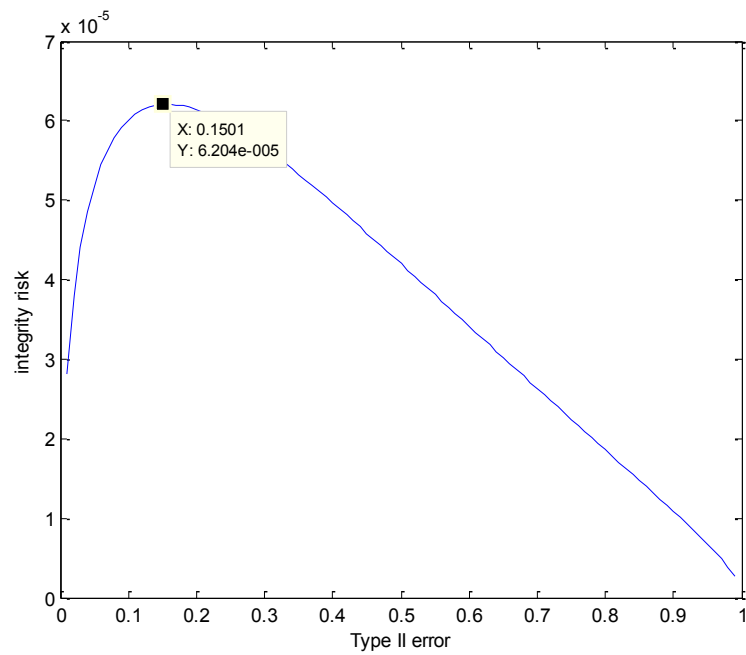


Figure 46: Type II error and Integrity Risk with given HPL

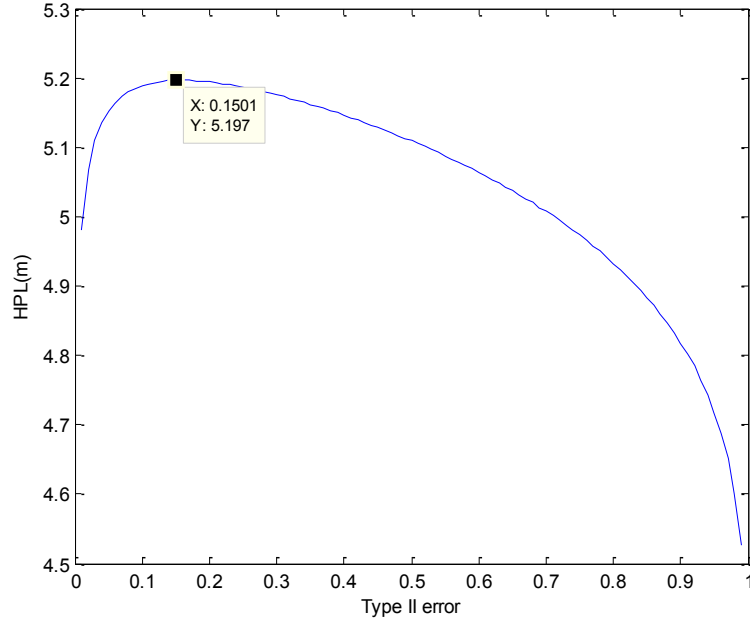


Figure 47: Type II error and HPL with given Integrity Risk

A procedure is defined in Milner and Ochieng (2011) with maximum integrity risk as the worst case to calculate the ideal VPL, which can be applied for HPL too and referred as the *iterative A* method. There are two iterative search loops with the inner loops as the bias range and the outer one as the input HPL range. For each inner loop, there is a worst bias point that has the maximum integrity risk with the given input HPL. For all the input HPL values in the outer loop, the one that generates the maximum integrity risk closest with the given integrity risk is the desired value. The process is described as follows. In the outer loop, an upper value U is chosen to decide the range $0 < HPL < U$ with HPL_k as the value at step k . The β range $10^{-3} < \beta_i < 1 - \alpha$ is used in the inner loop with β_{ij} as the value at step j . In each step j , the integrity risk $P\{\sqrt{\|\tilde{x}_H\|^2} > HPL_k | H_i\} \beta_{ij}$ is calculated and the maximum one among the inner loop is chosen. The HPL_k that generates the maximum integrity risk which is closet to 10^{-3} is the final result. Therefore, the accuracy of the results and computational time is dependent on the number of steps in two loops.

A new criterion is designed to obtain the maximum HPL within a fixed interval of β_i , which has the same worst case and result as the maximum integrity risk,

$$\max f_{HPL}(\beta_i) \text{ with } 10^{-3} < \beta_i < 1 - \alpha \quad (6.6)$$

where $f_{HPL}(\beta_i)$ stands for HPL as function of β_i , which is derived by the equation $P\{\sqrt{\|\tilde{x}_H\|^2} > HPL|H_i\}\beta_i = 10^{-3}$.

An iterative method is designed as follows. First, the β_i range is divided by the number of steps N with β_j as the value at step j . Then, the HPL_j corresponding to each β_{ij} are derived by equation $P\{\sqrt{\|\tilde{x}_H\|^2} > HPL_j|H_i\}\beta_{ij} = 10^{-3}$, where optimization tool to solve non-linear equations are used. The maximum HPL_j is therefore the desired result. In this way, the outer loop is removed and it is referred as the *iterative B* method. The accuracy of the results and computational time is only dependent on the number of steps in one search loop.

In these two iterative methods, the result would be close to the theoretical value if the steps are close to infinite. However, the number of steps cannot afford to be too big with the requirement of TTA in RAIM. Otherwise the integrity information cannot be transmitted to users in time. Normally, TTA should be within a few seconds, for example the TTA requirement for the LPV-200 service is 6.2 seconds. With smaller steps scale, it is observed that the accuracy of the results is not necessarily better with more steps. The reason lies in the uncertainty of the location of the worst case and the step size. An example is given in Figure 48 with various steps: 5, 10, 20 and 30. The worst case under each steps are marked with a rectangular box. It can be seen that the HPL with 20 steps is closer to the correct HPL than with 30 steps. With all the uncertainties, it is concluded that the iterative methods are not only too time consuming, but also lacks sufficient accuracy. Therefore, a new method is desirable that is able to control the result within a pre-defined accuracy level.

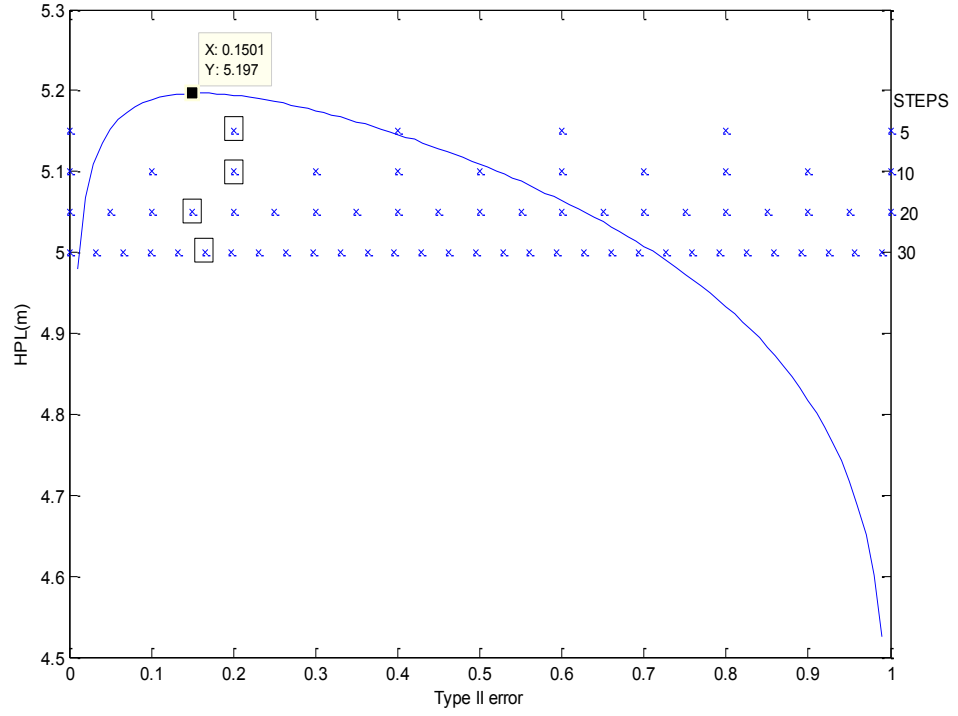


Figure 48: The uncertainty in iterative methods with the number of steps

To gain a HPL value with higher accuracy and computational efficiency, an optimization algorithm is used to find the maximum value within a fixed interval. The MATLAB implementation *fminbnd* is used, which is able to find single local minima with a continuous function of one variable. It is based on golden section search and parabolic interpolation (Forsythe 1976). The criterion is then adapted to be used in this optimization tool, where β_i is treated as the unknown parameter that needs to be solved and HPL is expressed by β_i with $P\{\sqrt{\|\tilde{x}_H\|^2} > HPL|H_i\}\beta_i = 10^{-3}$. The termination tolerance is set as 10^{-8} to guarantee the accuracy of the final results. The maximization problem is adapted as minimization problem by being subtracted from 100. The initial value is set as $HPL_{WEi}-2$ according to experiment data to speed up the solving process. The performance of this method is evaluated in the next section.

Based on the definition of the exact HPL, the theoretical proof of conservativeness for current HPLs is provided in the Appendix D.

6.1.3 Numerical Results

Results from two iterative methods with different steps for β_i range are compared in Table 11, where the HPL is ranged between 0~50 with 50,000 steps to achieve 0.001m accuracy in the *iterative A* method. With the error tolerance of β_i set as 10^{-8} , the result from the optimization method 7.3384m is used as the reference point.

Table 11: Different HPL values in one epoch with various steps

Steps	10	30	40	50	100	200	10000
Iterative A (m)	7.241	7.337	7.337	7.332	7.338	7.338	7.338
Iterative B(m)	7.2407	7.3368	7.3377	7.3319	7.3382	7.3383	7.3384

It can be seen from Table 11 that with the result from the *iterative B* method is not necessarily getting better accuracy with larger steps comparing step 40 and 50, which is consistent with the analysis in Figure 48. But with extremely large steps 10000, the value is close to the optimization one. Also, with search step larger than 100, the result stays relatively stable with 10^{-4} accuracy. With an additional search loop in the *iterative A* method, the HPL precision is constrained by the outer the number of steps with 0.01m accuracy. But this accuracy is not reliable since it is still susceptible to the uncertainty caused by the search in the β_i range. An example is the result with 40 and 50 steps in Table 11, where the result with larger steps obtains less accurate result, which is the same as the *iterative B* method. Therefore, it is concluded that another search loop in the *iterative A* method is still not able to control the accuracy of the result.

To evaluate the result with more geometry varieties, the *iterative B* method with 150 steps and 10 steps are compared with the optimization method in Figure 49 with the same collected data used in Figure 36. It is assumed that the error is of standard normal distribution without correlation.

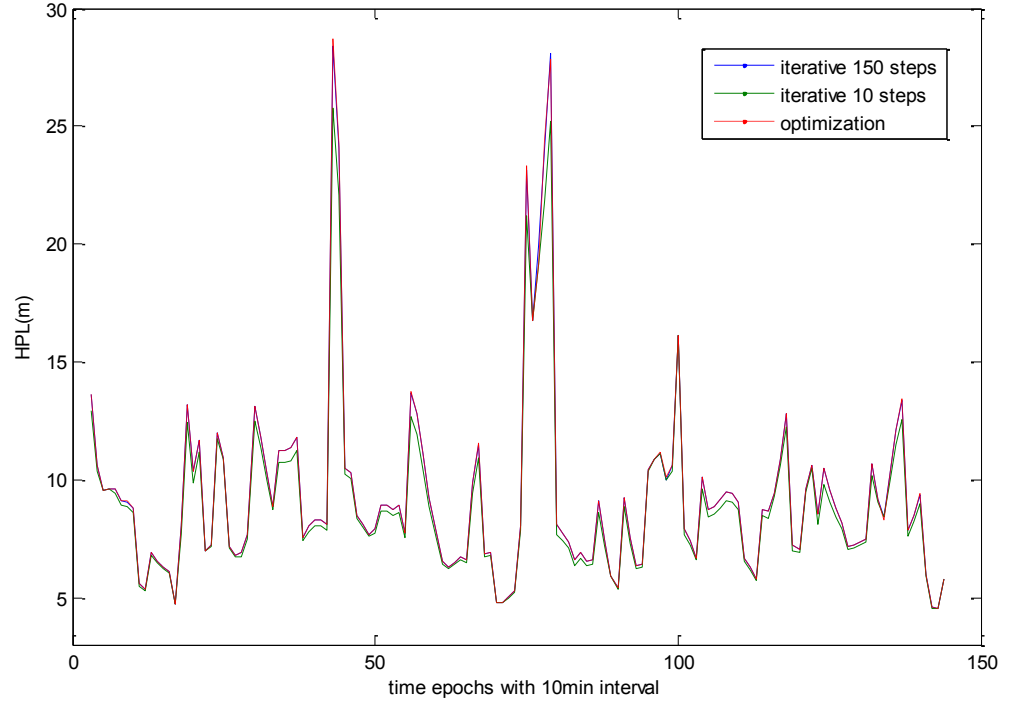


Figure 49: The iterative methods and the optimization approach for the new HPL

It is shown in Figure 49 that the result from the iterative method with 150 steps is very close with the result from the optimization method. But the result from the iterative method with 10 steps is smaller than the optimization method at the scale of 0.1m, and therefore the accuracy of the result from the iterative method is more uncertain depending on the number of steps, while the optimization method is more reliable.

With the Intel Core 2 Duo Processor E8400, the average computational time per epoch is shown in Table 12. For both iterative methods, the total search step is 100 in the β_i range. HPL is ranged between 0~35 with 350 steps with 0.1m accuracy.

Table 12: The average computational time of HPL in one epoch

	<i>per SV</i>	<i>7SV</i>	<i>8SV</i>	<i>9SV</i>	<i>10SV</i>
Iterative A(s)	2.60	19.2	20.4	23.2	25.4
Iterative B (s)	1.30	4.86	9.44	13.8	17.8
Optimization (s)	0.56	2.31	3.93	5.98	7.66

With 100 search steps, the result from the *iterative B* and optimization method is close, but it is shown in Table 12 that the optimization method is faster with less than half of the time used per SV than the *iterative B* method. All existing approximated algorithms to calculate HPL are examined by comparing with the new optimization value in Figure 50.

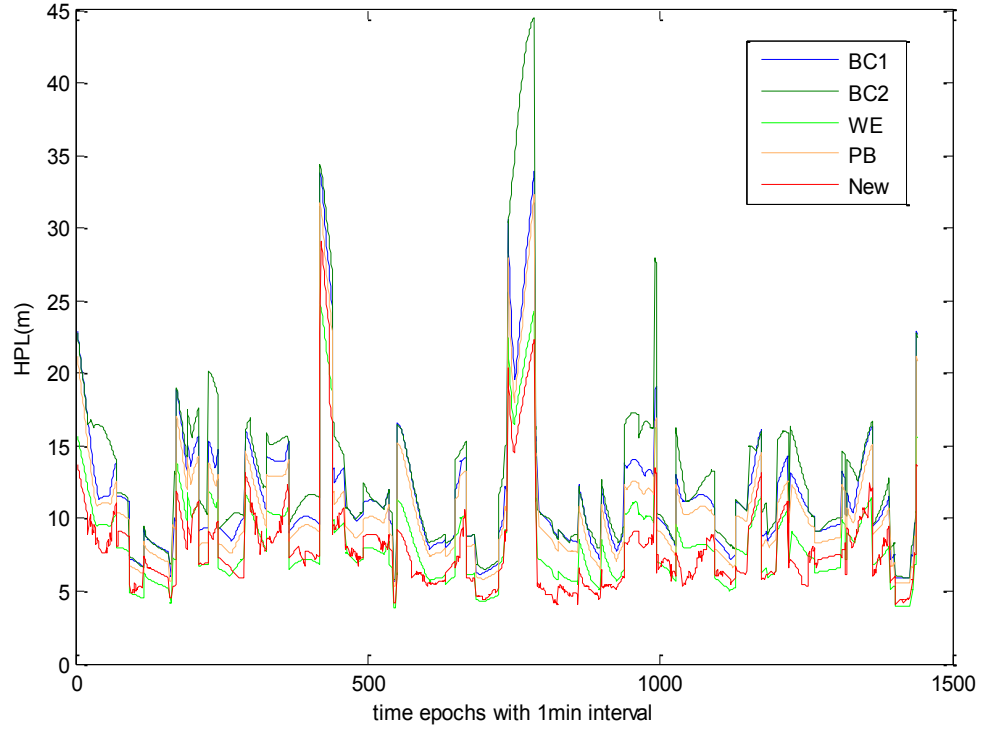


Figure 50: the new HPL and other approximated HPLs

As shown in Figure 50, the two HPL_{BCS} and HPL_{PB} are conservative which is consistent with the theoretical proof in the Appendix. HPL_{WE} is not safe with cases with values bigger than the new HPL in some cases. Although the normal approximation distribution is not safe compared with the exact distribution, the HPL_{BC2} based on it is conservative in this example, which needs further examination.

To quantify the performance improvement with the new HPL, the simulation for worldwide availability distribution is set up as follows. The almanac data for the standard 24 GPS constellation and 27 Galileo constellations was used respectively to determine the geometry at each location with a 5×5 degree grid on the world map at 50m altitude. The error model is adopted from GEAS (2008) for A-RAIM, and a bias term was added to gain more conservative results. The values for the nominal bias and the maximum bias were 0.1m and 0.75m separately. The URE and URA were 0.25m and 0.5m. The risk

definition is the multiple hypothesis requirements for HPL defined in Chapter 2. Results of HPL at each location are decided every 6min among the 24 hour duration. Mask angle of GPS is set at 5° . The availability was determined by comparing each HPL value with the alert limit (35m) for each location in one day. The percentage of having over 99% availability over this time is shown worldwide. The simulation software is based on the MATLAB Algorithm Availability Simulation Tool provided by the Stanford University.

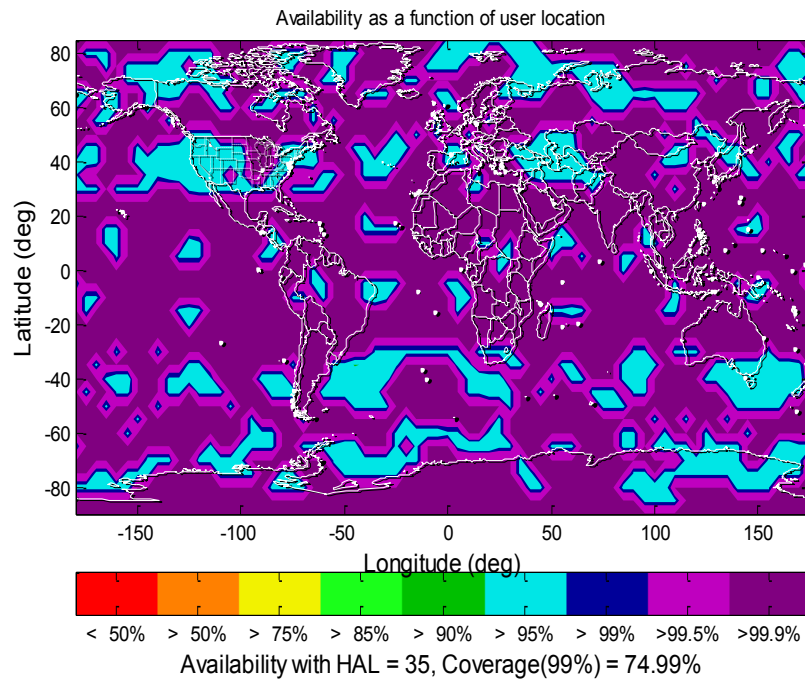


Figure 51: 99% Availability with HPL_{BC1} , 24 GPS

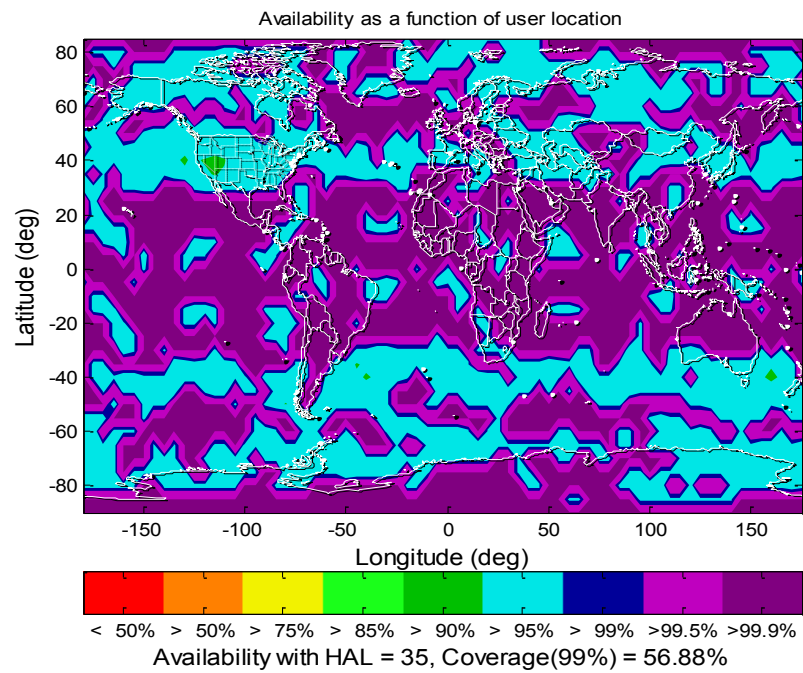


Figure 52: 99% Availability with HPL_{BC2} , 24 GPS

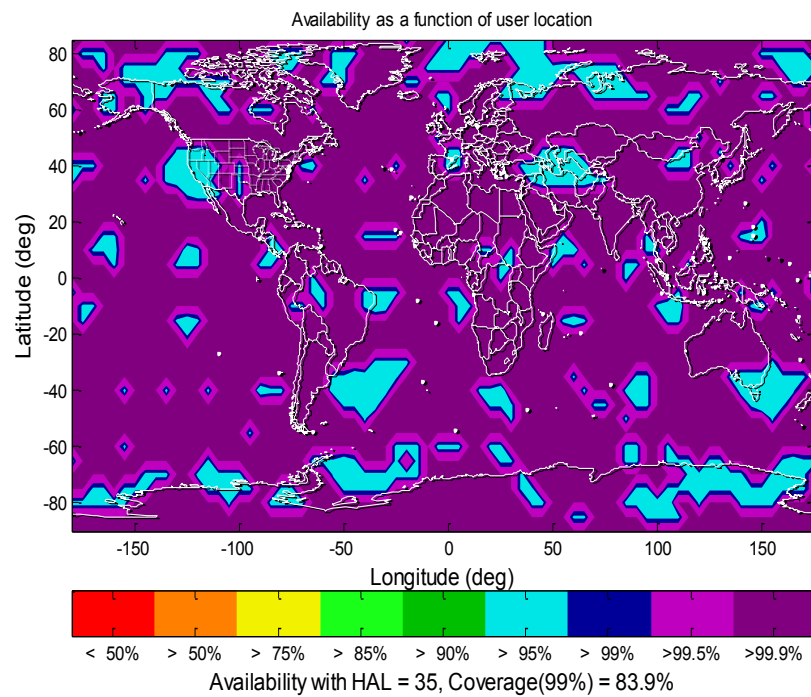


Figure 53: 99% Availability with HPL_{PB} , 24 GPS

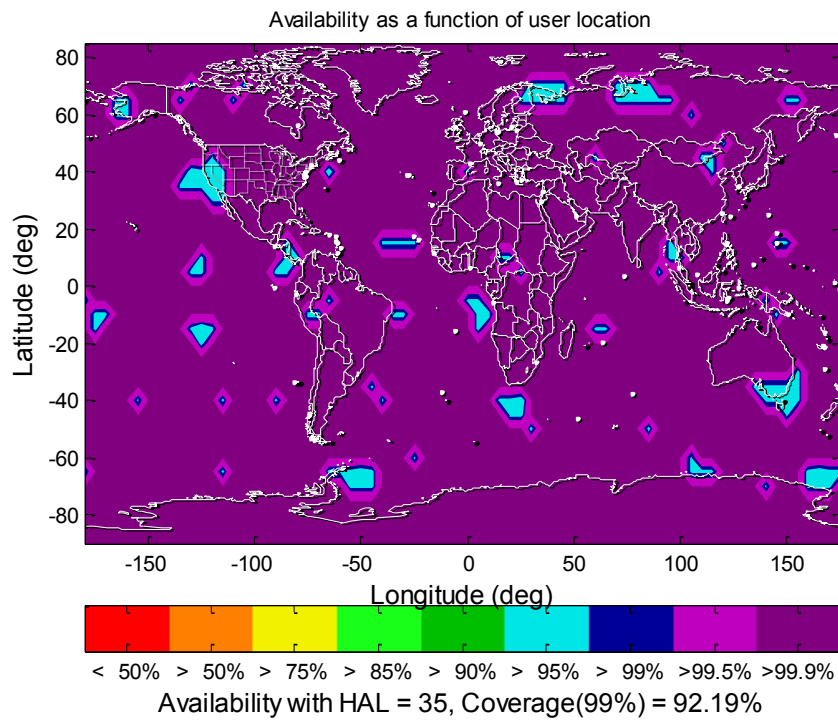


Figure 54: 99% Availability with the new HPL, 24 GPS

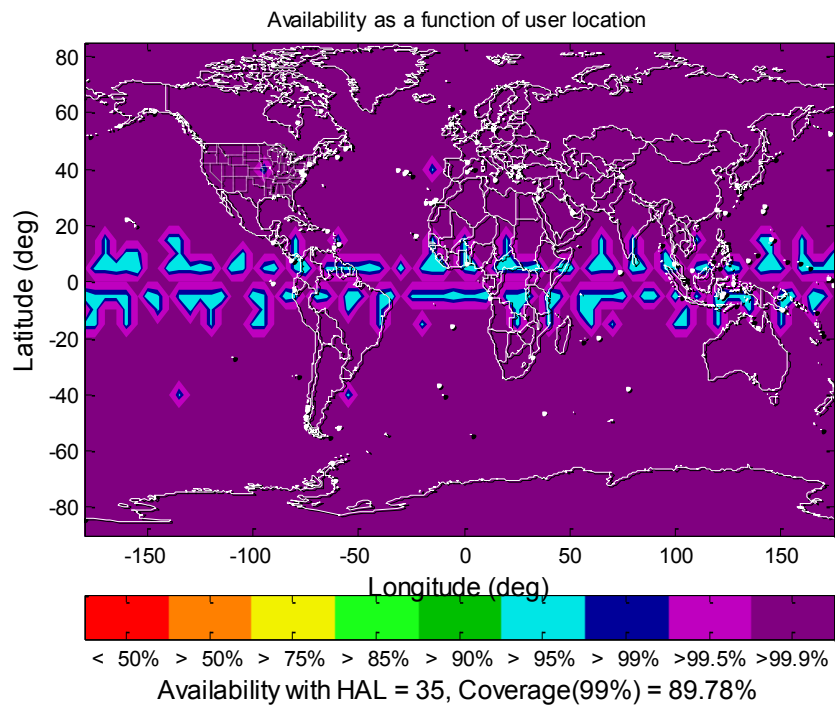


Figure 55: 99% Availability with HPL_{BC1}, 27 Galileo

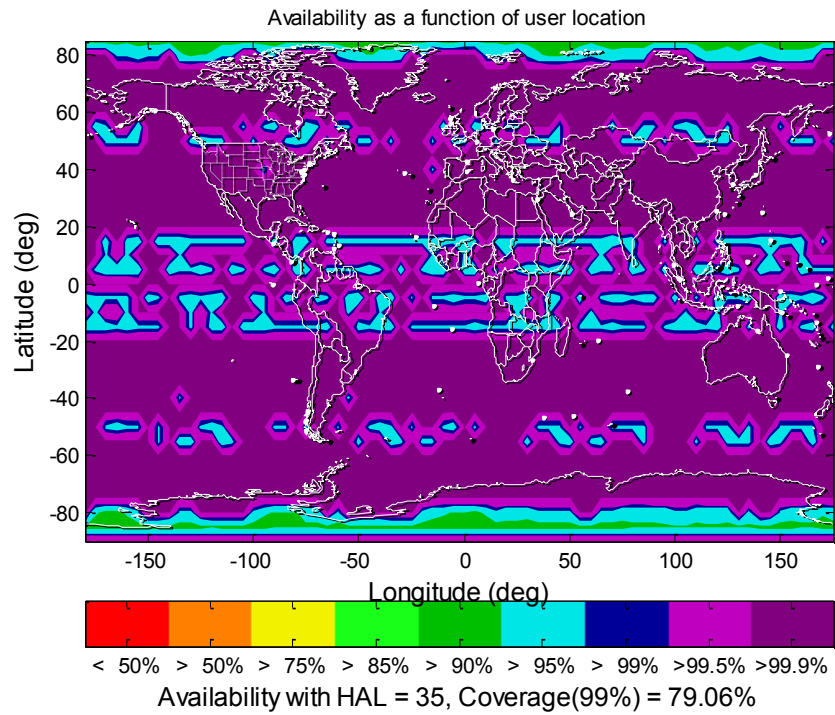


Figure 56: 99% Availability with HPL_{BC2} , 27 Galileo

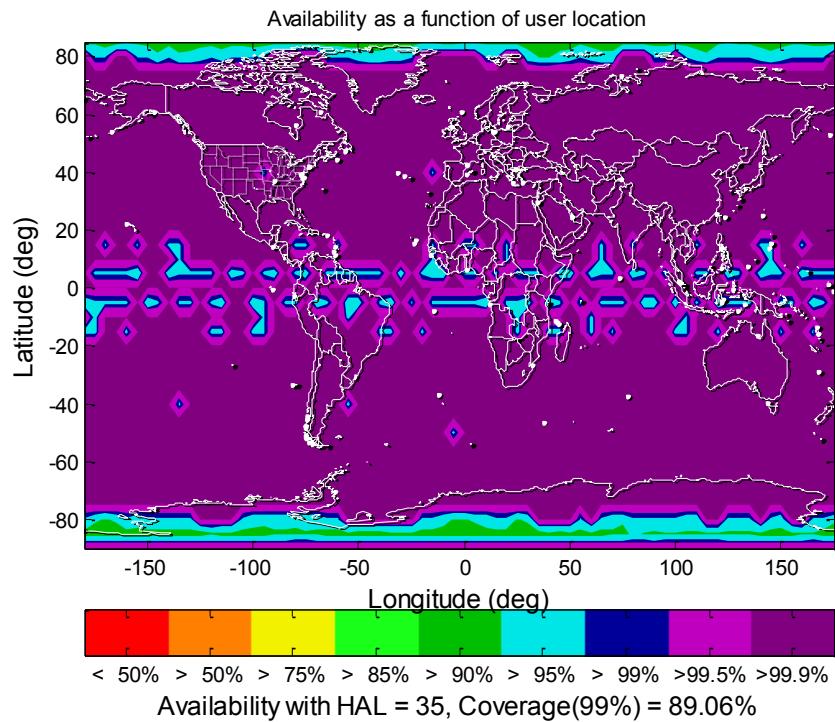


Figure 57: 99% Availability with HPL_{PB} , 27 Galileo

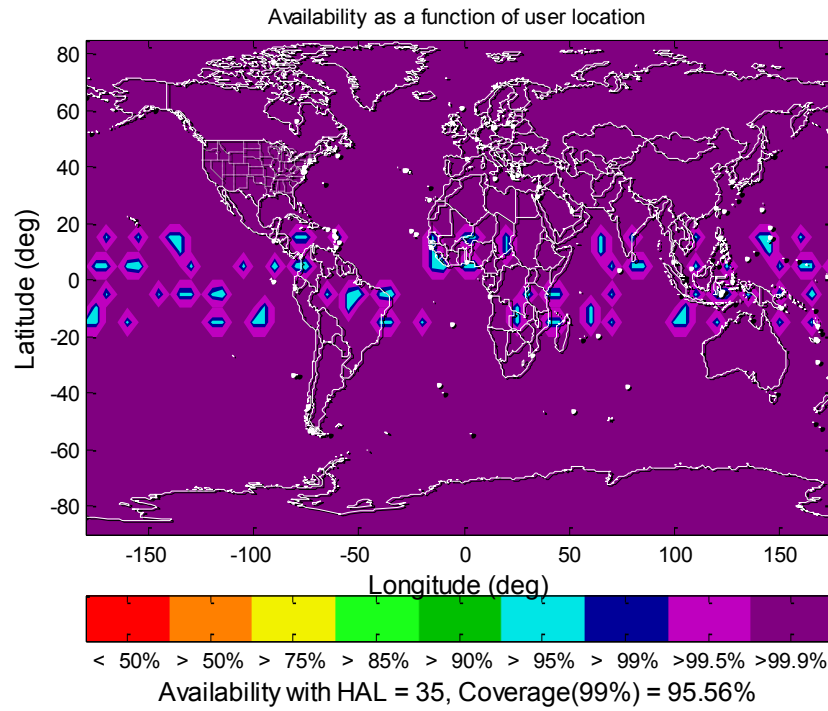


Figure 58: 99% Availability with new HPL, 27 Galileo

Table 13: 99% HPL Availability with multiple hypothesis RAIM

RAIM Algorithms	HPL _{BC1}	HPL _{BC2}	HPL _{PB}	New HPL
24 GPS	74.99%	56.88%	83.90%	92.19%
27 Galileo	89.78%	79.06%	89.06%	95.56%

It is shown that RAIM performance is greatly improved with the 99% availability worldwide. Although HPL_{PB} showed lower value than HPL_{BC1} in Figure 50, the service availability is higher than HPL_{BC1} with 24 GPS and lower with 27 Galileo. This is another example beside the similar case with VPL in Chapter 5 to conclude that there is no definite conclusion comparing the size of HPL_{PB} and HPL_{BC1}, which is dependent on geometry.

6.2 Higher Dimensional Protection Levels

For applications like UAV positioning, it is necessary to generalize current PL with one and two dimensions into higher dimensions. Three dimensional protection level (PPL) is pursued in this Chapter as a starting point of higher dimensional PL with different ways to obtain an approximated value and the exact value. Based on this, higher dimensional PL can be easily expanded.

6.2.1 The Positional Protection Levels

To calculate the position error with three dimensions, the two exact distributions applied for HPL are also applicable for PPL: the Imhof distribution (Imhof 1961) can be used directly and the simplified multivariate normal distribution can be found in DiDonato (1988).

The two approximations used for HPL can be applied for PPL in a similar way. With the normal approximation, PPL_{BC} under H_i is,

$$PPL_{BC1i} = Pslope1_i \delta_i + K(1 - \frac{IR_{Hi}}{2P_{Hi}}) \sigma_{\nabla i} \quad (6.7)$$

where δ_i is derived by given α_i and $\beta_i = \frac{IR_{Hi}}{P_{Hi}} = 10^{-3}$; The horizontal slope parameter is defined as the project matrix from the i^{th} observation domain to the horizontal position error domain (Brown and Chin 1998) with $S_{ENU} = [S_E \ S_N \ S_U]^T$,

$$Pslope1_i = \sqrt{\frac{e_i^T S_{ENU}^T S_{ENU} e_i}{e_i^T Q_y^{-1} Q_v Q_y^{-1} e_i}} \quad (6.8)$$

In a similar way, PPL_{BC} under H_i with the chi-squared approximation is derived as,

$$PPL_{BC2i} = \sqrt{\frac{1}{\lambda_m}} [Pslope2_i \delta_i + \sqrt{\chi^2(2, 1 - \frac{IR_{Hi}}{P_{Hi}})}] \quad (6.9)$$

where δ_i is also derived by given α_i and $\beta_i = \frac{IR_{Hi}}{P_{Hi}} = 10^{-3}$; $\chi^2(2, 1 - \frac{IR_{Hi}}{P_{Hi}})$ represents the value at probability $1 - \frac{IR_{Hi}}{P_{Hi}}$ with the central chi-squared inverse cumulative distribution function and 2 degrees of freedom; λ_m is the minimum eigenvalue of Q_H^{-1} . The slope factor for each hypothesis with chi-squared approximation is,

$$Pslope2_i = \sqrt{\frac{e_i^T S_{ENU}^T Q_H^{-1} S_{ENU} e_i}{e_i^T Q_y^{-1} Q_v Q_y^{-1} e_i}} \quad (6.10)$$

The search method is also applicable here to obtain a PPL that is able to accommodate all bias values.

6.2.2 Numerical Results

First, the exact and approximated distribution to calculate probability of position error as a function of PPL is shown in Figure 59, where it is shown that the normal approximation is also not safe to be used in PPL.

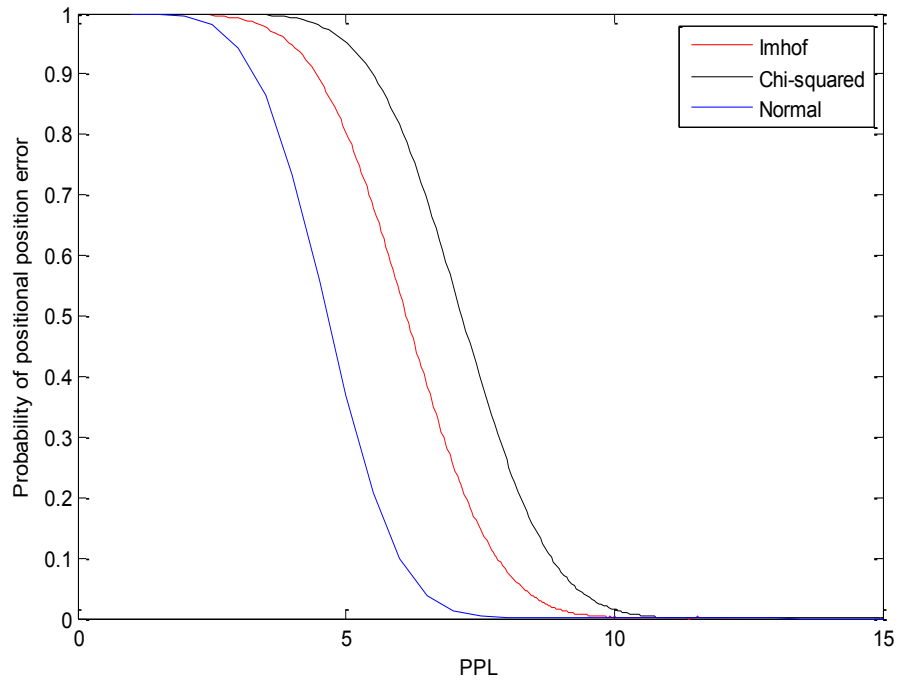


Figure 59: probability of the three dimensional position error

Then the exact and approximated PPLs are shown in Figure 60, where the two approximated PPLs are shown to be conservative with values smaller than the new PPL within a pre-defined accuracy.

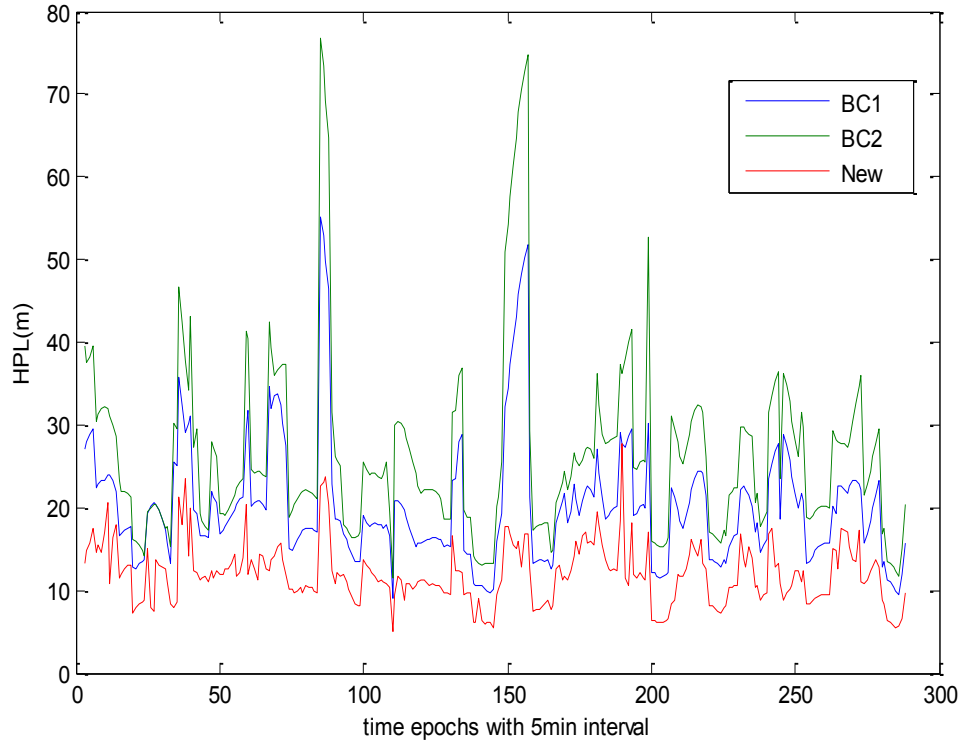


Figure 60: the new PPL with other approximated PPLs

The 99% PPL availability with worldwide distribution and the standard 24 GPS constellation is shown with the error model adapted based on GEAS (2008) and the risk definition adopted from the definition for HPL.

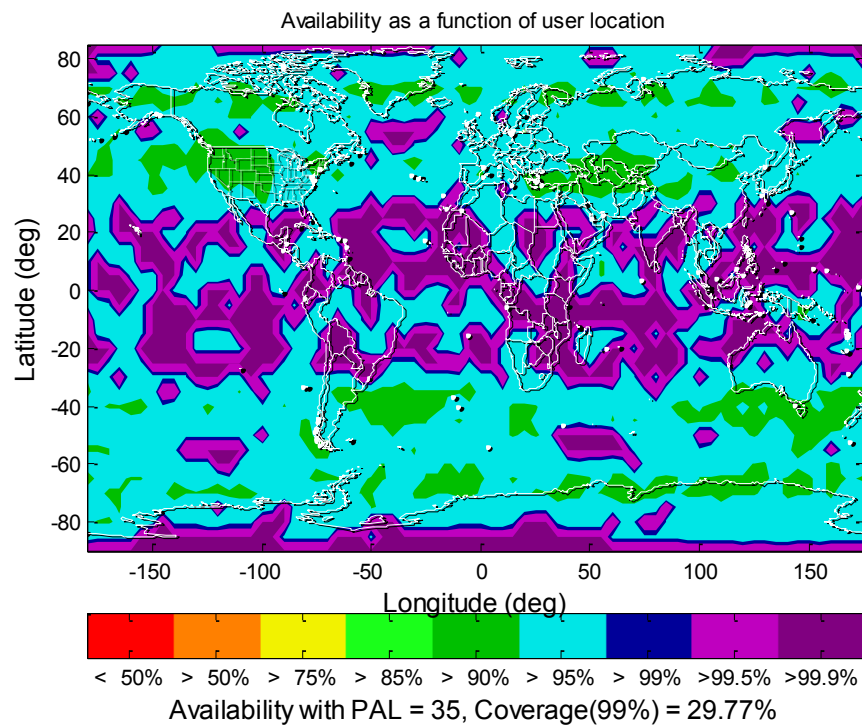


Figure 61: 99% PPL Availability with PPL_{BC1}, 24GPS

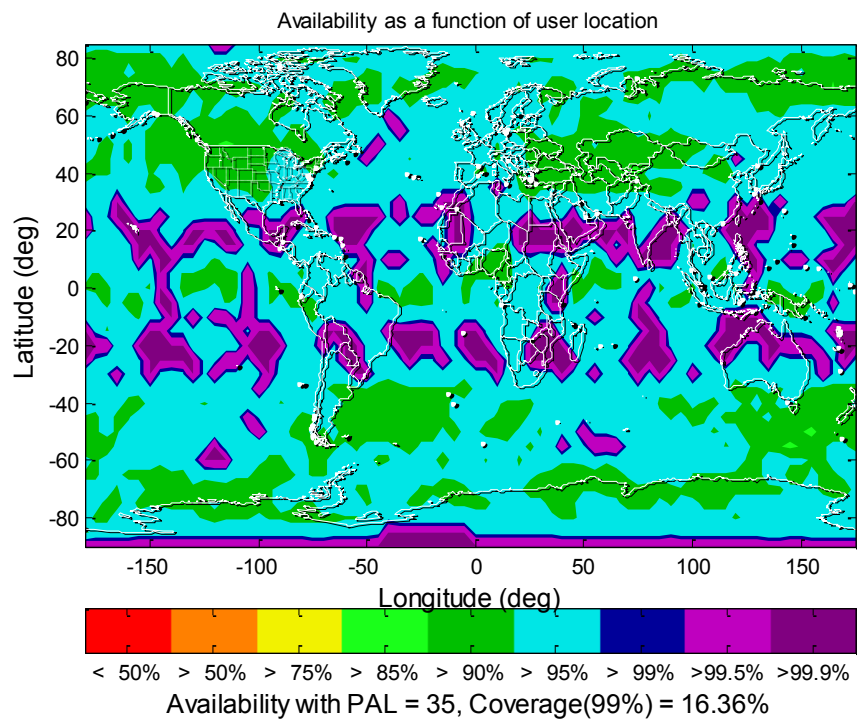


Figure 62: 99% PPL Availability with PPL_{BC2}, 24GPS

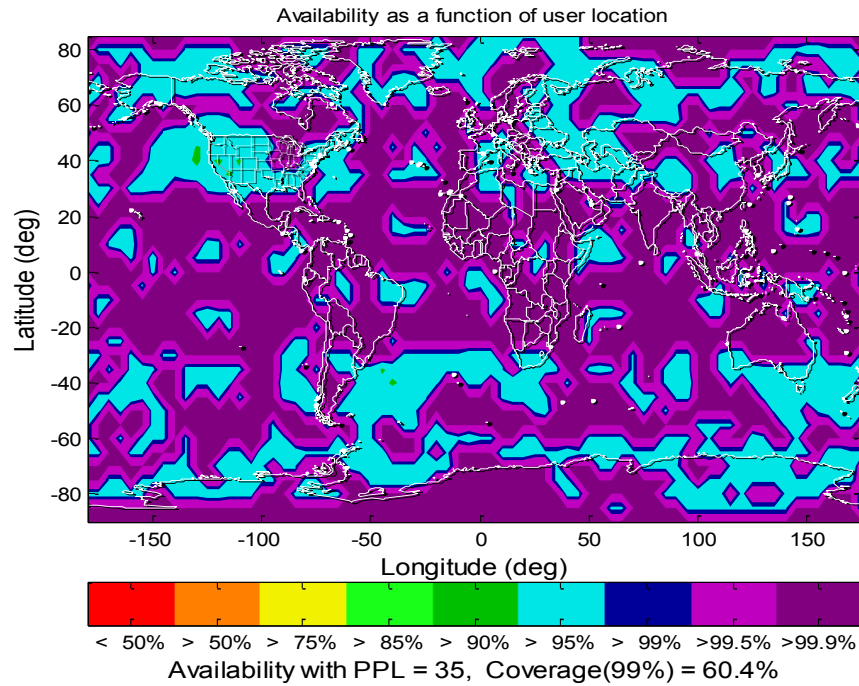


Figure 63: 99% PPL Availability with new PPL, 24GPS

Table 14: 99% PPL Availability with multiple hypothesis RAIM

RAIM Algorithms	PPL _{BC1}	PPL _{BC2}	New PPL
24 GPS	29.77%	16.36%	60.40%
27 Galileo	46.29%	47.19%	72.65%

Comparing the availability results with VPL, HPL and PPL in Tables 9, 13 and 14, the size order is PPL > VPL > HPL. In A-RAIM, the alarm limit is set at 35m for both HPL and VPL, and therefore a higher limit should be used in applications where PPL is used.

6.3 Summary

It has been shown that the new approach to calculate HPL has higher accuracy and computational efficiency, and therefore service availability can be improved in RAIM and GPS can be used in more stringent applications. Also the new iterative method has better performance than the old iterative method in the way that it is simple to be

implemented and faster to compute. With the exact HPL value validated in this paper, the conservativeness of current conservative HPLs is analyzed. It is theoretically proved that the chi-squared distribution is a safe choice to approximate the exact distribution, and also both HPL_{PB} and HPL_{BC} are conservative. Numerical results show that the normal distribution and HPL_{WE} are not safe to be used. Also, HPL is generalized towards higher dimensional protection level with PPL as an example.

CHAPTER 7 RAIM WITH A NEW SEPARABILITY MEASURE

With the data snooping method and reliability theory (Baarda 1967; 1968), the detectability of outliers and the influence of the undetected outliers are described with measures of internal reliability and external reliability, respectively. Further developments of the reliability theory include: 1) the influence of geometry on reliability was studied in Förstner (1985), which has been generalized with correlated observations (Wang and Chen 1994a; Schaffrin 1997; Prószyński 1994); 2) difficulties to apply the data snooping method with multiple outliers due to the outlier mask effects were recognized (Kok 1984); 3) the w-test statistic has been concluded to be uniformly most powerful (Teunissen 1991; 2000). To separate the outlier test from the estimation, parity space (Potter and Sunman 1977; Chow and Willsky 1984; Lou et al. 1986) is used to as a framework to generalize these developments in this study.

Various outlier isolation tests are available in the current literature: reapplication of the detection test by a comparison to the threshold (Parkinson and Axelrad 1988); maximization of test statistics to be compared with the threshold (Kelly 1998); the separability distance was tested (Wang and Knight 2012) and the hypothetical test with two alternative hypotheses was proposed by Förstner (1983) and Li (1986), based on which, the separability multiplying factor and Minimum Separability Bias (MSB) were defined with given confidence level. With detectability being the measure of the ability to distinguish between the null hypothesis and the alternative hypothesis, separability is the measure for distinguishing two alternative hypotheses in outlier isolation, which is of concern here. The probability of making wrong decisions in separability is described by

the event when the null hypothesis is correctly rejected, but the wrong alternative hypothesis is accepted, as Type III error (Hawkins 1980).

There are two factors available to represent separability: the correlation coefficient (Förstner 1983; Wang and Chen 1994a; Li and Yuan 2002) and the separability multiplying factor (Li 1986; Wang and Chen 1994b). Yet correlation coefficient is not a function of a given confidence level and this study has found that it is not applicable to some statistics. Since separability multiplying factor is a function of correlation coefficient and Type I/II/III errors, it represents both separability and detectability. Therefore a new separability measure in the range domain as a function of Type III error is desirable.

7.1 A New Criterion to Design Test Statistics

Another way to derive the test statistic is from the perspective of the robustness of the parity vector (Lou et al. 1986; Patton et al. 1992). The optimal parity space method was proposed by Zhang and Patton (1993), which was proved to be equivalent with the GLT method (Daly et al. 1979; Potter and Sunman 1977) as an UMP test. Later work based on this method can be found in Jin and Zhang (1999), which was also proved equivalent with the GLT method (Zhang et al. 2005).

The purpose is to design a robust parity vector, which have maximized sensitivity on certain fault mode and minimized sensitivity on random errors. To achieve this, the criterion is designed as the maximization of the norm ratio of two vectors. With the notion that statistical characteristics should not be neglected, the covariance of the random error is used in the criterion as the weight here. The new optimization criterion is designed as the ratio of two norms (statistical quadratic forms).

With an optimized parity matrix for each fault mode, the parity vector is different for each hypothesis. The parity vector under H_i is defined as,

$$p_i = P_i y = P_i e_i f + P_i \varepsilon \quad (7.1)$$

where $P_i \in R^{1 \times m}$, $P_i A = 0$.

The new criterion is,

$$\max_{P_i} \frac{\|P_i e_i\|^2}{\|P_i\|_{Q_y}^2} = \max_{P_i} \frac{P_i e_i e_i^T P_i^T}{P_i Q_y P_i^T} \quad (7.2)$$

Since $P_i A = 0$ and $P_s A = 0$, P_i can be expressed as the linear combination of P_s with $c_i \in R^{1 \times (m-n)}$,

$$P_i = c_i^T P_s \quad (7.3)$$

With Theorem 2 in Jin and Zhang (1999) and a as an arbitrary non-zero real number, the maximum value is obtained when

$$c_i = a(P_s Q_y P_s^T)^{-1} P_s e_i \quad (7.4)$$

The optimized parity matrix and its variance σ_{p_i} is therefore obtained. The studentized optimal parity vector is used as the test statistic, which is equivalent to the w-test statistic,

$$p_{s_i} = \frac{p_i}{\sigma_{p_i}} = \frac{e_i^T P_s^T (P_s Q_y P_s^T)^{-1} P_s y}{\sqrt{e_i^T P_s^T (P_s Q_y P_s^T)^{-1} P_s e_i}} = w_i \quad (7.5)$$

7.2 Optimality in Fault Detectability and Separability

7.2.1 Detectability

The fault detectability is studied with the expectation of the test statistic and the MDB. The MDB vector for multiple faults is defined in a similar way as for the single fault (Teunissen 2000; Wang and Chen 1999). With given Type I error α_i and Type II error β_i , MDB_i as the scalar component of MDB vector is,

$$MDB_i = \frac{\delta_i \sqrt{e_i^T P Q_y P^T e_i}}{|e_i^T P e_i|} \quad (7.6)$$

The external reliability is (Knight et al. 2010),

$$y_d = MDB_i |(A^T Q_y^{-1} A)^{-1} A^T Q_y^{-1} | e_i \quad (7.7)$$

Theorem A: With fault mode i , $E(|ts_i|)$ is maximum and MDB_i is minimum when the w-test statistic is used.

Proof: Since P_s is the orthonormal basis of the left null space of the design matrix, $e_i^T P$ can be expressed as a linear combination of P_s with $c_i \in R^{1 \times (m-n)}$,

$$e_i^T P = c_i P_s \quad (7.8)$$

Therefore the square of the expectation is expressed as,

$$E^2(|ts_i|) = \frac{f_i^2 (c_i P_s e_i)^2}{c_i (P_s Q_y P_s^T)^{-1} c_i^T} \quad (7.9)$$

Since $P_s Q_y P_s^T$ is symmetric positive definite, The Cauchy-Schwarz inequality and Theorem 2 in Jin and Zhang (1999) is used. With k as an arbitrary non-zero real number, the maximum value of the above equation is obtained when

$$c_i = k e_i^T P_s^T (P_s Q_y P_s^T)^{-1} \quad (7.10)$$

Therefore, $E(|ts_i|)$ is maximum when w-test statistic is used. Similar approach can be applied on the proof of the minimum MDB.

7.2.2 Conditions of Best Detection and Separation

Theorem B: With fault mode i , if the parity matrix satisfying the following two conditions: $P = P^T$ and $P = P Q_y P^T$,

$$\max\{E(|ts_j| | H_i)\} = E(|ts_i| | H_i), \quad j = 1 \dots m \quad (7.11)$$

The w-test statistic is able to obtain this conclusion, while the v-test statistic is not.

Proof: With $P = P^T$ and $P = PQ_y P^T$, it is concluded that P is symmetric semi-positive definite, and the diagonal entries are real and non-negative. Therefore, the following equation is derived,

$$E(|ts_i||H_i) = \sqrt{e_i^T P e_i} \quad (7.12)$$

The other expectations can be expressed as,

$$E(|ts_j||H_i) = \frac{e_j^T P e_i}{\sqrt{e_j^T P e_j}} \quad (7.13)$$

Since P is symmetric semi-positive, the following inequality is obtained,

$$\sqrt{e_i^T P e_i} \sqrt{e_j^T P e_j} > |e_j^T P e_i|, j = 1 \dots m, j \neq i \quad (7.14)$$

In other words, with fault mode i , if $j \neq i$,

$$E(|ts_j||H_i) < E(|ts_i||H_i) \quad (7.15)$$

Theorem B is thereby proved. The v-test statistic should not be used for fault isolation without the conclusion if there is any correlation in observations.

7.3 A New Separability Measure

7.3.1 The Design Process

To design a new separability measure, the probability of choosing a wrong alternative hypothesis is defined,

$$\theta_{ij} = P\{|ts_j| > |ts_i||H_i\} \quad (7.16)$$

To obtain the measure in the range domain, the fault size with given θ_{ij} is desirable. The calculation process is described below. The probability density of a bivariate normal distribution of two test statistics ts_i, ts_j with fault mode i is f_{ij} ,

$$f_{ij} = \frac{1}{2\pi\sqrt{1-\rho_{ij}^2}} \exp\left\{-\frac{1}{2(1-\rho_{ij}^2)} \left[(ts_i - u_i)^2 + (ts_j - k_{ij}u_i)^2 - 2\rho_{ij}(ts_i - u_i)(ts_j - k_{ij}u_i) \right] \right\} \quad (7.17)$$

where u_i is the expectation of ts_i and ρ_{ij} is the correlation coefficient of ts_i and ts_j . $u_j = k_{ij}u_i$ is the expectation of ts_j with k_{ij} as the ratio of expectations of test statistics ts_j and ts_i . As described in Theorem B, to satisfy the isolation performance, the condition of $|k_{ij}| < 1$ should be met. With $|k_{ij}| \geq 1$, the test statistic should not be used since θ_{ij} is larger than 50%. With the w-test, k_{ij} is equal to ρ_{ij} . Therefore, $|k_{ij}|$ is guaranteed to be less than 1. With the v-test, ρ_{ij} and k_{ij} are not equal, and $|k_{ij}|$ is not guaranteed to be less than 1.

The probability density is a function of both ρ_{ij} and k_{ij} . It is therefore reasonable to use ρ_{ij} as the separability measure for the w-test statistic since $\rho_{ij} = k_{ij}$. Without loss of generality, the new separability in range domain is designed as a function of θ_{ij} , ρ_{ij} and k_{ij} . With the region defined as $D = \{(ts_i, ts_j) | |ts_j| > |ts_i|\}$, double integral is used to derive the non-centrality parameter u_i ,

$$\iint_D f_{ij} d_{ts_i} d_{ts_j} = \theta_{ij} \quad (7.18)$$

Figure 64 depicts the mechanism,

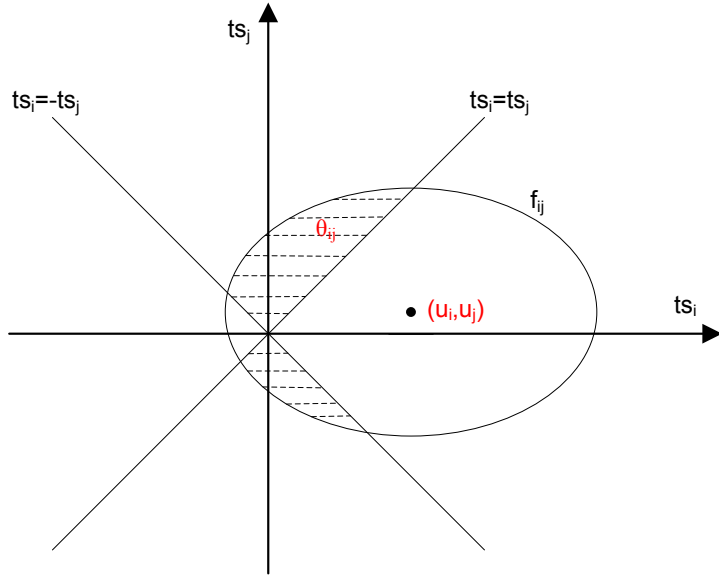


Figure 64: the mechanism to calculate the non-centrality parameter u_i

The relationship among $u_i, \theta_{ij}, \rho_{ij}, k_{ij}$ is illustrated in the following figures.

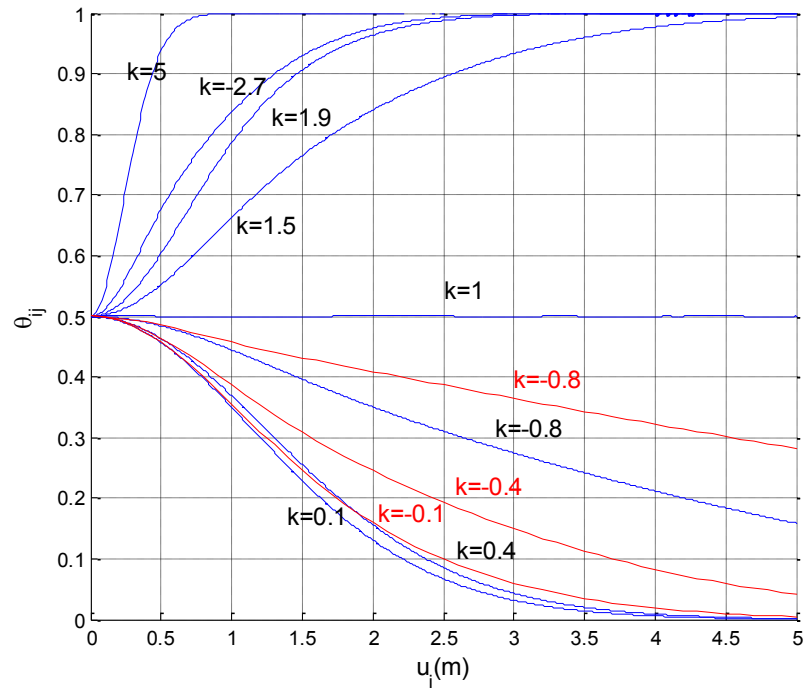


Figure 65: θ_{ij} and u_i with $\rho_{ij} = 0.5$ and varying k

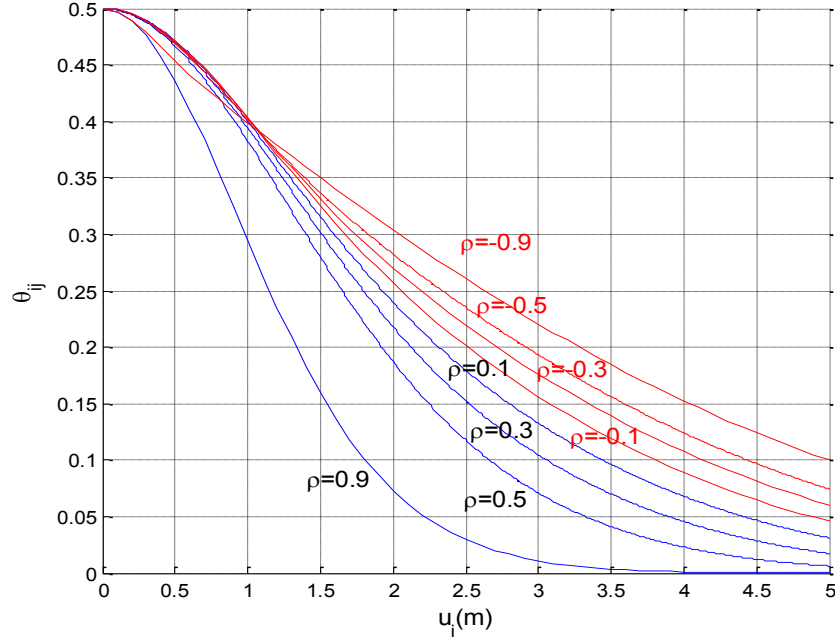


Figure 66: θ_{ij} and u_i with $k_{ij} = 0.5$ and varying ρ_{ij}

From Figure 65, if $|k_{ij}| < 1$, then $\theta_{ij} < 50\%$, and if $|k_{ij}| \geq 1$, then $\theta_{ij} \geq 50\%$.

Therefore, the following analysis only applies to cases when $|k_{ij}| < 1$. From Figure 65 and Figure 66, as u_i increases, the probability θ_{ij} decreases, which means the bigger the fault is, the easier it is to separate ts_i and ts_j . With given fault size, the size of k_{ij} and ρ_{ij} has no direct relationship with θ_{ij} . Therefore, the separability measure is defined as the fault size with given θ_{ij} . With the non-centrality parameter u_i derived in eq. (7.18), the new separability measure is,

$$S_{ij} = \begin{cases} \frac{u_i \sqrt{e_i^T P Q_y P^T e_i}}{|e_i^T P e_i|} & |k_{ij}| < 1 \\ +\infty & |k_{ij}| \geq 1 \end{cases} \quad (7.19)$$

The proposal of S_{ij} is under the context of the classical reliability theory (Baarda 1967; 1968). Please refer to (Förstner 1983; Li and Yuan 2002) for more background

information. It has been a critical issue to define a quality measure for separability of alternative hypotheses which are correlated. Under the context of RAIM, it is the exclusion test that will use this measure if it is deeply investigated.

The bigger value S_{ij} is, the more difficult it is to separate these two alternative hypotheses. The infinite value is defined for the case when $\theta_{ij} \geq 50\%$. The corresponding external reliability for separability is defined as,

$$y_{s,ij} = S_{ij}(A^T Q_y^{-1} A)^{-1} A^T Q_y^{-1} e_i \quad (7.20)$$

7.3.2 A Numerical Example

To further validate the reliability measures, a numerical experiment is designed with four observations, one unknown parameter and two faults. The total number of fault modes is 6. Assuming these two faults have the same size, the vector components for all fault modes are: $e_1^T = [1,1,0,0]$, $e_2^T = [1,0,1,0]$, $e_3^T = [1,0,0,1]$, $e_4^T = [0,1,1,0]$, $e_5^T = [0,1,0,1]$, $e_6^T = [0,0,1,1]$. The probabilities of making wrong decisions are: $\alpha_i = 0.1$, $\beta_i = 0.05$, $\theta_{ij} = 0.08$. The geometry of leveling observations is shown in Figure 67.

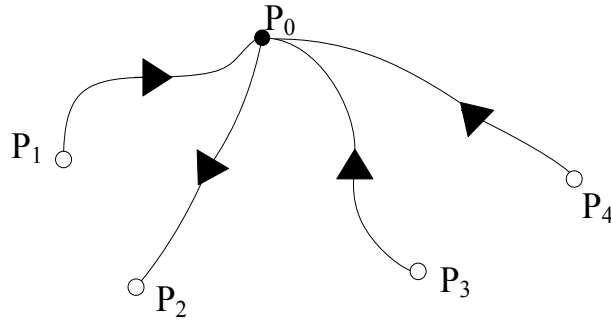


Figure 67: an example of the Observation Geometry

The design matrix and the covariance matrix are:

$$A^T = [1 \quad -1 \quad 1 \quad 1]$$

$$Q_y = \begin{bmatrix} 1.0 & 0.7 & 0.2 & 0.0 \\ 0.7 & 1.0 & 0.0 & 0.0 \\ 0.2 & 0.0 & 1.0 & 0.0 \\ 0.0 & 0.0 & 0.0 & 1.0 \end{bmatrix}$$

With known geometry, covariance and the probabilities of making wrong decisions, results of MDB, correlation coefficient, expectation ratio, the separability measure and external reliability are shown in Tables below.

Table 15: the scalar component of MDB

	1	2	3	4	5	6
w-test	3.014	3.823	3.524	2.016	2.123	2.421
v-test	3.033	4.155	4.343	2.326	2.326	2.430

Table 16: correlation coefficient with the v-test statistic

<i>v-test</i>	1	2	3	4	5	6
1	1.0000	0.7502	0.7562	0.7286	0.6529	0.0890
2		1.0000	0.4099	0.9782	0.3604	0.4099
3			1.0000	0.5220	0.9860	0.4618
4				1.0000	0.5000	0.5800
5					1.0000	0.5800
6						1.0000

Table 17: expectation ratio with the v-test statistic

<i>v-test</i>	1	2	3	4	5	6
H1	1.0000	0.6786	0.7645	0.6519	0.6519	0.0083
H2	0.6850	1.0000	0.0906	0.8931	0.0000	0.0906
H3	0.7160	-0.0735	1.0000	0.0000	0.9335	-0.0828
H4	0.3835	0.8946	0.4279	1.0000	0.5000	<i>1.0079</i>
H5	0.3835	0.2954	0.9128	0.5000	1.0000	0.9128
H6	0.0000	0.3498	0.3940	0.5224	0.5224	1.0000

Table 18: separability with the w-test statistic

<i>w-test</i>	1	2	3	4	5	6
H1	0	2.7976	3.0863	2.3104	2.3805	2.2507
H2	3.5485	0	2.9578	3.5142	2.8707	2.8462
H3	3.6082	2.7262	0	2.7101	3.0717	2.6444
H4	1.5450	1.8527	1.5502	0	1.9418	3.1425
H5	1.6766	1.5940	1.8504	2.0451	0	2.8796
H6	1.8075	1.8021	1.8165	3.7740	3.2836	0

Table 19: separability with the v-test statistic

<i>v-test</i>	1	2	3	4	5	6
H1	0	2.8783	3.8413	2.7831	3.1184	2.2558
H2	4.0152	0	3.0217	3.5222	3.1158	3.0217
H3	4.5737	3.4330	0	3.3063	4.6728	3.4982
H4	1.5573	1.9977	1.8288	0	2.0390	$+\infty$
H5	1.6324	1.7776	1.9397	2.0390	0	10.4378
H6	1.8089	1.8916	1.9154	2.0626	2.0626	0

Table 20: external reliability of separability with the w-test statistic

<i>w-test</i>	1	2	3	4	5	6
H1	0	-0.0153	-0.0169	-0.0126	-0.0130	-0.0123
H2	1.6191	0	1.3496	1.6035	1.3099	1.2987
H3	1.9421	1.4674	0	1.4587	1.6533	1.4234
H4	-0.5699	-0.6834	-0.5718	0	-0.7162	-1.1591
H5	-0.4810	-0.4573	-0.5309	-0.5867	0	-0.8261
H6	0.3161	0.3151	0.3176	0.6599	0.5742	0

As shown in Table 15, MDB with w-test is smaller than the v-test, which is consistent with Theorem A. To validate the separability measure, a Monte Carlo experiment with 100,000 samples is designed to get θ_{ij} with two 4m faults for each fault mode. The

random error is of Gaussian distribution with zero mean and covariance matrix given in eq. (7.22). The simulated θ_{ij} are in the Table 21 and Table 22.

Table 21: θ_{ij} with two 4m faults on w-statistics

<i>w-test</i>	1	2	3	4	5	6
H1	0	0.0208	0.0336	0.0035	0.0055	0.0024
H2	0.0551	0	0.0221	0.0541	0.0165	0.0151
H3	0.0584	0.0136	0	0.0121	0.0307	0.0092
H4	0.0000	0.0010	0.0000	0	0.0017	0.0375
H5	0.0002	0.0000	0.0011	0.0028	0	0.0259
H6	0.0002	0.0002	0.0002	0.0678	0.0433	0

Table 22: θ_{ij} with two 4m faults on v-test statistics

<i>v-test</i>	1	2	3	4	5	6
H1	0	0.0246	0.0722	0.0207	0.0355	0.0023
H2	0.0812	0	0.0244	0.0544	0.0304	0.0239
H3	0.1107	0.0488	0	0.0421	0.1176	0.0524
H4	0.0000	0.0023	0.0005	0	0.0024	0.5193
H5	0.0000	0.0002	0.0016	0.0023	0	0.2934
H6	0.0002	0.0005	0.0010	0.0023	0.0026	0

It is shown in the above tables that the new separability measure has better consistency with the θ_{ij} results than the correlation coefficient. An example is the bold θ_{ij} value 0.2934 in Table 22 with the v-test. The corresponding correlation coefficient is 0.5800, which is not reasonable comparing with other values in the table. The corresponding separability value is 10.4378, which is more consistent with θ_{ij} . Also, the $+\infty$ separability in Table 22 is corresponding to the situation when $|k_{ij}| \geq 1$ and $\theta_{ij} > 50\%$.

The constraint of the new separability measure is that it is only able to represent each pair of alternative hypotheses, and the relationship between the maximization and the separability should be further studied with correlation among test statistics.

7.4 Extended RAIM with Separability

7.4.1 Extended Risk Definition

The global test is used for FD, and therefore both the Type I error and the Type II error are defined in a global test as in eq. (2.18) and eq. (2.19). The local test is used for FDE if the detection is positive in the global test, and therefore both the Type I error and the Type II error are defined in a local test as in eq. (2.26) and eq. (2.27). Also the probability related to the exclusion in last section is applied here with the Type III error defined as the probability of choosing wrong hypotheses γ_i ,

$$\gamma_i = 1 - P\{\max(|ts_j|) = |ts_i| | H_i\} \quad (7.21)$$

γ_i can be expressed with a local probability θ_{ij} , and the distribution of γ_i onto each hypothesis θ_{ij} is assumed to be known.

$$\gamma_i = 1 - \sum_{j=1}^{m, j \neq i} \theta_{ij} \quad (7.22)$$

With the condition that $\rho_{ij} = k_{ij}$ for the given statistic, the non-central parameter $\delta_{ij} = u_i$ is able to be derived for fault exclusion, which is a function of θ_{ij}, ρ_{ij} with eq. (7.16).

With VPL as an example, the following risk and formulas are defined, and similar conclusions can be derived for HPL, PPL and etc. The integrity risk on the vertical level with FD is defined as,

$$IR_{VD} = P\{|\tilde{x}_v| > VPL|H_a\}P\{C < T|H_a\}P_{H_a} \quad (7.23)$$

With Type III error defined above, the integrity risk on the vertical level with FDE is a sum of all single hypotheses

$$IR_{VE} = \sum_{i=0}^m \sum_{j=1}^{m, j \neq i} IR_{VEij} \quad (7.24)$$

With faulty mode i, the IR_{VEi} is defined as,

$$IR_{VEij} = P\{|\tilde{x}_v| > VPL|H_i\}P\{|ts_j| > |ts_i||H_i\}P_{H_i} \quad (7.25)$$

7.4.2 The Extended Protection Level

With the classic RAIM as an example, the following VPL formulas are derived, and similar conclusions can be derived with the MHSS method and VPL_{new} . The VPL after FD is $VPL_{BC,D}$,

$$VPL_{BC,D} = \delta \cdot \max(Vslope_i) + K(1 - \frac{IR_{Va}}{2P_{Ha}})\sigma_U \quad (7.26)$$

where δ is derived with given α and $\beta = \frac{IR_{Va}}{P_{Ha}}$ in a global test.

The VPL after fault exclusion under H_{ij} is $VPL_{BC,Eij}$,

$$VPL_{BC,Eij} = \delta_{ij} \cdot Vslope_i + K(1 - \frac{IR_{VEij}}{2P_{Hij}})\sigma_{Ui} \quad (7.27)$$

where δ_{ij} is the u_i in eq. (7.17) as the non-centrality parameter derived with given θ_{ij}

The VPL after fault exclusion under H_i is $VPL_{BC,Ei}$

$$VPL_{BC,Ei} = \max(VPL_{BC,Eij}) \quad (7.28)$$

The final result is,

$$VPL_{BC,E} = \max(VPL_{BC,Ei}) \quad (7.29)$$

It should be noted that VPL_{PB} is not applicable to derive VPL for detection since it can only be used with multiple hypothesis, while a global test is used here. Both VPL_{BC} and the new VPL can be used in extended RAIM. Similarly, HPL_{PB} cannot be used.

7.4.3 Numerical Results

The risk definition for the detection part is based on the one in Chapter 5 except that each risk is not distributed to each hypothesis anymore with the global test used. Therefore, the prior probability of the alternative hypothesis is 1×10^{-5} . The integrity risk under faulty case is 2.175×10^{-8} . The P_{FA} of the alternative hypothesis is 4×10^{-6} . The risk definition for the exclusion part is also based on the one in Chapter 5, except that the risk is further divided into each local hypothesis. Therefore, the prior probability of the alternative hypothesis is 1×10^{-5} . The integrity risk under faulty case is 2.175×10^{-8} . The Type III error for each single hypothesis is 1×10^{-6} . The VPL/HPL/PPL results for detection and exclusion separately are shown in the following figures.

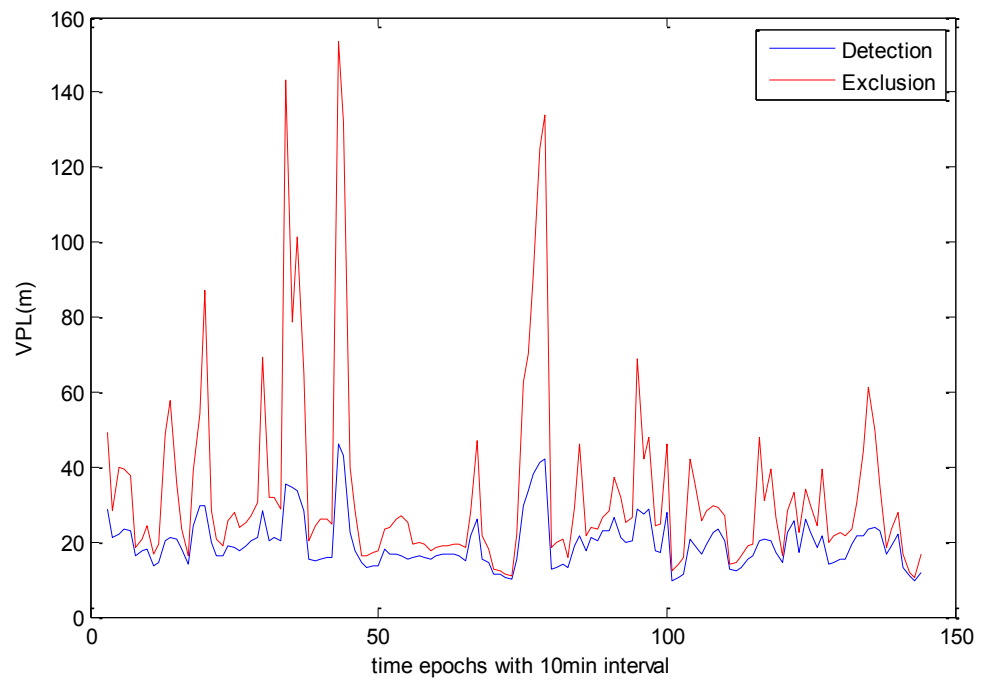


Figure 68: VPL_{BC} with FD and VPL_{BC} with FDE

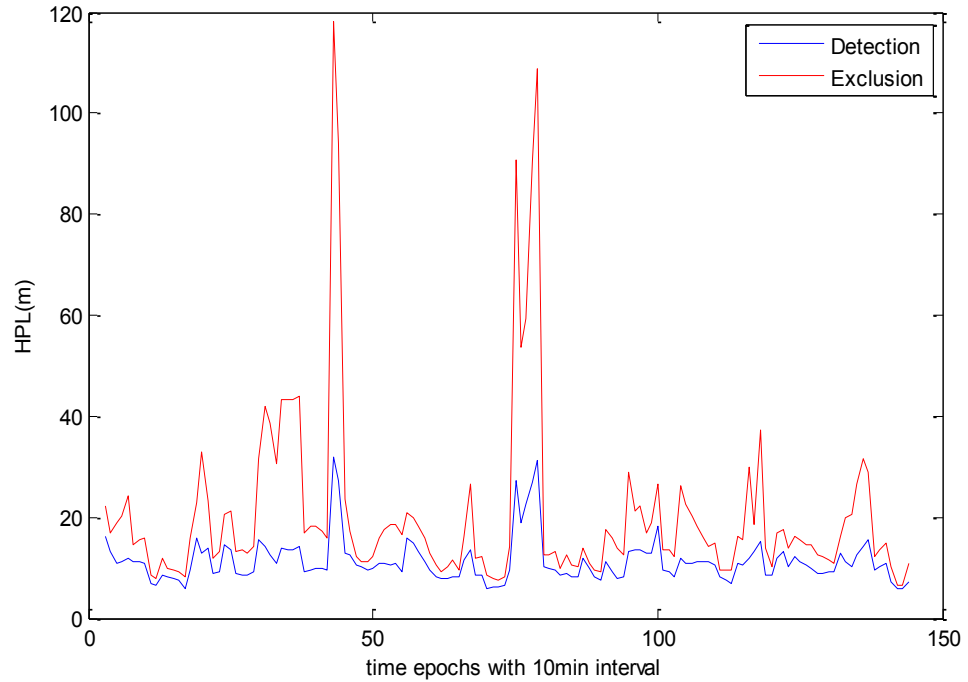


Figure 69: HPL_{BC1} with FD and HPL_{BC1} with FDE

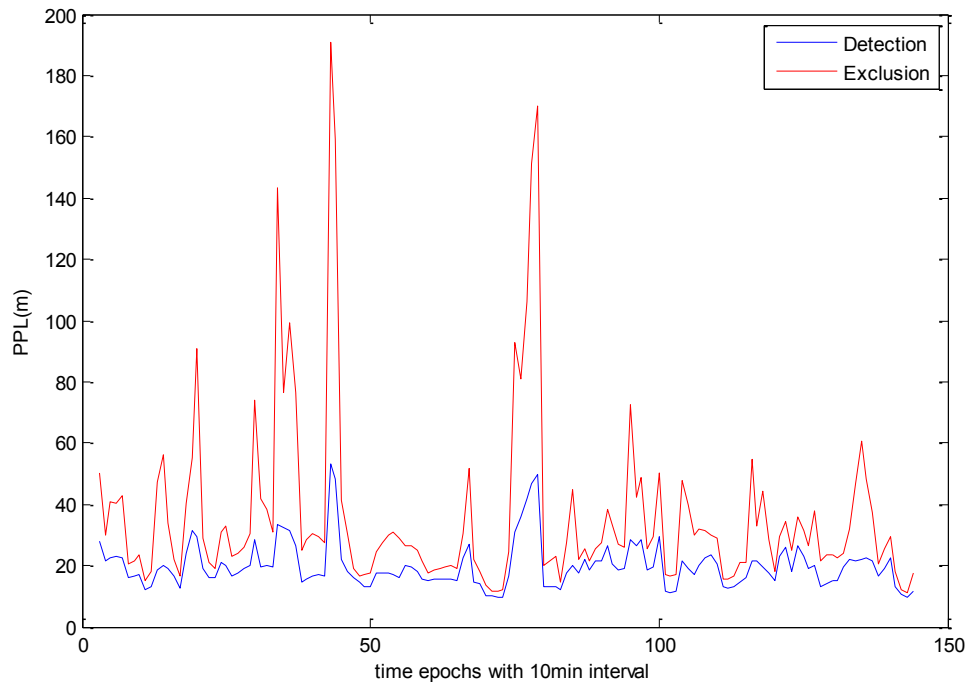


Figure 70 PPL_{BC1} with FD and PPL_{BC1} with FDE

It is shown in the figures that PL after FDE is worse than the PL after FD especially at the peak points. With the same risk definition, the 99% availability with 35m AL is shown below.

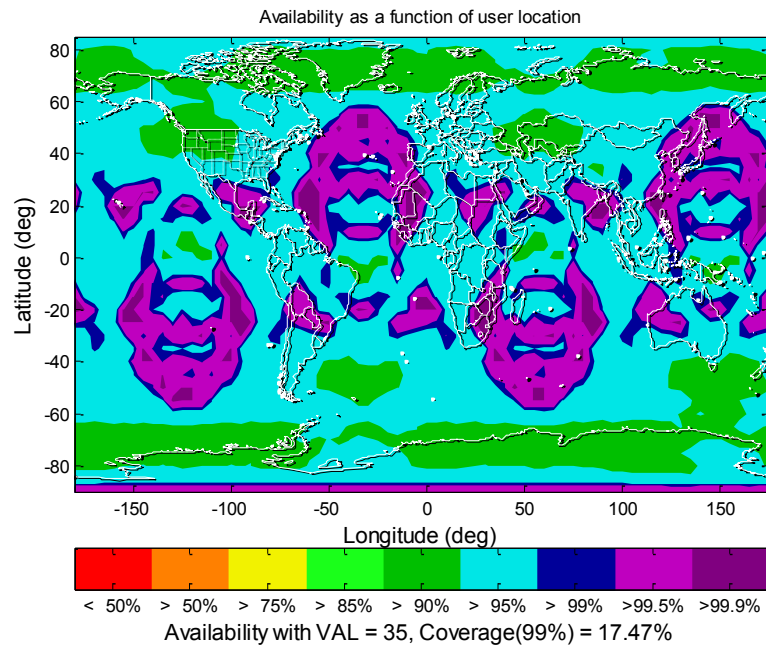


Figure 71: 99% VPL Availability with VPL_{BC} Exclusion, 24GPS

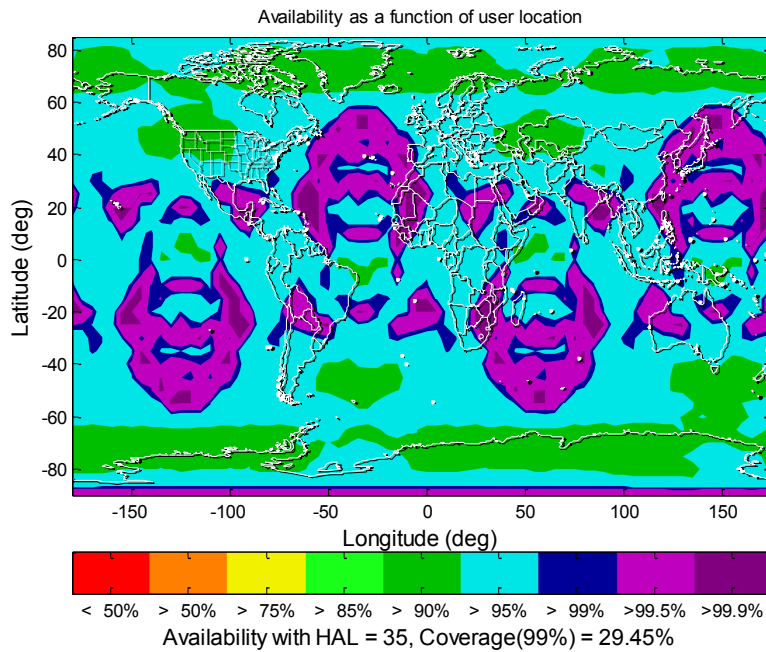


Figure 72: 99% HPL Availability with HPL_{BC1} Exclusion, 24GPS

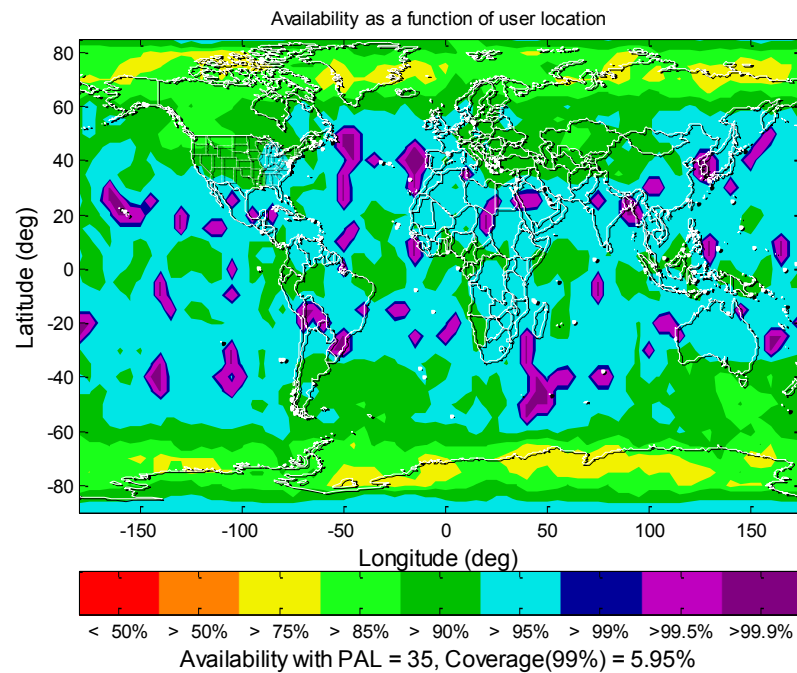


Figure 73: 99% PPL Availability with PPL_{BC1} Exclusion, 24GPS

Table 23: 99% Availability with the extended RAIM and 24 GPS

RAIM Algorithms	VPL _{BC}	HPL _{BC1}	PPL _{BC1}
Detection	78.46%	94.97%	62.35%
Exclusion	17.47%	29.45%	5.95%

As shown in

Table 23, the different dimensional PL values with the same given integrity risk and RAIM algorithms have the size order as: PPL>VPL>HPL. The same conclusion can be obtained comparing results with the original RAIM algorithm in Figure 36, Figure 50 and Figure 60. The results for exclusion are shown to have less availability than the RAIM results for detection with given Type III error in the classic method.

7.5 Summary

A new separation measure in the range domain based on the probability of choosing a wrong alternative hypothesis has been proposed. The results show that the new measure is more consistent with the performance to separate two alternative hypotheses and more general for both statistics compared to the correlation coefficient. The constraint of the new separability measure is that it is only able to represent each pair of alternative hypotheses, and the relationship between the maximization and the separability should be further studied with correlation among test statistics. RAIM is therefore generalized using this separability measure, with PL defined for FD and FDE separately.

CHAPTER 8 CONCLUSIONS AND RECOMMENDATIONS

The conventional RAIM algorithms are studied under the future integrity monitoring structures including A-RAIM and R-RAIM with multiple hypothesis. Then, these algorithms are optimized in the way to calculate both VPL and HPL to improve the service availability. The new approach aims to obtain the exact VPL and HPL value within a pre-defined accuracy. With the exact PL value, it is able to analyze if current algorithms are safe to be used. Also, the single dimensional VPL and the two dimensional HPL are generalized into a higher dimensional PPL by proposing two approximated algorithms and an approach for the exact PPL value, wherein the conservativeness analysis is also provided.

Furthermore, the FDE as a component of RAIM is studied in background of the classical reliability theory. The optimality of test statistics on detectability and separability is concluded in a generalized parity space. Also, a new quality control measure is proposed for separability of two alternative hypotheses to improve the generality of the current measure. The new measure is in the range domain, similar with MDB, which can be further applied in other applications. Therefore, RAIM is expanded with two different scenarios: RAIM for FD and RAIM for FDE, with the new separability measure applied in the latter one.

With the work summarized as above, the following conclusions and suggestions are obtained.

8.1 Conclusions

- a) The two positioning methods in R-RAIM including the range domain method and the position domain method have similar estimation precision, while the two RAIM algorithms including the classic method with a global test and the MHSS method with a local test have different VPL results with the classic method produce smaller PL values.
- b) With better results in R-RAIM than A-RAIM, the coasting time is an uncertain element in the design that cannot be too big or too small. The optimal value does not show stable characteristics and needs further investigation.
- c) The major difference between the A-RAIM and R-RAIM structure is the positioning method with the first one using the static single point positioning mode and the second one using a relative positioning method. The influence of different estimation methods on RAIM is investigated with the position domain R-RAIM showing obvious advantages. The 24h 99.9% LPV-200 availability worldwide is 99% with the MHSS method compared with the 31%~35% with other structures, and 100% with the classic method compared with the 78%~85% with other structures. Since the implementation of R-RAIM is more complicated, the current design is to use A-RAIM most of the time and R-RAIM is used only when A-RAIM is not available.
- d) The new approach to obtain the worst case bias and calculate the exact VPL is proved to have accuracy within a pre-defined level of enough computational efficiency. The A-RAIM improvement in the 99% LPV-200 availability is from 32%-38% with the conventional methods to 74%.
- e) With the exact VPL, two conventional VPL methods are theoretically proved to be conservative, while one is numerically proved to be not safe to be used whose value is smaller than the exact one, causing dangerous situations.
- f) Two approximations in calculation of HPL are identified including the approximated distribution of two dimensional position error and the

approximated worst case bias. Two exact distributions are compared with two approximated distributions with the conclusion that the normal approximation is not safe to be used and the chi-squared one is safe.

- g) With the exact HPL value obtained, one of the conventional methods is theoretically proved to be conservative, and one is numerically proved to be not safe.
- h) Similar conclusions are obtained for the PPL with two conservative methods proposed. The method to calculate the exact PPL is similar with the HPL, and the higher dimensional case can be easily obtained.
- i) There is no definite conclusion when comparing the size VPL_{PB} and VPL_{BC} . There are different results with different constellations, such as GPS and Galileo. This leads to the conclusion that geometry plays a key role in deciding which one produces better results. Similar results exist in the HPL results.
- j) Conclusions on MDB as the measure of detectability are made to obtain the optimal test statistic for FD. The w-test statistic is proved to be the best one with smallest MDB in all cases. Other statistics has larger MDB, in another word, worse FD performance, especially when observations are correlated.
- k) The correlation coefficient as the conventional quality measure of separability is found to be not applicable with the v-test when observations are correlated. Therefore a new measure is proposed without loss of generality. Results show that the new measure is consistent with the performance of identifying between two alternative hypotheses.
- l) The expanded RAIM result is dependent on the FDE process with two possible modes: RAIM with FD and RAIM with FDE. The exclusion performance is integrated with the new separability measure used to derive the PL results, which has worse integrity performance than the PL results with FD only.

8.2 Recommendations

- a) The solution separation method to calculate both the HPL and the VPL adopted in the latest EU-US study (A-RAIM report 2012) is proved to be conservative in this thesis. But it should be noted that this method is based on a different definition of integrity risk compared with the classic method, which needs further justification. The proposed RAIM method in this thesis to calculate the HPL and the VPL can be used in A-RAIM with higher availability. If the proposed extended RAIM is used, A-RAIM can be generalized with both detection and exclusion for multiple dimensional protection level calculation.
- b) The multiple hypothesis structure is adopted in the latest EU-US study (A-RAIM report 2012). But the assumption on the design of the multiple hypotheses RAIM should be noted, which is that there is no correlation among different hypotheses. But it is not true in the sense of FDE with multiple alternative hypotheses, which needs further investigation.
- c) Similar assumption exists in the even distribution of the Type I error on each hypothesis with a local test. The complexity and uncertainty exists between the relationship of a global test and a local test needs more attention in academia.
- d) The design to use R-RAIM when A-RAIM is not available is possible, since R-RAIM is shown to have better integrity results within all possible algorithms. But the complexity of R-RAIM should also be noted, such as the increased computation burden, the risk of any fault in the initial position and the choice of coasting time. The GIC information for the initial position estimation is trusted 100% with no risk probability distributed here. If there is any fault in the initial measurement, the current design of R-RAIM is not able to protect the user from it. Also, the coasting time should be properly chosen since it can influence the probability of cycle slip and satellite fault, the geometry change during this time and the parameters in the error model.

- e) The new approach to decide the worst case bias for calculation of both the VPL and the HPL in this thesis can be further optimized by customizing available MATLAB tool for this specific problem with the purpose to further improve the efficiency.
- f) The application for higher dimensional PL may be considered further. But with the increase of the variety of the positioning applications, it is expected that the requirement definition and algorithms to compute the higher dimensional PL would attract more attention.
- g) To apply the extended RAIM in real time applications, the computational efficiency to obtain the non-central parameter with given Type III error needs to be further optimized.
- h) The reliability theory for detection is mature, but more attention is needed for exclusion. A reliable method to exclude a fault is urgent, including the definition of the procedure, the choice of test statistics and the definition of the quality control measure. The latter two are discussed in this thesis, while the first one needs more investigation. The difficulty exists in the separability of all the alternative hypotheses, which are correlated.
- i) There are limitations on the design of statistical tests, such as the single fault assumption, the pre-defined fault mode, and etc. Efforts are made to generalize for multiple faults and modeling of existing fault modes. Any breakthrough in this direction would be mostly valuable.

APPENDIX A: COMPARING TWO MDB SIZE

First, Q_y , Q_v , Q_y^{-1} and $Q_v Q_y^{-1}$ are expressed as block matrices,

$$Q_y = \begin{bmatrix} q_{ii} & Q_{i2} \\ Q_{2i} & Q_{22} \end{bmatrix} \quad (\text{a.1})$$

$$Q_v = \begin{bmatrix} d_{ii} & D_{i2} \\ D_{2i} & D_{22} \end{bmatrix} \quad (\text{a.2})$$

$$Q_y^{-1} = \begin{bmatrix} p_{ii} & P_{i2} \\ P_{2i} & P_{22} \end{bmatrix} \quad (\text{a.3})$$

where $p_{ii} = \frac{q_{ii}^{-1}}{1-\rho_i}$, $\rho_i = \frac{Q_{i2}Q_{22}^{-1}Q_{2i}}{q_{ii}}$, $0 < \rho_i < 1$; $P_{i2} = P_{2i}^T = -\frac{Q_{i2}Q_{22}^{-1}}{q_{ii}(1-\rho_i)}$.

$$Q_v Q_y^{-1} = \begin{bmatrix} b_{ii} & B_{i2} \\ B_{2i} & B_{22} \end{bmatrix} \quad (\text{a.4})$$

where

$$b_{ii} = d_{ii}p_{ii} + D_{i2}P_{2i} = \frac{d_{ii}-D_{i2}Q_{22}^{-1}Q_{2i}}{q_{ii}(1-\rho_i)}, B_{2i} = B_{i2}^T = p_{ii}D_{2i} + D_{22}P_{2i} = \frac{D_{2i}-D_{22}Q_{22}^{-1}Q_{2i}}{q_{ii}(1-\rho_i)}.$$

The following derivations are made:

$$\Rightarrow e_i^T Q_v e_i = d_{ii} \quad (\text{a.5})$$

$$\Rightarrow e_i^T Q_v Q_y^{-1} e_i = b_{ii} = \frac{d_{ii}-D_{i2}Q_{22}^{-1}Q_{2i}}{q_{ii}(1-\rho_i)} \quad (\text{a.6})$$

$$\Rightarrow e_i^T Q_y^{-1} Q_v Q_y^{-1} e_i = p_{ii}b_{ii} + P_{i2}B_{2i} \quad (\text{a.7})$$

$$= \frac{1}{q_{ii}(1-\rho_i)} \cdot \frac{d_{ii}-D_{i2}Q_{22}^{-1}Q_{2i}}{q_{ii}(1-\rho_i)} - \frac{Q_{i2}Q_{22}^{-1}}{q_{ii}(1-\rho_i)} \cdot \frac{D_{2i}-D_{22}Q_{22}^{-1}Q_{2i}}{q_{ii}(1-\rho_i)} \quad (\text{a.8})$$

$$= \frac{d_{ii}-D_{i2}Q_{22}^{-1}Q_{2i}-Q_{i2}Q_{22}^{-1}D_{2i}+Q_{i2}Q_{22}^{-1}D_{22}Q_{22}^{-1}Q_{2i}}{q_{ii}^2(1-\rho_i)^2} \quad (\text{a.9})$$

$$\Rightarrow MDB_{vi}^2 = \frac{\delta^2 d_{ii} q_{ii}^2 (1-\rho_i)^2}{d_{ii}^2 - 2d_{ii} D_{i2} Q_{22}^{-1} Q_{2i} + (D_{i2} Q_{22}^{-1} Q_{2i})^2} \quad (\text{a.10})$$

$$\begin{aligned} \Rightarrow MDB_{wi}^2 &= \frac{\delta^2 q_{ii}^2 (1-\rho_i)^2}{d_{ii} - D_{i2} Q_{22}^{-1} Q_{2i} - Q_{i2} Q_{22}^{-1} D_{2i} + Q_{i2} Q_{22}^{-1} D_{22} Q_{22}^{-1} Q_{2i}} \\ &= \frac{\delta^2 d_{ii} q_{ii}^2 (1-\rho_i)^2}{d_{ii}^2 - 2d_{ii} D_{i2} Q_{22}^{-1} Q_{2i} + d_{ii} Q_{i2} Q_{22}^{-1} D_{22} Q_{22}^{-1} Q_{2i}} \end{aligned} \quad (\text{a.11})$$

Therefore, based on the above two terms, to compare the size between MDB_{vi}^2 and MDB_{wi}^2 , the size of $(D_{i2} Q_{22}^{-1} Q_{2i})^2$ and $d_{ii} Q_{i2} Q_{22}^{-1} D_{22} Q_{22}^{-1} Q_{2i}$ should be compared first. The difference between these two terms is,

$$\begin{aligned} &(D_{i2} Q_{22}^{-1} Q_{2i})^2 - d_{ii} Q_{i2} Q_{22}^{-1} D_{22} Q_{22}^{-1} Q_{2i} \\ &= Q_{i2} Q_{22}^{-1} D_{2i} D_{i2} Q_{22}^{-1} Q_{2i} - Q_{i2} Q_{22}^{-1} d_{ii} D_{22} Q_{22}^{-1} Q_{2i} \\ &= Q_{i2} Q_{22}^{-1} (D_{2i} D_{i2} - d_{ii} D_{22}) Q_{22}^{-1} Q_{2i} \end{aligned} \quad (\text{a.12})$$

With Schur Complement, if Q_v is symmetric positive semidefinite and d_{ii} is positive definite, then $D_{22} - D_{2i} d_{ii}^{-1} D_{i2}$ is positive semidefinite.

$$\Rightarrow Q_{i2} Q_{22}^{-1} (D_{22} - \frac{1}{d_{ii}} D_{2i} D_{i2}) Q_{22}^{-1} Q_{2i} \geq 0 \quad (\text{a.13})$$

$$\Rightarrow \frac{1}{d_{ii}} (D_{i2} Q_{22}^{-1} Q_{2i})^2 \leq Q_{i2} Q_{22}^{-1} D_{22} Q_{22}^{-1} Q_{2i} \quad (\text{a.14})$$

$$\Rightarrow (D_{i2} Q_{22}^{-1} Q_{2i})^2 \leq d_{ii} Q_{i2} Q_{22}^{-1} D_{22} Q_{22}^{-1} Q_{2i} \quad (\text{a.15})$$

$$\Rightarrow \frac{1}{d_{ii}^2 - 2d_{ii} D_{i2} Q_{22}^{-1} Q_{2i} + (D_{i2} Q_{22}^{-1} Q_{2i})^2} \geq \frac{1}{d_{ii}^2 - 2d_{ii} D_{i2} Q_{22}^{-1} Q_{2i} + d_{ii} Q_{i2} Q_{22}^{-1} D_{22} Q_{22}^{-1} Q_{2i}} \quad (\text{a.16})$$

$$\Rightarrow MDB_{vi}^2 \geq MDB_{wi}^2 \quad (\text{a.17})$$

$$\Rightarrow MDB_{vi} \geq MDB_{wi} \quad (\text{a.18})$$

Also, the condition for $MDB_{vi} = MDB_{wi}$ is proved as follows.

$$\frac{MDB_{vi}^2}{MDB_{wi}^2} = \frac{e_i^T Q_v e_i e_i^T Q_y^{-1} Q_v Q_y^{-1} e_i}{(e_i^T Q_v Q_y^{-1} e_i)^2} = \frac{e_i^T Q_v e_i e_i^T Q_y^{-1} Q_v Q_y^{-1} e_i}{e_i^T Q_v Q_y^{-1} e_i e_i^T Q_v Q_y^{-1} e_i} = \frac{e_i^T Q_v (e_i e_i^T Q_y^{-1}) Q_v Q_y^{-1} e_i}{e_i^T Q_v (Q_y^{-1} e_i e_i^T) Q_v Q_y^{-1} e_i} \quad (\text{a.19})$$

Therefore, when $e_i e_i^T Q_y^{-1} = Q_y^{-1} e_i e_i^T$, which is equivalent to when Q_y^{-1} or Q_y is a diagonal square matrix for any i , $MDB_{vi} = MDB_{wi}$.

$$MDB_{vi} = MDB_{wi} \Rightarrow Q_y \text{ is diagonal} \quad (\text{a.20})$$

$$Q_y \text{ is diagonal} \Rightarrow MDB_{vi} = MDB_{wi} \quad (\text{a.21})$$

Therefore, the relationship of both necessity and sufficient is obtained,

$$MDB_{vi} = MDB_{wi} \Leftrightarrow Q_y \text{ is diagonal} \quad (\text{a.22})$$

APPENDIX B: THE SOLUTION SEPARATION STATISTIC

The subset solution estimation \hat{x}_i is,

$$\hat{x}_i = (A_i^T Q_{yi}^{-1} A_i)^{-1} A_i^T Q_{yi}^{-1} y_i \quad (b.1)$$

where A_i , Q_{yi} , y_i are A , Q_y , y with the i th element as zeros.

The subset solution estimation without correlation is (Deggelen and Brown 1994),

$$\hat{x}_i = \hat{x} - S e_i \nabla \hat{S}_i \quad (b.2)$$

The solution separation on the vertical level and its variance are,

$$U_{SS} = \hat{x}_U - \hat{x}_{Ui} = \frac{S_U e_i e_i^T Q_y^{-1} v}{e_i^T Q_y^{-1} Q_v Q_y^{-1} e_i} \quad (b.3)$$

$$\sigma_{U_{SS}} = \frac{S_U e_i}{\sqrt{e_i^T Q_y^{-1} Q_v Q_y^{-1} e_i}} = V_{slope_i} \quad (b.4)$$

Same conclusion can be derived for the horizontal case as shown below.

$$H_{SS} = \sqrt{(\hat{x}_E - \hat{x}_{Ei})^2 + (\hat{x}_N - \hat{x}_{Ni})^2} = \frac{e_i^T Q_y^{-1} v \sqrt{(S_E e_i)^2 + (S_N e_i)^2}}{e_i^T Q_y^{-1} Q_v Q_y^{-1} e_i} \quad (b.5)$$

$$\sigma_{H_{SS}} = \frac{\sqrt{(S_E e_i)^2 + (S_N e_i)^2}}{\sqrt{e_i^T Q_y^{-1} Q_v Q_y^{-1} e_i}} = H_{slope1_i} \quad (b.6)$$

Also for the full solution, the statistic and its covariance matrix are,

$$P_{SS} = \hat{x} - \hat{x}_i = S e_i \nabla \hat{S}_i \quad (b.7)$$

$$Q_{P_{SS}} = \frac{S e_i e_i^T S^T}{e_i^T Q_y^{-1} Q_v Q_y^{-1} e_i} \quad (b.8)$$

Therefore, the equivalence of the test statistics from the vertical and horizontal solution separation is obtained.

$$w_i = \frac{H_{SS}}{\sigma_{H_{SS}}} = \frac{U_{SS}}{\sigma_{U_{SS}}} = \sqrt{P_{SS}^T Q_{P_{SS}}^{-1} P_{SS}} \quad (b.9)$$

APPENDIX C: CONSERVATIVENESS OF VPL

VPL_{ex} as the exact value is compared with other VPLs to analyze their conservativeness. VPL_{ex} can be expressed as a combination of the non-centrality part ∇x_i and the random part,

$$VPL_{ex,i} = \nabla x_i + Q\left(\nabla x_i, \frac{IR_{Vi}}{P_{H_i}\beta_i}\right) \quad (c.1)$$

where the second parameter is the random part as a function of ∇x_i and $\frac{IR_{Vi}}{P_{H_i}\beta_i}$.

Based on the range value of β_i , the following inequality is derived,

$$\nabla x_i < \left[K \left(1 - \frac{\alpha_i}{2} \right) + K \left(1 - \frac{IR_{Vi}}{P_{H_i}} \right) \right] Vslope_i \quad (c.2)$$

When $\nabla x_i \neq 0$, the following inequality is derived,

$$Q\left(\nabla x_i, \frac{IR_{Vi}}{P_{H_i}\beta_i}\right) < K \left(1 - \frac{IR_{Vi}}{2P_{H_i}\beta_i} \right) \sigma_v < K \left(1 - \frac{IR_{Vi}}{2P_{H_i}} \right) \sigma_v \quad (c.3)$$

Therefore, the conservativeness of the VPL_{BC} is obtained,

$$VPL_{ex,i} < VPL_{BCi} \quad (c.4)$$

The position error can be regarded as a sum of two parts: solution separation and subset solution error,

$$|\tilde{x}_v| < |\hat{x}_v - \hat{x}_{vi}| + |\hat{x}_{vi} - x_v| \quad (c.5)$$

With the relationship of test statistic and solution separation, a given P_{MD} can conclude,

$$P\{|\hat{x}_v - \hat{x}_{vi}| < T_i \sigma_{ss,i} | H_i\} = \beta_i \quad (c.6)$$

Consequently,

$$P\{|\hat{x}_{vi} - x_v| > VPL_{ex,i} - T_i \sigma_{ss,i} | H_i\} > \frac{IR_{Vi}}{P_{H_i}\beta_i} \quad (c.7)$$

Therefore,

$$VPL_{ex,i} < K \left(1 - \frac{IR_{Vi}}{2P_{H_i}\beta_i} \right) + K \left(1 - \frac{\alpha_i}{2} \right) \sigma_{ss,i} < VPL_{PB_i} \quad (\text{c.8})$$

Consequently, VPL_{BC} and VPL_{PB} are always conservative irrespective of the size of the bias.

APPENDIX D: CONSERVATIVENESS OF HPL

The conservativeness proof of HPL_{BC1i} is as follows with HPL_{1i} as the exact HPL_{BC} value under normal approximation, which can be regarded as a combination of the non-centrality part ∇HPL_i and the random part $HPL_{\varepsilon i}$.

$$HPL_{1i} = \nabla HPL_i + HPL_{\varepsilon i} \quad (d.1)$$

Since HPL_{1i} is the value under worst case bias with β_i 's range, ∇HPL_i have an upper bound,

$$\nabla HPL_i < [K \left(1 - \frac{\alpha_i}{2}\right) + K(1 - \frac{IR_{Hi}}{P_{Hi}})] Hslope1_i \quad (d.2)$$

Also, since $\nabla HPL_i \neq 0$ under H_i , the following inequalities can be obtained,

$$HPL_{\varepsilon i} < K \left(1 - \frac{IR_{Hi}}{2P_{Hi}\beta_i}\right) \sigma_{\nabla i} < K \left(1 - \frac{IR_{Hi}}{2P_{Hi}}\right) \sigma_{\nabla i} \quad (d.3)$$

Therefore, the conservativeness of the HPL_{BC1} regardless of the bias size is obtained based on normal approximation,

$$HPL_{BC1i} > HPL_{1i} \quad (d.4)$$

Similar proof can be applied on the chi-squared approximation. With HPL_{2i} as the exact value under chi-squared approximation, the proof of the conservativeness of HPL_{BC2i} is as follows. HPL_{2i} is larger $\beta_i = \frac{IR_{Hi}}{P_{Hi}}$ is used to derive the non-centrality parameter $(Hslope2_i \delta_i)^2$ and $\beta_i = 1 - \alpha_i$ is used for the probability of $P_{HPE} = \frac{IR_{Hi}}{P_{Hi}}$. Therefore, the following inequality is obtained with $\chi^2()$ as the non-central chi-squared inverse cumulative distribution with 2 degrees of freedom,

$$HPL_{2i} < \sqrt{\frac{1}{\lambda_m} \chi^2[2, 1 - \frac{IR_{Hi}}{P_{Hi}}, (Hslope2_i \delta_i)^2]} \quad (d.5)$$

With the Triangle Inequality, it is derived that,

$$\sqrt{\frac{1}{\lambda_m} \chi^2 [2, 1 - \frac{IR_{Hi}}{P_{Hi}}, (Hslope2_i \delta_i)^2]} < HPL_{BC2i} \quad (d.6)$$

Therefore, the HPL_{BC2} under the chi-squared approximation is proved to be conservative,

$$HPL_{BC2i} > HPL_{2i} \quad (d.7)$$

REFERENCES

- Angus, J. E. (2007) RAIM with Multiple Faults, *NAVIGATION*, 53(4):249-257.
- Annex 10 (2006) To the Convention on International Civil Aviation, Volume I - Radio Navigation Aids, International Standards and Recommended Practices (SARPs). ICAO Doc. AN10-1, 6th Edition.
- A-RAIM report (2012) Interim Report of the EU/US Cooperation on Satellite navigation released, Working Group C, A-RAIM Technical Subgroup, http://ec.europa.eu/enterprise/policies/satnav/galileo/files/wgc-A-RAIM-tsg-interim-report-1-0_en.pdf.
- Baarda, W. (1967) *Statistical concepts in geodesy*. Netherlands Geodetic, Commission, Publications on Geodesy, New Series 2, No. 4, Delft, the Netherlands.
- Baarda, W. (1968) *A testing procedure for use in geodetic networks*, Netherlands Geodetic Commission, Publications on Geodesy - New Series, 2(5).
- Banett, V. and Lewis, T. (1994) *Outliers in Statistical Data*, 3rd ed., John Wiley & Son.
- Blanch, J., Ene, A., Walter, T. and Enge, P. (2007) An Optimized Multiple Hypothesis RAIM Algorithm for Vertical Guidance, ION GNSS, Fort Worth, TX.
- Blanch, J., Walter, T. and Enge, P. (2008) A Simple Algorithm for Dual Frequency Ground Monitoring Compatible with A-RAIM, ION GNSS, Savannah, GA, 1911-1917.
- Blanch, J., Walter, T. and Enge, P. (2010) RAIM with Optimal Integrity and Continuity Allocations under Multiple Failures, *Aerospace and Electronic Systems, IEEE Transactions on*, 46(3),1235-1247.

- Blanch, J., Walter, T. and Enge, P. (2012a) Optimal Positioning for Advanced RAIM, Proceedings of the 2012 International Technical Meeting of The Institute of Navigation, Newport Beach, CA, 1624.
- Blanch, J., Walter, T., Enge, P., Lee, Y., Pervan, B., Rippl, M., Spletter, A. (2012b) Advanced RAIM user Algorithm Description: Integrity Support Message Processing, Fault Detection, Exclusion, and Protection Level Calculation, ION GNSS 2012, Nashville, TN, September 2012, pp. 2828-2849.
- Brenner, M. (1990) Implementation of a RAIM Monitor in a GPS Receiver and an Integrated GPS/ZRS, Proceedings of ION GPS-90, Colorado Springs, CO, September 19-21.
- Brenner, M. (1996) Integrated GPS/Inertial Fault Detection Availability, *NAVIGATION*, 43(2):111-130.
- Brown, R. G. (1992) A Baseline GPS RAIM Scheme and a Note on the Equivalence of Three RAIM Methods, *NAVIGATION*, 39(3): 301-316.
- Brown, R. G. and Chin, G. Y. (1997) GPS RAIM: Calculation of threshold and protection radius using chi-squared methods-a geometric approach, in *Global Positioning System: Inst. Navigation.*, vol. V, pp. 155-179.
- Brown, R. G. and Chin, G. Y. (1998) Calculation of threshold and protection radius using chi-squared methods-a geometric approach, ION Red Books.
- Chin, G., Kraemer, J., and Brown, R. (1992) GPS RAIM: Screening Out Geometries Under Worst-Case Bias Conditions, *NAVIGATION, Journal of The Institute of Navigation*, Vol. 39, No. 4, Winter 1992-93.
- Choi, M., Blanch, J., Walter, T. and Enge, P. (2011a) Advanced RAIM Demonstration Using Four Months of Ground Data, Proceedings of the 2011 International Technical Meeting of The Institute of Navigation, San Diego, CA, 279-284.
- Choi, M., Blanch, J., Akos, D., Heng, L., Gao, G., Walter, T. and Enge P. (2011b) Demonstrations of Multi-constellation Advanced RAIM for Vertical Guidance Using GPS and GLONASS Signals, ION GNSS 2011, Portland, OR, 3227.

- Daly, K. C., Gai, E., and Harrison, J. V. (1979) Generalized likelihood test for FDI in redundant sensor configuration. *Journal of Guidance and Control*, 2(1): 9-17.
- DiDonato, A. R. and Jarnagin, M. P. (1961) Integration of the general bivariate Gaussian distribution over an offset circle. *J Math Comput JSTOR Database* 15(76):375–382.
- DiDonato, A. R. (1988) Integration of the Trivariate Normal Distribution Over an Offset Sphere and an Inverse Problem, Volume 87, Issue 27 of NSWC TR, Dahlgren Laboratory.
- Diggelen, F. and Brown, A. (1994) Mathematical aspects of GPS RAIM, Position Location and Navigation Symposium, IEEE, pp.733-738.
- Ding, W. and Wang, J. (2011) Precise velocity estimation with a stand-alone GPS receiver, *Journal of Navigation*, 64(2): 311-325.
- DO-229 (2006) Minimum Operational Performance Standards for Global Positioning System/Wide Area Augmentation System Airborne Equipment. *RTCA DO-229*.
- Duchesne, P. and Lafaye de Micheaux, P. (2010) Computing the distribution of quadratic forms: Further comparisons between the Liu-Tang-Zhang approximation and exact methods, *Computational Statistics and Data Analysis*, 54: 858-862.
- Forsythe, G. E., Malcolm, M. A. and Moler, C. B. (1976) *Computer Methods for Mathematical Computations*, Prentice-Hall.
- Förstner, W. (1983) Reliability and discernability of extended gauss-markov models. In: Seminar on Mathematical Models to Outliers and Systematic Errors, Deutsche Geodatische Kommission, Series A, no. 98, Munich, 79-103.
- Förstner, W. (1985) The Reliability of Block Triangulation. *Photogramm. Eng. & Remote. Sens.*, 51(6): 1137-1149.
- GEAS (2008) GNSS Evolutionary Architecture Study, *GEAS Phase I - Panel Report, FAA*.
- GEAS (2010) GNSS Evolutionary Architecture Study, *GEAS Phase II - Panel Report, FAA*.

- GPS SPS (2008) Global Positioning System Standard Positioning Service Performance Standard.
- Gratton, L., Mathieu, J. and Boris, P. (2010) Carrier Phase Relative RAIM Algorithms and Protection Level Derivation, *Journal of Navigation*, 63(2): 215-231.
- Hawkins, D. M. (1980) *Identification of Outliers*. Chapman and Hall, London/New York.
- Hewitson, S. and Wang, J. (2006) GNSS Receiver Autonomous Integrity Monitoring (RAIM) Performance Analysis. *GPS Solutions*. 10(3):155-170
- Hewitson, S. and Wang, J. (2007) GNSS Receiver Autonomous Integrity Monitoring (RAIM) with a dynamic model. *Journal of Navigation*, 60(2): 247- 263.
- Hwang, P. Y. and Brown, R. G. (2005) RAIM FDE Revisited: A New Breakthrough In Availability Performance With NIORAIM (Novel Integrity-Optimized RAIM), NTM ION, San Diego, CA.
- Imhof, J. P. (1961) Computing the Distribution of Quadratic Forms in Normal Variables, *Biometrika*, Volume 48(3-4): 419-426.
- Jiang, Y., Wang, J., Knight, N. and Ding, W. (2010) Optimization of position domain relative RAIM for weak geometries, 23rd Int. Tech. Meeting of the Satellite Division of the U.S. Inst. of Navigation, Portland, Oregon, USA, 2182-2189.
- Jiang, Y. and Wang, J. (2011) A-RAIM vs. R-RAIM: A Comparative Study. IGNSS Symp., Sydney, Australia, paper 154.
- Jiang, Y. and Wang, J. (2014a) A-RAIM and R-RAIM Performance using the Classic and MHSS Methods. *Journal of Navigation*, 67: 49-61.
- Jiang, Y. and Wang, J. (2014b) A new approach to calculate the Vertical Protection Level in A-RAIM, *Journal of Navigation*, 67(4):711-725..
- Jin, H. and Zhang, H. (1999) Optimal parity vector sensitive to designated sensor fault, *Aerospace and Electronic Systems, IEEE Transactions on*, 35(4):1122-1128.
- Johnson, N. L. and Kotz, S. (1970) *Continuous Univariate Distributions*, volume 2, first edition, John Wiley & Sons Inc.

- Kaplan, D. E. and Hegarty, C. (2005) *Understanding GPS: Principles and Applications*, Artech House, Second Edition.
- Kelly, R. J. (1998) The linear model, RNP, and the near optimum fault detection and exclusion algorithm, US Institute of Navigation Red Book, Vol., 5:227-259.
- Knight, N. L., Wang, J., and Rizos, C., (2010) Generalised measures of reliability for multiple outliers. *Journal of Geodesy*, 84(10): 625-635.
- Kok, J. J. (1984) On Data Snooping and Multiple Outlier Testing. NOAA Technical Report, NOS NGS. 30, U.S. Department of Commerce, Rockville, Maryland.
- Lee, Y. C. (1986) Analysis of Range and Position Comparison Methods as a Means to Provide GPS Integrity in the User Receiver. In: *Global Positioning System*, Vol. 5. The Institute of Navigation, Fairfax, Virginia, 5-19.
- Lee, Y. C (1995) New techniques relating fault detection and exclusion Performance to GPS Primary Means Integrity Requirements, The 8th international technical meeting of the ION.
- Lee, Y., Van Dyke, K., DeCleen,e B., Studenny, J. and Beckmann, M. (1996) SUMMARY OF RTCA SC-159 GPS INTEGRITY WORKING GROUP ACTIVITIES, *NAVIGATION*, 43(3) : 307-362.
- Lee, Y. C. (2008) Optimization of Position Domain Relative RAIM, ION GNSS, Savannah.
- Lee, Y. C. and McLaughlin, M. (2008) A Position Domain Relative RAIM Method, Proceedings of the IEEE/ION PLANS 2008 Conference, Monterey, California.
- Li, D. (1987) Theory and research on the disjunction of cross passage errors and systematic image errors in photogrammetric point determination, Ph.D. Thesis, Stuttgart Univ., West Germany.
- Li, D. and Yuan, X. (2002) *Error Processing and reliability theory*, The press of Wuhan University, Wuhan, China, in Chinese.
- Lou, X. C., Willsky, A. S., and Verghese, G. C. (1986) Optimally robust redundancy relations for failure detection in uncertain systems. *Automatica*, 22(3):333-343.

- Macdonald, K. (2002) The Modernization of GPS: Plans, New Capabilities and the Future Relationship to Galileo, *Positioning*, vol. 1 No. 3.
- Milner, C. and Ochieng, W. (2010a) A-RAIM for LPV-200: The Ideal Protection Level, ION GNSS, Portland, OR, 3191-3198.
- Milner, C. D. and Ochieng, W. Y. (2010b), A fast and efficient integrity computation for non-precision approach performance assessment, *GPS Solutions*, Vol:14, ISSN:1080-5370, Pages:193-205
- Milner, C. and Ochieng, W. (2011) Weighted RAIM for APV: The Ideal Protection Level, *Journal of Navigation*, 64: 61-73.
- Ober, P. B. (1997) Ways to improve RAIM/AAIM availability using position domain performance computations. In: The proceedings of the 1997 National technical meeting of the Institute of Navigation, Lowes Santa Monica Beach Hotel, Santa Monica, pp 485–498
- Ober, P. B. (1998) RAIM Performance: How Algorithms Differ, Proceedings of the 11th International Technical Meeting of the Satellite Division of The Institute of Navigation (ION GPS 1998), Nashville, TN, pp. 2021-2030.
- Ober, P. B. (2003) Integrity Prediction and Monitoring of Navigation Systems, PhD Thesis. TU Delft.
- Patton, R. J., Chen, J. and Zhang, H. Y. (1992) Modelling methods for improving robustness in fault diagnosis of jet engine system, Decision and Control, Proceedings of the 31st IEEE Conference on ,2:2330-2335.
- Patton, R. J, Robert, N., Paul, C. and Frank, M. (2000) *Issues of Fault Diagnosis for Dynamic Systems*, Springer.
- Parkinson, B. W. and Axelrad, P. (1988) Autonomous GPS Integrity Monitoring Using the Pseudorange Residual, *Navigation*, 35(2): 255-74.
- Pervan, B. S. (1996) Navigation integrity for aircraft precision landing using the global positioning system, Thesis (Ph.D.), Stanford University.

- Pervan, B. S., Lawrence, D. G.; Cohen, C. E. and Parkinson, B. W. (1996) Parity Space Methods For Autonomous Fault Detection and Exclusion Algorithms Using Carrier Phase, Proceedings of PLANS 96 Symposium, Atlanta, GA, April 22-26.
- Pervan, B., Pullen, S. and Christie, J. (1998) A Multiple Hypothesis Approach to Satellite Navigation Integrity, *Navigation*, 45(1): 61-71.
- Plan (2008) US Federal Radionavigation Plan, DOT-VNTSC-RITA-08-02/DoD-4650.5
- Potter, I. E. and Sunman, M. C. (1977) Thresholdless redundancy management with arrays of skewed instruments, *Integrity in Electronic Flight Control Systems*, AGARDOGRAPH-224, pp. 15–11 to 15–25.
- Prószyński, W. (1994) Criteria for internal reliability of linear least squares models. *Bulletin Géodésique*, 68: 161-167.
- Rippl, M., Spletter, A. and Günther, C. (2011) Parametric Performance Study of Advanced Receiver Autonomous Integrity Monitoring (A-RAIM) for Combined GNSS Constellations, Proceedings of the 2011 International Technical Meeting of The Institute of Navigation, San Diego, CA, 285-295.
- Serrano, L., Kim, D. and Langley, R. B. (2004a) A single GPS receiver as a real-time, accurate velocity and acceleration sensor. ION GNSS 17th international technical meeting of the satellite division, Long Beach CA. 2021–2034.
- Serrano, L., Kim, D., Langley, R. B., Itani, K. and Ueno, M. (2004b) A GPS velocity sensor: How accurate can it be? – A first look. ION NTM 2004, San Diego CA. 875–885.
- Schaffrin, B. (1997) Reliability measures for correlated observations. *Journal of Surveying Engineering*, 123(3):126-137.
- Sturza, M. A. (1988) Navigation System Integrity Monitoring Using Redundant Measurements, *NAVIGATION*, 35(4): 483-502.
- Teunissen P.J.G. (1990) Quality Control in Integrated Navigation Systems. *IEEE Aerosp. Electron. Syst. Mag.* 5(7): 35-41.

- Teunissen, P. J. G. (1991) On the Minimal Detectable Biases of GPS Phase Ambiguity Slips. In: First International Symposium on Real Time Differential Applications of the GPS, Stuttgart, Germany, Vol 2, 679-686.
- Teunissen, P. J. G. (2000) *Testing Theory: an introduction*, VSSD, Delft.
- Teunissen, P. J. G. (2004) *Adjustment Theory: an introduction*, VSSD, Delft
- Teunissen, P. J. G. (2006) *Network Quality Control*, VSSD, Delft
- Van Dyke, K. (1993) RAIM Availability for Supplemental GPS Navigation, *NAVIGATION*, 39(4): 1993-94.
- Van Graas, F. and Farrell, J. (1993) Fault Detection and Exclusion Baseline Algorithm, *NAVIGATION*, Vol. 40, No. 2, Summer 1993.
- Van Graas, F. and Soloviev, A. (2004) Precise Velocity Estimation Using a Stand-Alone GPS Receiver, *Navigation*, 51(4): 283-292.
- Walter, T. and Enge, P. (1995) Weighted RAIM for Precision Approach, Proceedings of ION GPS-95, Palm Springs, CA, pp. 1995-2004.
- Wang, J. and Chen, Y. (1994a) On the reliability measure of observations. *Acta Geodaetica et Cartographica Sinica*, English Edition, 42-51.
- Wang, J. and Chen, Y. (1994b) On the Localizability of Blunders in Correlated Coordinates of Junction Points in Densification Networks, *Aust.J.Geod.Photogram.Surv.*, 60:109-119.
- Wang, J. and Chen, Y. (1999) Outlier Detection And Reliability Measures For Singular Adjustment Models. *Geomat. Res. Aust* 71:57-72.
- Wang, J. and Knight, N. L. (2012) New Outlier Separability Test and its Application in GNSS Positioning, *Journal of global positioning systems*, 11(1):46-57.
- Wang, J. and Kubo, Y. (2010) GNSS Receiver Autonomous Integrity Monitoring, In: (Eds. Sugimoto S & R. Shibasaki): *GPS Handbook*, Asakura, Tokyo, ISBN978-4-254-20137-6, 197-207.

- Wang, J. and Ober, P. B. (2009) On the Availability of Fault Detection and Exclusion in GNSS Receiver Autonomous Integrity Monitoring, *Journal of Navigation*, 62(2): 251–261.
- Wu, Y., Wang, J. and Jiang, Y. (2013) Advanced receiver autonomous integrity monitoring (A-RAIM) schemes with GNSS time offsets, *Advances in Space Research*, 52(1): 52-61.
- Yang L., Wang J., Knight N. L. and Yunzhong, S. (2013) Outlier separability analysis with a multiple alternative hypotheses test, *Journal of Geodesy*, 87(6): 591-604.
- Young, R. S. Y., McGraw, G. A. (2003) Fault Detection and Exclusion Using Normalized Solution Separation and Residual Monitoring Methods, *NAVIGATION*, 50(3): 151-170.
- Zhao, S. (1990) On Separability for Deformations and Gross Errors, *Journal of Geodesy*, 64(4):383-396.
- Zhang, H. Y., and Patton, R. J. (1993) Optimal design of robust analytical redundancy for uncertain systems. Presented at the IEEE Region 10 Conference on Computer, Communication, Control and Power Engineering, 1993, Beijing, China.
- Zhang, L., Chen, M. and Liu, C. (2005) Is OPT better than GLT in fault diagnosis of redundant sensor system? (Translation Journals) *Journal of Northwestern Polytechnical University*, 23(2).

PUBLICATIONS DURING PHD STUDIES

Referred journal papers:

- Jiang, Y. and Wang, J. (2014) A-RAIM and R-RAIM Performance with the Classic Method and the MHSS Method, *Journal of Navigation*, 67: 49-61.
- Jiang, Y. and Wang, J. (2014) a new approach to calculate the Vertical Protection Level in A-RAIM, *Journal of Navigation*, 67(4):711-725.
- Jiang, Y. and Wang, J. (2014) a new approach to calculate the Horizontal Protection Level, *Journal of Navigation*, under revision.
- Jiang, Y. and Wang, J. (2013) a new Separability Measure in Parity Space, *Journal of Surveying Engineering*, Submitted.
- Wu, Y., Wang, J. and Jiang, Y. (2013) Advanced Receiver Autonomous Integrity Monitoring (A-RAIM) Schemes with GNSS Time Offsets, *Advances in Space Research*, 52(1):52-61.

Referred conference papers:

- Jiang, Y. and Wang, J. (2011) A-RAIM vs. R-RAIM: A comparative study. IGNSS Symp., Sydney, Australia, 15-17 November, paper 154.

Abstract Referred conference papers:

- Jiang, Y. and Wang, J. (2010) Fault detection and exclusion for future generation GNSS using an improved parity space method, 2010 Int. Symp. on GPS/GNSS, Taipei, Taiwan, 26-28 October, 344-349.
- Jiang, Y., Wang, J., Knight, N. and Ding, W. (2010) Optimization of position domain relative RAIM for weak geometries. 23rd Int. Tech. Meeting of the Satellite Division of the U.S. Inst. of Navigation, Portland, Oregon, USA, 21-24 September, 2182-2189.

Jiang, Y. and Wang, J. (2012) Optimization of the Multiple Hypotheses Solution Separation RAIM Method, Proceedings of the 25th International Technical Meeting of The Satellite Division of the Institute of Navigation (ION GNSS 2012), Nashville, TN, September 2012.

Conference Presentations:

Fault detection and exclusion for future generation GNSS using an improved parity space method, International Symposium on GPS/GNSS 2010, Taipei, Taiwan, October 2010.

A-RAIM vs. R-RAIM: A comparative study, IGNSS 2011, Sydney, Australia, November 2011.

Optimization of position domain relative RAIM for weak geometries, ION GNSS 2012, Nashville, TN, September 2012.